BIOPHYSICAL STUDIES OF M2GLYR MODIFIED SEQUENCES: THE EFFECT OF ELECTROSTATICS ON ION CHANNEL SELECTIVITY

by

URŠKA BUKOVNIK

M. S., University of Ljubljana, Slovenia, 2003

AN ABSTRACT OF A DISSERTATION

submitted in partial fulfillment of the requirements for the degree

DOCTOR OF PHILOSOPHY

Department of Biochemistry
College of Arts and Sciences

KANSAS STATE UNIVERSITY
Manhattan, Kansas

2011

Abstract

Channel replacement therapy represents a new treatment modality that could augment existing therapies against cystic fibrosis. It is based on designing synthetic channel-forming peptides (CFPs) with desirable selectivity, high ion transport rates and overall ability to supersede defective endogenous chloride channels. We derived synthetic CFPs from a peptide initially reconstituted from the second transmembrane segment of the α-subunit of Glycine receptor (M2GlyR). Our best candidate peptide NK_4-M2GlyR T19R, S22W (p22-T19R, S22W) is soluble in aqueous solutions, has the ability to deliver itself to the epithelial cell membranes without the use of a delivery system, is non-immunogenic, but when assembled into a pore, lacks the structural properties for anion selectivity. Previous findings suggested that threonine residues at positions 13, 17 and 20 line the pore of assembled p22-T19R, S22W and recent studies indicated that an introduction of positively charged 2, 3-diaminopropionic acid (Dap) at either T13 or T17 in the sequence increases transepithelial ion transport rates across the apical membranes of Madin-Darby canine kidney (MDCK) epithelial cells. This study focused on further structural modifications of the pore-lining interface of p22-T19R, S22W assembled pore. It was hypothesized that singly, doubly or triply introduced Dap residues modify the pore geometry and that their positively charged side chains impact discrimination for anions. Dap-substituted p22-T19R, S22W peptides retain the α-helical secondary structure characteristic for their parent p22-T19R, S22W. The sequences containing multiple Dap-substituted residues induce higher short circuit current across the epithelial MDCK cells compared to peptides with single Dap-substitutions or no Dap-substitutions. Whole-cell voltage clamp recordings using *Xenopus* oocytes indicate that Dap-substituted peptide assemblies induce higher levels of

voltage-dependent but non-selective ion current relative to p22-T19R, S22W. Studies using the D-enantiomer of p22-T19R, S22W and shorter truncated sequences of a full length L-p22-T19R, S22W and L-Dap-substituted peptides provided evidence that peptide-induced ion transport rates can be attributed to formation of *de novo* pathways. Results of preliminary computer modeling studies indicate that Dap residues affect the pore geometry but not ion selectivity. Future studies focusing on modifying the existing electrostatic environment towards anion selectivity will focus on staggering the charged residues of Dap at various locations inside synthetic pores.

BIOPHYSICAL STUDIES OF M2GLYR MODIFIED SEQUENCES: THE EFFECT OF THE ELECTROSTATICS ON ION CHANNEL SELECTIVITY

by

URŠKA BUKOVNIK

M. S., University of Ljubljana, Slovenia, 2003

A DISSERTATION

submitted in partial fulfillment of the requirements for the degree

DOCTOR OF PHILOSOPHY

Department of Biochemistry
College of Arts and Sciences

KANSAS STATE UNIVERSITY
Manhattan, Kansas

2011

Approved by:

Major Professor
John M. Tomich

Abstract

Channel replacement therapy represents a new treatment modality that could augment existing therapies against cystic fibrosis. It is based on designing synthetic channel-forming peptides (CFPs) with desirable selectivity, high ion transport rates and overall ability to supersede defective endogenous chloride channels. We derived synthetic CFPs from a peptide initially reconstituted from the second transmembrane segment of the α-subunit of Glycine receptor (M2GlyR). Our best candidate peptide NK_4-M2GlyR T19R, S22W (p22-T19R, S22W) is soluble in aqueous solutions, has the ability to deliver itself to the epithelial cell membranes without the use of a delivery system, is non-immunogenic, but when assembled into a pore, lacks the structural properties for anion selectivity. Previous findings suggested that threonine residues at positions 13, 17 and 20 line the pore of assembled p22-T19R, S22W and recent studies indicated that an introduction of positively charged 2, 3-diaminopropionic acid (Dap) at either T13 or T17 in the sequence increases transepithelial ion transport rates across the apical membranes of Madin-Darby canine kidney (MDCK) epithelial cells. This study focused on further structural modifications of the pore-lining interface of p22-T19R, S22W assembled pore. It was hypothesized that singly, doubly or triply introduced Dap residues modify the pore geometry and that their positively charged side chains impact discrimination for anions. Dap-substituted p22-T19R, S22W peptides retain the α-helical secondary structure characteristic for their parent p22-T19R, S22W. The sequences containing multiple Dap-substituted residues induce higher short circuit current across the epithelial MDCK cells compared to peptides with single Dap-substitutions or no Dap-substitutions. Whole-cell voltage clamp recordings using *Xenopus* oocytes indicate that Dap-substituted peptide assemblies induce higher levels of voltage-dependent but non-selective ion current relative to p22-T19R, S22W. Studies using the

D-enantiomer of p22-T19R, S22W and shorter truncated sequences of a full length L-p22-T19R, S22W and L-Dap-substituted peptides provided evidence that peptide-induced ion transport rates can be attributed to formation of *de novo* pathways. Results of preliminary computer modeling studies indicate that Dap residues affect the pore geometry but not ion selectivity. Future studies focusing on modifying the existing electrostatic environment towards anion selectivity will focus on staggering the charged residues of Dap at various locations inside synthetic pores

Table of Contents

List of Figures

List of Tables

Acknowledgements

I will be always thankful to my major advisor and mentor Prof. John M. Tomich for his mentorship, professional guidance and encouragement. Thank you also to Prof. Colin Nichols for sharing his rich knowledge of electrophysiology and guidance throughout the time I spent working in his laboratory at the University of Washington School of Medicine, St. Louis, MO.

I am grateful to Dr. Takeo Iwamoto for his guidance and willingness to share his rich knowledge of peptide synthesis with me.

I would like to express my appreciation to the following individuals who have contributed to this work and helped me grow professionally: Prof. Bruce D. Schultz, Dr. Monica Sala-Rabanal, and Dr. Nazzareno D'Avanzo. I am grateful for their helpful suggestions and sharing the knowledge of electrophysiology.

Thank you also to my committee members: Prof. Om Prakash, Prof. Michal Zolkiewski and Prof. Peying Fong and the outside chairperson Prof. Christine Aikens.

My gratitude goes to my lab colleagues: Pinakin Sukthankar, Dr. Yasuaki Hiromasa, Sushanth Gudlur, Luz Adriana Avila Flores, Nozomi Matsumiya Caton and Xiao Xao, whom I enjoyed their friendship and working with at the Biotechnology Core laboratory, at the Biochemistry Department at Kansas State University. Thank you also to my friend Priscilla Mfombep for her support and friendship.

I am especially thankful to my parents and my brother for their great support and trust on my path through all the years spent on PhD program at Kansas State University.

Dedication

I dedicate this work to the cystic fibrosis patients. I hope my research contributes a new step towards development of a successful therapy against cystic fibrosis.

Chapter 1 - Introduction and background

Cystic Fibrosis

Epithelial cells form the tissues lining cavities and ducts in animals and humans. The main function of epithelial cells is to act as a barrier to the movement of small solutes, inorganic ions and drugs between body compartments. The ions traverse epithelial apical and basolateral membranes *via* a combination of tightly regulated ion-specific transporters and channels. Mutations of genes encoding ion channels result in malfunction of channels that lead to disease pathogenesis. One such channelopathy is cystic fibrosis (CF), a chronic hereditary autosomal recessive disease (Becq, 2010) caused by mutations in the cystic fibrosis transmembrane conductance regulator (CFTR). CFTR functions as an anion selective transmembrane regulator protein (McCarty, 2000) and belongs to the ABC transporter/channel superfamily (Higgins, 1995). The structure of CFTR consists of two hydrophobic membrane-spanning domains, two hydrophilic membrane-associated domains and a regulatory domain (Riordan et al., 1989; Devidas and Guggino, 1997; McCarty, 2000); the latter carries multiple sites for regulation by protein kinase A (Devidas and Guggino, 1997; McCarty, 2000). The absence of proper CFTR activity alters expression of several genes encoding membrane transport proteins known for their direct interaction with CFTR as well as expression of genes involved in inflammation, intracellular trafficking and signal transduction (Xu et al., 2003).

CFTR is cAMP regulated membrane protein (Sheppard and Welsh, 1999; Davis, 2006) expressed primarily in tissues with epithelia as sweat duct, airway, pancreatic duct, gastrointestinal tract and vas deferens (Quinton, 1999; Davis, 2006). CFTR mutations give rise to increased sweat chloride concentration, lung disease characterized by bacterial infection and

bronchiectasis, pancreatic insufficiency, intestinal obstruction and congenital bilateral absence of the vas deferens (CBAVD). Often a combination is observed (Davis, 2006).

Development of CF is a result of mutations. Defects of CF-associated mutations are well documented and grouped into 5 different classes, based on the mechanism by which they disrupt CFTR function (Pilewski and Frizzell, 1999). Mutations affecting the CFTR biosynthesis belong to class 1 and result in a failure of CFTR translation. Further, mutations affecting the protein maturation belong to the second class. One of the representatives of this class is a deletion of phenylalanine (ΔF508) where CFTR fails to mature and is prone to degradation in the endoplasmic reticulum (Mall et al., 2004; Kopito, 1999; Pilewski and Frizzell, 1999). Class 1 and 2 mutations are associated with multi-organ disease, especially progressive pulmonary disease, pancreatic insufficiency and male infertility (Rowntree and Harris, 2003). The third class of mutations affects channel regulation and gating, with perhaps the G551D mutation being the best characterized. The pancreatic and pulmonary insufficiency manifested by these mutations is indistinguishable from class 1 and 2 mutations. A much milder phenotype is observed with class 4 mutations. These result in diminished chloride conductance even though mature CFTR protein is activated normally. Milder phenotypes are observed also for class 5 mutations. The splice mutations resulting in decreased abundance of a full-length mRNA decrease the quantity of functional CFTR at the cell membrane. Two phenotypes are associated with this class: a mild phenotype for pancreatic disease and a phenotype of CBAVD (Pilewski and Frizzell, 1999; Rowntree and Harris, 2003). CF patients with CBAVD make normal sperm but are missing their vas deferens that connects the testes to the ejaculatory ducts of the external male sex organ used to copulate and ejaculate semen and convey urine.

Altogether, CF-associated mutations result in abnormal chloride transport and diminished chloride conductance of epithelia, leading to reduced chloride and fluid secretion by the secretory epithelia (Welsh, 1987; Liedtke, 1989; Anderson et al., 1992; Smith et al., 1994; Zhou et al., 1994). In addition, other CFTR-dependent processes contribute to the disease. CFTR plays a role in a regulation of Cl^--coupled HCO_3^- transport (Choi et al., 2001; Quinton, 2001), a process mediated by Cl^-/HCO_3^- exchanger, found in the apical membrane of the pancreatic duct and airway epithelia (Kim and Stewart, 2009).

Recent studies have indicated that CFTR plays a major role in early organogenesis in the CF pig. Within only few months of birth CF pigs developed the hallmark features of CF lung disease and showed impaired ability to eradicate bacteria in lungs. It seems that there is more than just infection that leads to the pathological state of the disease (Stoltz et al., 2010).

In CF airway epithelium, reduced chloride secretion, increased sodium absorption and insufficient airway luminal fluid (Rowe et al., 2005; Davis, 2006) result in viscid secretions (Taylor and Ashwani, 2002). Mucus hydration and its clearance depend on the volume of the airway surface liquid (ASL) that can be regulated by the active ion transport (Tarran, 2004). ASL contains antibacterial agents and immune cells, such as neutrophils and macrophages that protect lungs against infection (Tarran, 2004). In CF patients this is compromised due to reduced volume of ASL (Pilewski and Frizzell, 1999). Reduced HCO_3^- secretion, dehydration of mucus and reduced height of the periciliary fluid layer (PCL) altogether result in poor mucus clearance (Boucher, 2007; Fahy and Dickey, 2010). Abnormally thick and sticky mucus (Quinton, 1999; Planells-Cases and Jentsch, 2009) containing polymerized actin, mucins (Davis, 2006) and DNA, is released by the apoptosis of leukocytes. Leukocytes migrate into the airway in response to

infections. Mucus clearance plays major role in lung`s innate immune defense against disease.

The mucus serves as a substrate on which pathogens such as *Pseudomonas aeruginosa, Burkholderia cepacia, Staphylococcus aureus,* and *Haemophilus influenza* can thrive. The pathogens establish and propagate within these immobile airway secretions, trigger development of host pulmonary inflammation, chronic infections and ultimately a decline in respiratory function (Rowe et al., 2005). CFTR may also play role in deregulation of the inflammatory response through the mechanisms that include defective apoptosis, impaired antioxidant secretion and elevated oxidant production (Pilewski and Frizzell, 1999).

Disrupted transport of ions and water across the intestinal wall results in meconium ileus in newborns. This is caused by distal intestinal obstructions resulting from the impact of a thick meconium in the bowel. While the primary effect of CF in the pancreatic duct is a reduction in water secretion involving a Cl^-/HCO_3^- exchange (Taylor and Ashwani, 2002), since CFTR provides the pathway for HCO_3^- transport in pancreatic duct cells (Ishiguro et al., 2009). Pancreatic secretions block the duct thus obstructing the flow of pancreatic juice containing digestive enzymes. Degeneration of acinar cells where the enzymes are synthesized and secreted from and the subsequent pancreatic fibrosis result in impaired digestion of fat, proteins and starch (Taylor and Ashwani, 2002).

In sweat glands, the absence of functional CFTR restricts the chloride absorption in the duct and affects the reabsorption of its counter-ion, sodium. A lack of chloride reabsorption and a poor sodium intake contribute to higher concentrations of salt in the sweat (Rowe et al., 2005).

Pharmacological treatments for CF

Currently available treatments for CF focus on replacing or restoring function to defective CFTR channels by employing mutation-specific pharmacotherapies (Proesmans et al., 2008), pharmacoagents alone (Gao et al., 2001; Van Goor et al., 2009) or a variety of genetic approaches. Many of the available approaches increase the life span of CF patients beyond 30 years by reducing inflammation and fighting off infections.

Diet supplements

Vitamin deficiency of fat-soluble vitamins A, E and K (Dodge, 1986) and the lack of antioxidants in CF patients are considered to contribute to the poor host response to lung inflammation. A commercially available vitamin supplement, AquADEKs®, developed by Yasoo Health (Sagel et al., 2011), reportedly increase the systemic antioxidant levels, improved the vitamin A levels but did not completely normalize vitamin D and K status. Additionally, increased β-carotene levels were associated with improved growth parameters, such as changes in weight and body mass index percentiles (Sagel et al., 2011).

Enzyme replacement therapies

Digestive tract enzyme deficiency in CF patients can be treated with pancreatic enzyme products consisting of lipases, proteases and amylases from porcine pancreatic glands. Active compounds in these products increase the digestion and absorption of fats, proteins, and starches and promote the absorption of certain vitamins. The FDA-approved products include: Creon® (Abbot Pharmaceuticals) and Pancreaze™ (McNeil). Among the ones waiting approval is Liprotamase (Alnara Pharmaceuticals) a non-porcine pancreolipase enzyme which completed a

phase 3 clinical trial while a few more such as Pancrecarb® (DCI) and Ultrase® (Axcan Scandipharm) are still awaiting clinical trials (Lowry, 2011).

Antibiotics for chronic lung infections

CF patients with chronic lung infections require treatment with antibiotics to treat drug resistant infections. Antibiotics are administered orally, intravenously or via inhalation (Gibson et al., 2003). TOBI® and recently developed Cayston® (a aztreonam, (Z)-2-[[[(2-amino-4-thiazolyl)[[(2S,3S)-2-methyl-4-oxo-1-sulfo-3azetidinyl]carbamoyl]methylene]amino]oxy]-2-methylpropionic acid, in solution for inhalation) developed by Gilead Sciences, are two approved and commonly prescribed antibiotics for patients with CF. Both are effective against *Pseudomonas aeruginosa*, the most common pathogen present in airway mucus (Cheer et al., 2003). TOBI® developed by Novartis Pharmaceuticals, which has been used widely since its FDA approval in 1997. It is an aminoglycoside antibiotic produced by *Streptomyces tenebrarius*. Tobramycin disrupts protein synthesis and cell envelope and alters cell membrane permeability ("TOBI® - Description clinical pharmacology", n.d.). Aside from TOBI® and Cayston®, several other anti-infective agents are presently being evaluated for use. Mpex Pharmaceuticals has developed MP-376, an aerosol form of levofloxacin, also used to treat *P. aeruginosa* infections. It is currently undergoing phase 3 clinical trials ("Mpex – Product development programs", n.d.). Insmed Incorporated recently completed phase 2 trials of Arikace™, an inhaled version of the FDA-approved antibiotic amikacin in a liposomal formulation that is inhaled using a nebulizer. *In vitro* experiments, demonstrate that Arikace™ liposomes penetrate into the human CF sputum and the *Pseudomonas* macro-colonies. Virulence factors secreted from the targeted bacteria facilitate the release of amikacin from the Arikace™ liposomes, releasing the drug near bacteria and resulting in their destruction ("Arikace™ - Clinical trials", n.d.).

Airway rehydrating agents

Many therapies are directed toward allaying the pulmonary symptoms of CF focused on restoring the liquid necessary to hydrate the mucus or the underlying layer to facilitate expectoration (Pettit and Johnson, 2011) or to reduce the mucus viscosity. Pulmozyme® by Genentech in use as a mucolytic for CF patients is a dornase α (recombinant human deoxyribonuclease) used to break down the DNA contributing to thickened pulmonary mucus, thereby promoting mucus clearance and thus reducing the environment that supports bacterial growth. Pulmozyme® reportedly increases lung function by 6% and reduces the risk of infection by 27% (Fuchs et al., 1994; "Pulmozyme – Full Prescribing Information", (n.d.)).

In another approach, the response to Lancovutide (Moli1901) inhalation solution, developed by Lantibio, was unaffected by the pretreatment of the pulmonary epithelium of CF patients with amiloride or cyclic adenosine monophosphate. The effect may not involve sodium channels or CFTR (Zeitlin et al., 2004) but alternative chloride channels to compensate for the deficiencies of CFTR. In phase 2 of European trials, Moli1901 was shown to increase the pulmonary function of CF patients and was well tolerated (Grasemann et al., 2007).

GS-9411 by Gilead is an epithelial sodium channel (ENaC) inhibitor blocking airway epithelial sodium transport and is predicted to reduce mucus dehydration. A phase 1 trial has been completed and the drug shown to be safe and well tolerated (Sears et al., 2011; "Clinical trial - GS-9411, 2010).

Mannitol was shown to help clear CF airways and improves pulmonary function. Mannitol draws water into the lungs osmotically and helps to clear mucus. Mannitol is well tolerated by patients having no serious adverse side effects (Jaques et al., 2008; Bilton et al., 2011). Phase 3 trials

have been completed and the therapy is currently being marketed in Europe ("Mannitol - Clinical trials and use", n.d.). Another approach is the use of inhaled hypertonic saline. The hypertonic saline increases the ionic concentration in the ASL, osmotically draws fluid into the airway lumen and replenishes the fluid layer. This helps to accelerate mucus clearance (Robinson et al., 1997). However, another approach to activate signal-transducing pathways independent of cAMP and a bicarbonate secretion across the epithelium is based on the use of extracellular nucleotides (Knowles et al., 1995; Clarke et al., 2000).

Anti-inflammatories

Immune cells, such as macrophages and neutrophils, defend against bacterial infections in CF patients. In doing so, they generate a greater problem in physical damage to the host airway cells due to nuclear factor (NF)-kappaB activation and elevated pro-inflammatory cytokines which results in scarring and fibrosis. Oral N-acetylcysteine (PharrmaNAC, BioAdvantex Pharma, Inc.) reduces inflammation and increases pulmonary function by restoring glutathione in neutrophils (Tirouvanziam et al., 2006; Atkuri et al., 2007).

Other therapies

Information on the mechanism triggered by CFTR mutations and clinical phenotypes tailor the designs for therapeutic interventions in CF.

Gene therapy focuses on focus on delivering the DNA encoding the full-length wild type CFTR protein (Ramalho et al., 2002). Viral vectors, such as adenovirus (AV) and adeno-associated viruses (AAV) are used as vehicles for delivery. Viruses are modified to be replication deficient and contain an expression cassette with CFTR cDNA (Wagner and Gardner, 1997). AV has higher efficiency but is more immunogenic than AAV or non-viral vectors (Wagner and Gardner, 1997; Schwiebert, 2004). Non-viral vectors combining CFTR cDNA with

a suitable promoter and lipids (liposomes) has been proposed as safer delivery system (Wagner and Gardner, 1997). However, lipid-based vesicles possess a number of shortcomings, especially with regard to stability, bioreactivity and toxicity (Torchilin et al., 2003). In particular cationic liposomes are known to trigger specific signaling pathways, including the protein kinase C (Tanaka et al., 2008), stimulate Toll-like receptor 4 in dendritic cells (Ouali et al., 2007) and directly binds to membrane lipids resulting in modulation of membrane protein activities (Koynova et al., 2007; Kumar et al., 2003).

Further therapies focus on designing therapeutic agents to rectify the effects of two mutations, G551D and G1349D. Both mutations are involved in ATP-binding and channel gating dysfunctions. The G551D mutation results in a severe clinical phenotype characterized by abolished responses of the channel to ATP and ADP, whereas the G1349D mutation leads to a milder clinical phenotype (Bompadre et al., 2007). Vertex Pharmaceuticals developed a CFTR potentiator, VX-770. The drug increases the function of CFTR proteins by holding the defective channels in the open conformation. In phase 3 clinical trials testing VX-770 in patients carrying a copy of G551D, treated patients showed an improvement in forced lung expiratory volume compared to the control patients ("VX-770 – product description", n.d.).

The most common CF mutation is a deletion of phenylalanine at position 508 (ΔF508) of the CFTR gene. Overexpression of this mutant protein can lead to escape of a small amount of ΔF508-CFTR to the cell membrane (Cheng et al., 1995). Treatment of CF airway epithelia with VX-770 from patient with F508del and G551D mutation increases ASL volume (Van Goor et al., 2009), but improved CFTR trafficking and activity was shown only when administering VX-770 in combination with VX-809. VX-809, also developed by Vertex Pharmaceuticals, increases ΔF508-CFTR trafficking. Phase 2 clinical trials in progress aimed to evaluate VX-770 and VX-

809 combination therapy on patients homozygous for ΔF508 mutation (Pollack, 2011; "VX-770 and VX-809 combination drug release", 2011).

Another drug, Ataluren®, by PTC Therapeutics, is classified as a protein restoration therapy agent. Its presence promotes the synthesis of functional copies from mutated forms of CFTR that harbor nonsense mutations. A nonsense mutation leads to insertion of a stop mutation codon into the protein-coding region of mRNA; thereby the ribosomal translation is interrupted, causing protein truncation and a loss of function (Sermet-Gaudelus et al., 2010). Alturen is a small molecule compound that overrides the premature stop codons to allow for the completion of the desired protein (Wilschanski et al., 2011). The study in children with nonsense mutations showed that Ataluren is correcting CFTR function by increasing the apical CFTR protein expression in respiratory epithelium. The study enrolled 30 patients, with a nonsense mutation in at least 1 allele of the CFTR gene, a classical CF phenotype, and abnormal baseline nasal epithelial chloride transport. Patients were assessed in two 28-day cycles, 3 times per day with randomized order of receiving a lower dose (4 or 8 mg/kg) and a higher dose (10 or 20 mg/kg) in two cycles (Sermet-Gaudelus et al., 2010).

Another set of treatments designed to reduce the progression of lung disease by augmenting the normal mucocilliary clearance and facilitating expectoration include a variety of approaches. Some of the approaches include: active cycle of breathing techniques (ACBT), autogenic drainage (AD), conventional chest physiotherapy (CCPT), high frequency chest wall oscillation (HFCWO), and intrapulmonary percussive ventilation (IPV) (Prasad et al., 2000).

Alternative to existing therapies – Channel replacement therapy

The restoration of CFTR activity has been an ultimate goal through CFTR rescue and in particular gene therapy. The therapeutic approaches described above have helped only limited numbers of patients. None of the available therapeutic approaches addresses the underlying cause of the disease at the cellular or tissue level: to reduce anion conductance that sets the chemiosmotic driving force for both paracellular and transcellular fluid movement. Therefore, we have advocated another approach: peptide-based channel replacement therapy. Under this scenario a synthetic channel-forming peptide (CFP) is applied to the apical surface of CF airway tissues to promote anion secretion and surface hydration. Gene therapy, to date, has involved the delivery of a CFTR-encoding DNA segment encased in a viral capsid to the affected epithelial tissues. There are serious problems with the gene therapy delivery vectors, transformation efficiency and CFTR production and delivery. Also airway epithelial cells have limited half-lives and the airway would need to undergo gene therapy on a regular basis to maintain expression. The new approach described here is much simpler and places the therapeutic directly on the target membrane (**Figure 1-1**).

Figure 1-1 Channel replacement therapy.

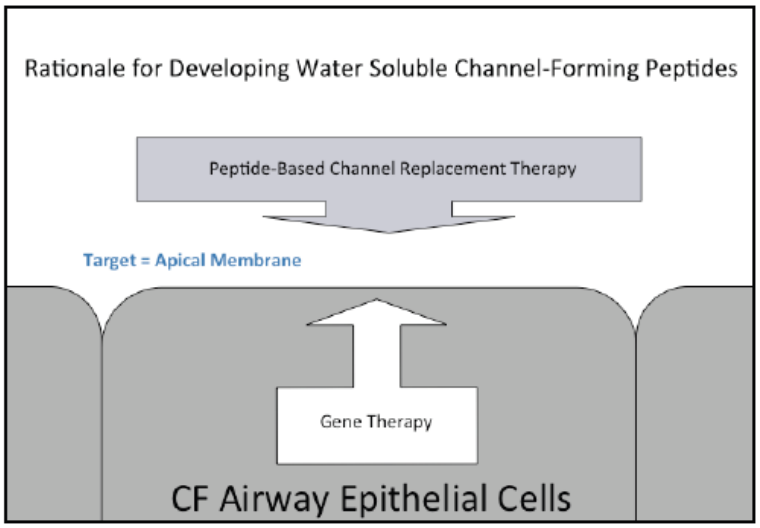

The channel-forming peptide can be instilled or delivered as an aerosol to the apical surface of CF airway cells. Upon binding to the surface it assembles to form an anion selective pathway. Fluid secretion in epithelia is regulated by apical chloride efflux through CFTR, followed by the

paracellular efflux of sodium. This facilitates the outward flow of water through osmosis. Water in the airway lumen hydrates the airway surface fluid/mucus layer and facilitates proper cilia-mediated airway clearance.

The validity of the peptide-based channel replacement therapy has so far been tested using nasal potential difference (PD) studies performed at the Gregory Fleming James Cystic Fibrosis Center at the University of Alabama, Birmingham, under the direction of Dr. Eric Sorscher. More than 40 ΔF508 homozygous transgenic mice were tested for effects of CK_4-M2GlyR or NK_4-M2GlyR peptides. The ΔF508 homozygous transgenic mouse nasal epithelia exhibit ion transport defects identical to those in CF human airways. Thus they are an excellent model to test for potential peptide therapeutic effects. A standardized protocol that uses transitions to amiloride, Cl^--free medium, and exposure to adrenergic stimuli was employed. Ion transport was assessed by repeated nasal PD measurements in both transgenic and wild type mice (Tomich et al., 2011). Nasal PD assay monitors changes in apical cell membrane potential. The potential difference is established using activators and inhibitors of both ion channels and transporters with and without the addition of the peptide. A perfusion protocol is used to either depolarize or hyperpolarize the membrane potential of the luminal cell side, to increase or decrease the potential difference (Kersting et al., 1998).

The presence of peptides resulted in sustained chloride conductance in CF mice for up to 6 h after a single application of peptide in solution, delivered in aerosol. However, for the optimal clinical results in treatments of CF patients, this type of treatment would likely have to be administered one or more times per day (Tomich et al., 2011).

Synthetic CFPs can be *de novo* sequences (Abel et al., 1997; Pajewski et al., 2006) or based on segments of native proteins. An advantage of these constructs is that they can be

studied in greater detail than their parent proteins, while their disadvantages include a difficult delivery from aqueous solution and lack of regulatory complexity-characteristics of native proteins. Early CFPs designs corresponding to putative transmembrane regions of natural proteins showed that CFPs possess detectable channel activities of CFPs in planar lipid bilayers (Tosteson et. al., 1989; Montal et al., 1990; Oiki et al., 1988) and human erythrocyte membranes (Kersh et al., 1989). Synthetic CFPs show either reduced or no ion selectivity, or poor ability to conduct ions (Tosteson et. al., 1989; Montal et al., 1990; Oiki et al., 1988). Experimental approaches to date have been limited. Our laboratory has developed synthetic membrane-active peptides that can be delivered efficiently, assemble into ion-conductive pores, trigger fluid secretion and elicit no detectable immune or inflammatory response. However, higher anion selectivity remains to be engineered into CFPs.

Glycine receptor and a design of CFPs

The glycine receptor (GlyR) is a ligand-gated anion channel (Le Novére and Changeux, 2001) and a member of the cys-loop super family of ligand-gated channels (Cascio, 2004). GlyR is a heteropentameric oligomer (Kersh et al., 1989; Cascio, 2004) with three α subunits and two β subunits (Ryan et al., 1994). Both, β and α subunits contribute to a ligand binding domain (Grudzinska et al., 2005). The water-filled pores are formed by the association of the second transmembrane segments (M2) contributed by each of the five subunits. *Xenopus* oocytes, expressing just the α-subunit, form homo-pentameric channels having functional characteristics typical of the native GlyR (Schmieden et al., 1989). This result suggests that homomeric α-M2 assemblies generate a functional anion-selective channel. Indeed, the native α-subunit M2 segment, PARVGLGITTVLTMTTQSSGSRA, forms chloride-selective channels in lipid bilayers and single cells, and facilitates ion transport across epithelial monolayers (Reddy et

al., 1993; Wallace et al., 1997). This provides the rationale for choosing GlyR as a lead structure for developing anion-selective CFPs in our laboratory. These sequences are amphipathic, containing distinct clusters of hydrophobic and hydrophilic residues. In aqueous solution, the hydrophobic patches associate and the hydrophilic ones remaining exposed to the solvent. This property generally leads to aggregation through a concentration-dependent process.

The model in **Figure 1-2** illustrates the formation of multiple, higher molecular weight assemblies which do not readily interact with membranes. Based on perfusion washout experiments (indicated by the double-ended arrows) we do know that much of the process is slowly reversible. Two possible routes are shown. One (left) has the peptide folding event occurring at the surface, followed by assembly as a prerequisite for insertion. The second (right) has the peptide inserting and folding as a single step followed by assembly. A preferred outcome, however, would be to have a peptide that remained predominantly monomeric in solution while retaining membrane binding and insertion activities. The actual sequences of insertion and assembly events leading to a functional channel are still unresolved.

Figure 1-2 Solution and membrane inserted states for channel-forming peptides.

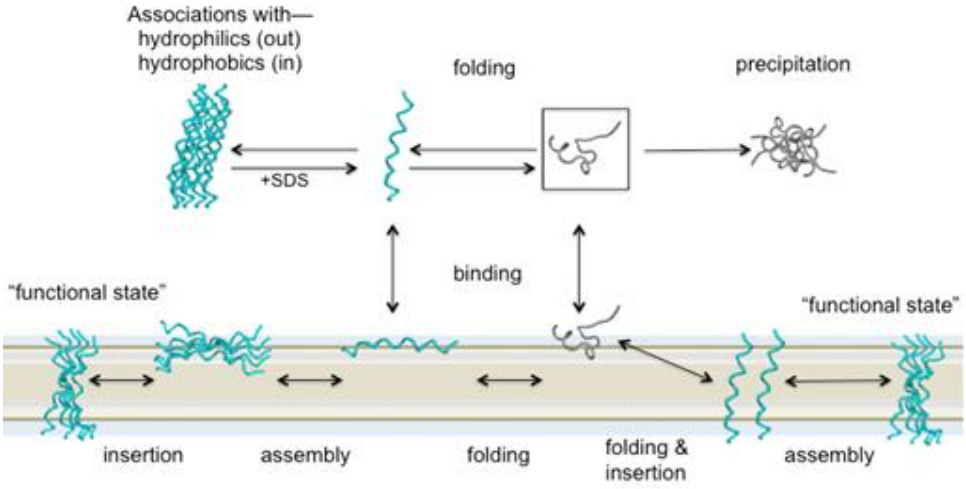

The early studies tethered pore-lining M2 segment variants to the template in order to

control the stoichiometry and evaluate the functional properties of the resultant pores (Montal et al., 1990; Reddy et al., 1993; Montal et al., 1993a; Montal et al., 1993b; Montal et al., 1994; Iwamoto et al., 1994). Comparing the measured ionic conductances of template-tethered peptide constructs to those of monomers revealed that all monomers inserted in the membrane with the same orientation and assembled into pentameric structures, based on similarities.

Preparing the large peptide templates, however, proved too labor intensive and too expensive to be practical from a therapeutic standpoint. Studies were thus focused on preparing a monomer capable of self-assembly into an ion-selective pore.

Peptides corresponding to the wild type M2 sequence conferred net transepithelial ion transport comparable to the parent GlyR channel pore (Reddy et al., 1993), but had poor efficiency with regard to membrane insertion and a tendency to form aggregates in aqueous solutions (Reddy et al., 1993; Wallace et al., 1997). To address these limitations, peptide sequences were modified by introducing multiple lysyl-residues at either terminus to improve the solubility of the peptide and ensure the uniformity of orientation in the membrane (Tomich et al., 1998). Lysines placed at the termini of transmembrane sequences position themselves in the aqueous phase near the lipid phosphate groups (de Planque et al., 1999) while their side chains direct electrostatic interactions with ions (Faraldo-Gómez and Roux, 2004); the latter could aid in anion selectivity. A tetralysyl tail on these peptides proved optimal, giving enhanced solubility without any apparent alteration of channel properties (Tomich et al., 1998) as assayed for induction of short circuit current using Ussing chambers and MDCK monolayers. Subsequently, the sequence was truncated by five residues at the C-terminus and the resulting C-terminal serine was replaced by tryptophan to reduce or eliminate solution aggregation (Broughman et al., 2001,

Broughman et al., 2002; Cook et al., 2004; Shank et al., 2006). Resultant peptide relative to the wild-type M2GlyR sequence showed better efficiency of insertion into epithelial cell membranes (Broughman et al., 2001), a decreased propensity for aggregation in aqueous solution (Tomich et al., 1998; Broughman et al., 2002), and increased transepithelial net ion transport at lower peptide concentrations (Broughman et al., 2002). Tryptophan and lysine both play important roles in peptide orientation and membrane insertion (de Planque et al., 1999). Tryptophan in proteins with transmembrane segments is known for its specific affinity for sites near the lipid carbonyl region (de Planque et al., 1999). The tryptophan-containing sequence exhibited a decrease in the concentration required for net transepithelial ion conductance and more readily adopt a helical secondary structure (Cook et al., 2004, Shank et al., 2006; Herrera et al., 2010). Furthermore, tryptophan and arginine reportedly anchor transmembrane helices (White and Heijne, 2005). The threonine 19 (T19) in our peptides was replaced with arginine (T19R) to introduce a second anchor (Hererra et al., 2010; Shank et al., 2006). The resulting peptide, NK_4-M2GlyR p22-T19R S22W, showed increased net transepithelial ion conductance compared to the non-substituted wild type peptide (NK_4-M2GlyR) in Ussing chamber experiments employing MDCK cells (Figure 1-3) (Shank et al., 2006). NK_4-M2GlyR p22-T19R S22W also lacked antigenic activity in mice at proposed clinical dosages (van Ginkel et al., 2008). Altogether, analysis indicated that the best candidate from derivatives of α-M2 GlyR so far is NK_4-M2GlyR p22-T19R S22W.

Figure 1-3 Concentration-dependence of I_{SC} induced by NK_4-M2GlyR-p22-derived peptides with W and R amino acid substitutions on MDCK epithelial monolayers.

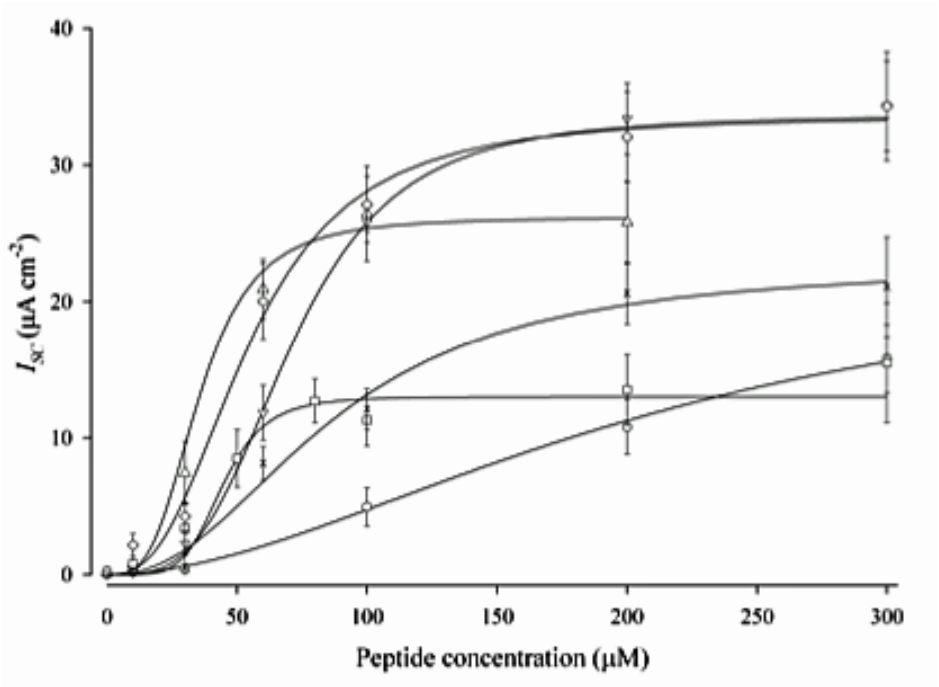

Symbols represent the mean and standard error of 6 or greater observations for each concentration tested. Solid lines represent the best fit of a modified Hill equation to each data set. Points comprising the curves for each NK_4-M2GlyR derived peptide concentration dependence are indicated as follow: NK_4-M2GlyRp22 (○), NK_4-M2GlyR-p22 S22W (□), NK_4-M2GlyR-p22 Q21R, S22W (Δ), NK_4-M2GlyR-p22 T20R, S22W (×), NK_4-M2GlyR-p22 T19R, S22W (∇) and NK_4-M2GlyR-p22 Q21W, S22R (◊) (Shank et al., 2006).

Structural and biophysical properties of the synthetic channel-forming peptide NK_4-M2GlyR p22-T19R, S22W

The NK_4-M2GlyR p27, one of the parent peptides of NK_4-M2GlyR p22-T19R, S22W, increases chloride permeability in epithelial cells through a distinct conduction pathway in cell membranes. Lines tested include: Madin-Darby canine kidney (MDCK) cells, human colonic epithelial cell line (T84) and CF airway human epithelial cells (IB3-1) (Mitchell et al., 2000). NK_4-M2GlyR p27 had several undesirable properties with respect to potential for therapeutic use. This peptide derivative demonstrated poor aqueous solubility and inconsistency in membrane insertion. Subsequent modifications of the sequence to address these problems led to a design of NK_4-M2GlyR p22-T19R, S22W peptide with many desirable properties that relate to improved aqueous solubility, decreased solution assemblies, undetectable immune and inflammatory responses and increased ion permeation rates.

The parent NK_4-M2GlyR p27 sequence had permeation selectivities greater than 25:1 for chloride over potassium ions (Tomich et al., 1998). Unfortunately, in the process of designing the NK_4-M2GlyR p22-T19R, S22W, the chosen sequence modifications affected the permselectivity ratio of NK_4-M2GlyR p22-T19R, S22W-assembled pores, reducing it to 1.4:1 for chloride over potassium ions (Shank et al., 2006). Before planning additional substitutions to remedy this shortcoming, we determined the structure of this peptide in detail (Bukovnik et al., 2011).

First, the monomeric structure of NK_4-M2GlyR p22-T19R, S22W was analyzed by circular dichroism (CD) and nuclear magnetic resonance (NMR). These analyses were conducted by Dr. G.A. Cook. (Bukovnik et al., 2011). Monomeric NK_4-M2GlyR p22-T19R, S22W adopts a linear helical structure in hydrophobic environments. The circular dichroism spectra indicated

that the propensity to adopt a helical conformation in a hydrophobic environment was not affected by T19R substitution. Detailed NMR analyses in both trifluoroethanol (TFE) and sodium dodecyl sulfate (SDS) micelles yielded structure of the monomer encapsulated within a C_{12} acyl chain anionic detergent micelle. All spectra were indistinguishable from the previously analyzed peptide, NK_4-M2GlyR p22-S22W (Herrera et al., 2010). These results showed that residues 10-20 of NK_4-M2GlyR p22-T19R, S22W had resonances consistent with a helical conformation, while the N-terminus was largely disordered. NK_4-M2GlyR p22-S22W adopts a conformation of a more curved structure compared to the more linear conformation of NK_4-M2GlyR p22-T19R, S22W. These sequences were subsequently analyzed as five-helix assemblies using molecular simulations. Results served as a starting point for further, more detailed molecular modeling studies.

Molecular modeling studies

All molecular modeling studies were a work of Dr. Gao in Professor Jianhan Chen's laboratory. The stability of NK_4-M2GlyR p22-T19R, S22W channel structure in equilibrated POPC bilayers, the handedness of peptide helical assembly, properties of helical packing, the identities of pore lining residues and pore profile simulations were carried out (Bukovnik et al., 2011).

Stability of channel structures in Palmitoyl-oleoyl-phosphatidylcholine (POPC) bilayers

Molecular dynamics simulations of the assembled channel structures in fully solvated POPC lipid bilayers predicted the stability of peptide's helix assembly. Three models of the putative pentameric pore of NK_4-M2GlyR p22-T19R, S22W were constructed with different handedness of helix packing: left-handed, straight and right-handed. Similar to previous work with NK_4-M2GlyR p22-S22W (Herrera et al., 2010), the tilt angle of the initial left-handed and

right-handed models was set at 15°. Interestingly, NK_4-M2GlyR p22-T19R, S22W channels appeared to show substantial vertical fluctuation along the membrane normal similar to NK_4-M2GlyR p22 channels (Herrera et al., 2010). This suggests that T19R mutation could attenuate the membrane anchoring effects seen in NK_4-M2GlyR p22-S22W. Importantly, the secondary structures and overall features of the pore assemblies (such as helix-helix packing interfaces and pore-lining residues analyzed below) were well conserved. The overall helicity stabilized at ~70%, similar to the values previously reported for NK_4-M2GlyR p22 and NK_4-M2GlyR p22-S22W pores (Herrera et al., 2010). General conservation of the secondary and tertiary fold across all three sequences (NK_4-M2GlyR p22, NK_4-M2GlyR p22-S22W, and NK_4-M2GlyR p22-T19R, S22W) is not surprising, as all these peptides are capable of inserting into the membrane and forming ion conducting channels, albeit with different levels of ion conductance. Results of the simulation suggest that the peptide forms stable and ordered pores in a model bilayer.

Handedness of helical assembly

Although all available crystal structures of cys-loop ligand-gated ion channels contain left-handed packing of pore-forming transmembrane helices (Moneé et al., 1998; Sine and Engel, 2006; Hilf and Dutzler, 2009), handedness of the helical assembly of the putative pores formed by M2GlyR-derived peptides remained unresolved. Previous simulations of limited length (20 ns) of NK_4-M2GlyR p22 and NK_4-M2GlyR p22-S22W channels failed to identify any apparent difference between right- and left-handed assemblies (Herrera et al., 2010). A key objective of the straight, right- and left-handed simulations was to resolve this issue. As mentioned earlier, three models of the putative pentameric pore of NK_4-M2GlyR p22-T19R, S22W were constructed. The straight assembly gradually drifted towards left-handedness over the course of 100ns simulation. The same was observed for the right-handed assembly that switched towards

left-handedness over a 200ns simulation. These simulations thus predicted that putative channels formed by M2GlyR-derived peptides assume left-handed pore assembly.

Helix packing, membrane-exposed and pore-lining residues

Details of helix packing and residue distribution of the pore were analyzed. Based on the previous work a left-handed assembly was employed. Results demonstrated that the pore is lined principally with residues A6, R7, L10, T13, T14, T17, T20 and Q21. The predicted pore-lining interface is consistent with the one derived from consideration of amphipathicity. The last N- and C-terminal residues, K1-4 and W22, were not considered as pore-lining, but were in contact with (bulk) water molecules.

The predicted pore-lining interface is broader due to substantial dynamic fluctuations of the pore. Participation of residues in helix-helix packing was characterized by calculating the average burial areas of side-chains. Clearly, most residues within the structured region contribute to helix-helix interactions, except G9, G11, I12, V15 and R19. These residues either lack side chains (G9 and G11) or are fully lipid exposed (I12, V15, L16 and R19). L10 and Q21 appear to be particularly important for stabilization of the pore assembly with the largest surface areas buried in the POPC bilayers used in the model membrane simulation.

Pore profiles

The profiles were derived from simulations of left-handed and straight assemblies. These two assemblies are similar, due to the observation that the straight assembly evolves completely to a left-handed one. All three pores, straight, left- and right-handed, had similar radii at the narrowest region (near Thr17). Curiously, the p22-T19R, S22W pore appears to be slightly narrower than the p22 or p22-S22W pore (Herrera et al., 2010). It is not clear that this is an artifact of much longer, 200 ns simulations used in these simulations compared to previous 20ns

simulations. Further free energy calculations using similarly refined structural models, together with new channel measurements are required in order to clarify whether the molecular modeling can recapitulate the expected difference in channel activity.

Cysteine scanning

A set of experiments included in Bukovnik et al. (2011) aimed to identify the pore-lining residues of assembled NK_4-M2GlyR p22-T19R, S22W. The solvent accessible residues in the assembled pore were mapped using cysteine-scanning analysis. Seventeen peptides incorporating cysteine substitutions along the length of NK_4-M2GlyR p22-T19R, S22W were tested for their ability to promote ion secretion across the MDCK monolayers. The N-terminal lysines at positions 1 and 2, the arginines at positions 7 and 19 and tryptophan at the C-terminus were not substituted due to their involvement in insertion orientation and membrane anchoring functions. Measurements of peptide-induced short circuit current ($\mu A/cm^2$) (I_{SC}) showed that the replacements at the more terminal sites, K3, K4, P5, A6 or T17, M18, T20 and Q21 yielded currents higher than those observed for the parent NK_4-M2GlyR p22-T19R, S22W. Replacements in the central membrane-embedded region generally led to lower flux values relative to NK_4-M2GlyR p22-T19R, S22W except for the pore contributing L10, which yielded results nearly identical to the parent sequence. The lowest activities were observed for the cysteine substitutions at positions G9, G11, I12, V15 and L16. These residues most likely face lipid and have either no side chain or extended hydrophobic side chains. Introduction of a short hydrophilic side chain in these positions could affect membrane insertion or helix-helix packing. When the threonine was replaced by cysteine at position 17 the replacement I_{SC} incremented, while the T13C replacement decreased I_{SC} compared to the NK_4-M2GlyR p22-T19R, S22W. This is an indication that T13 might not be a part of pore-lining surface, but could play a role in

structural properties of assembled pore. This is in agreement with calculations based on refined NMR monomer structure showing the potential involvement of T13 in structural modifications of the pore. The narrowing of the pore observed in NK_4-M2GlyR p22-S22W, which was absent in NK_4-M2GlyR p22-T19R, S22W indicates that the position of the ring of OH groups contributed by Thr13 in NK_4-M2GlyR p22-T19R, S22W have likely become repositioned thereby widening the pore and explaining the increased conductance observed. These results were followed by the assay of channel blockade using thiol binding mercurial salts (Bukovnik et al., 2011). Channel activity of the cysteine-substituted peptides was examined in artificial bilayers consisting of 70:30 POPC: Palmitoyl-oleoyl phosphatidylserine (POPS) (Tomich et al., 2011). Following induction of current, increasing concentrations of mercury chloride ($HgCl_2$) were added to determine pore-lining residues. Water-accessible residues to $HgCl_2$ and subsequent blocked channel activities indicate pore-lining residue positions: K3, A6, L10, T13, T17 and T20. Importantly, the identities of these pore-lining residues are fully consistent with those predicted by molecular simulations (Bukovnik et al., 2011). This supported the proposed structure of the pentameric channel formed by NK_4-M2GlyR p22-T19R, S22W. The model was realistic, and generated a structural basis for understanding channel activity, as well as providing a template for designing new sequences with improved functions.

Peptide insertion into artificial lipid membranes

The ability and efficiency of insertion of NK_4-M2GlyR p22-T19R, S22W into liposomes composed of different compositions and ratios of POPC, POPS, Palmitoyl-oleoyl-glycero-3-phosphoethanolamine (POPE) and Palmitoyl-oleoyl-phosphatidylglycerol (POPG) were examined (Bukovnik et al., 2011). The choice of lipid compositions was based on observations that the ability of synthetic peptides to interact with membranes does not depends both on peptide sequence (de Planque et al., 1999) and lipid composition of targeted membranes (de Planque et al., 1999; Smart et al., 1996). The lipids commonly present in bacterial and mammalian cell membranes were employed, as these surfaces will be encountered by CFPs when employed.

We first tested the ability and efficiency of NK_4-M2GlyR p22-T19R, S22W insertion into liposomes composed of POPC: POPS (70:30) and POPC: POPE (60:40). Optimal insertion of the peptide was obtained in phospholipid mixtures containing some anionic phospholipids (POPC: POPS; 70:30), possibly due to more favorable attractive electrostatic interactions. This agrees with previously reported information that the orientation of membrane proteins can be guided by contact between negatively charged phospholipids and positively charged amino acid residues (van Klompenburg et al., 1997). When the peptide was mixed with the vesicles composed of 100% POPC, which is considered a basic phospholipid, the peptide/liposome spectra did not give evidence of partition into the large unilamellar vesicles. One possible explanation is that the peptide may be lying on the surface of the liposome due to electrostatic interaction between the glycerol head groups on the phospholipids and the oligo lysine N-terminus on the peptide. Further, when the percentages of POPC: POPS and POPC: POPE were either at 10% or 20% of the anionic phospholipid, peptide insertion was also inhibited. Similarly

50% POPS or POPE also did not show an increase in the inserted tryptophan's blue shift, indicating unfavorable conditions for peptide insertion.

Aims and Goals

Designing synthetic channel forming peptides based on the transmembrane segments of natural ion channel proteins is a challenging task. When assembling into a pore, NK_4-M2GlyR p22-T19R, S22W peptides form a pentameric construct resembling the ion conductive ensemble of its parent protein. Such a construct lacks a complex set of regulated control of assembly and function owned by its natural parent with its full protein structure. However, lacking regulatory characteristics can be seen as limitations or a unique advantage. Various modifications of original putative protein sequences can lead to specific structure/function modified synthetic channels, carefully designed to meet the needs for targeted therapeutic use.

The study presented here addresses the last limitation of this channel-forming peptide, the anion selectivity. The detailed, modeled structure of NK_4-M2GlyR p22-T19R, S22W served as a starting point for devising strategies to redesign the monomer to incorporate selectivity. Substitutions were identified to modified hydrogen bonding and the electrostatic properties of the NK_4-M2GlyR p22-T19R, S22W-formed pore. One class of these replacements introduced 2, 3-diaminopropionic acid (Dap), a cationic non-encoded amino acid, at different positions along the pore. It was hypothesized that anion conductance of Dap-substituted NK_4-M2GlyR p22-T19R, S22W peptides would be improved with the addition of this small positively charged residue. The threonine residues at position 13, 17 and 20 were replaced individually and in combination with Dap (**Table 2-1)**. To gain further information on physiological activities of NK_4-M2GlyR p22-T19R, S22W and its Dap-substituted derivatives, electrophysiological studies were

conducted with both the all L- and all D-amino acids, as well as truncated parts of L-NK_4-M2GlyR p22-T19R, S22W-peptides (**Table 3-1**).

Significance of work

Peptide-based therapies for treatments of channelopathies create a novel treatment modality with an unbounded potential. The significance of this thesis is in preparation of sequences with rational alterations of residues that dictate the structure and ion-selective properties of synthetic pores. As a substitute for pore-lining residues, a non-natural amino acid Dap was chosen. Our study furthers the understanding of anion channels and carries a novel approach in designs of synthetic pores.

Chapter 2 - Use of 2, 3-diaminopropionic acid (Dap) in design of synthetic anion selective pores

Abstract

Earlier studies incorporating L-2, 3-Diaminopropionic acid in NK_4-M2GlyR T19R, S22W showed peptide-induced increases in short circuit current. It was hypothesized that introducing cationic side chains of Dap in place of the pore-lining threonine residues in NK_4-M2GlyR T19R, S22W (p22- T19R, S22W) would modulate anion selectivity through alterations in pore electrostatics and increased hydrogen bonding potential. The p-22 T19R, S22W was used as the scaffold for introducing up to three Dap residues at pore-lining positions 13, 17 and/or 20. The peptide-induced ion *transport measured* as I_{SC} using Madin-Darby canine kidney (MDCK) epithelial cell monolayers was assessed, as well as the permselectivity of the Dap-assembled pore examined using two-microelectrode voltage clamp (TEVC) recordings of *Xenopus* oocytes. All Dap-substituted peptides induced transepithelial current across polarized MDCK cells. Molecular dynamic simulations modeled the effect of introducing cationic residues on the pore's diameter and anion selectivity. Experimental work substantiated aspects of the virtual predictions. Dap-substituted peptides increased net transepithelial ion transport in MDCK cells producing larger effects. TEVC measurements using *Xenopus* oocytes provided similar evidence, with a difference that Dap-substituted peptide-induced ion currents were not sequence-dependent. Preliminary computer modeling of the Potential of Mean Force (PMF) predicted the flow of different ions from one side of the channel to the other and showed improved anion conductance of assemblies with Dap sequences. However, this prediction was not in agreement with experimental studies where the selectivity, varying slightly above or below unity, indicated that p-22 T19R, S22W and its Dap-substituted sequences formed non-selective pores.

Preliminary flux assays measuring ^{86}Rb influx across peptide-assembled pores in liposome membranes (POPE: POPG; 3:1) tested whether Dap-substituted peptides are able to form functional synthetic channels. Results indicated that Dap-substituted peptides did form *de novo* pores, however, the results from several replicate experiments were inconsistent. It is possible that similar as M2GlyR derivative peptides, the p22-T19R, S22W peptide-assembled pores require a specific membrane composition for successful insertion and channel activity.

Introduction

Ion channels are transmembrane protein complexes that control the movement of specific ions across barrier membrane. They are conceptualized generally as pores regulated by specific gating mechanism and dependent on the architecture of the pore, such as: pore size, pore length and dielectric constant (Futaki 1998; Stoikov et al., 2003). The ion current is driven by the electrochemical gradient and can be described by Ohm's law which states: $I = G (V)$. Thus the current (I) is the product of the conductance (G) and when I is plotted as a function of voltage (V), G can be derived from the slope of the resultant I vs. V curve. This means that an ion channel, when opened and when the permeant ions are present, carries the ion current at a certain membrane potential (Hille, 2001).

The permeability of the ion flow is the ease with which ions traverse the plasma membrane and depends on the number of ion selective channels open in the membrane (Hille, 2001). Ion conductance and ion selectivity are the two basic parameters of ion permeability. Ion selectivity is an ability of ion channel to favor the flow of one ion over another and is determined by the permselectivity ratio of the two ions, P_X/P_Y. Experimentally, this ratio is obtained by the

reversal potential of an ionic solution containing these two ions of interest (Pusch, 2008). Reversal potential (V_{rev}) is the transmembrane voltage at which diffusive and electrical forces counterbalance and result in no net ion flow across the membrane (Hille, 2001). The Nernst equation expresses this relationship and gives the equilibrium potential for an ion based on its charge (i.e., its valence) and the concentration gradient of this ion across the membrane. The negative or positive value of the calculated potential depends on the valence of the ion.

If one assumes the system with only one ion type and only one type of ion channel present mediating the transmembrane ion movements, then the Nernst potential determines the resulting membrane potential (V_m).

Equation 1: Nernst equation.

$$E_x = RT/(z)F \ln [X]_{ext}/ [X]_{int}$$

Legend to equation 1: E_x **–** equilibrium potential; R – gas constant (8.3145 J mol^{-1} K^{-1}; T – absolute temperature in K (273. 15 + T (25° C) estimated for room temperature)); F – Faraday's constant (9.6485 x 10^4 Coulombs x mol^{-1}); (z) – the valence number of the ion (for anions the sign of the reversal potential has to be inverted); X = type of ions (K^+, Na^+, Cl^-, Na^+, Ca^{2+}, Mag^{2+}, etc.); $[X]_{ext}$ = concentration of given ion in external solution; $[X]_{int}$ = concentration of given ion in internal solution.

But biological membranes have multi-ion transport systems, with ion channels and transporters allowing the movement of different types of ions simultaneously. In this case the reversal potential is the membrane potential at which the summed currents of the multiple ions equal zero. It is also the potential at which membrane current reverses direction and is calculated using the Goldman-Hodgkin-Katz equation (GHK equation).

Equation 2: Goldman-Hodgkin-Katz equation (GHK equation).

$$E_{rev} = \frac{RT}{F} \ln \frac{PK^+_i[K^+]_{out} + PNa^+_i [Na+]_{out} + PCl^-_i [Cl^-]_{in}}{PK^+_i[K^+]_{out} + PNa^+_i [Na^+]_{in} + PCl^-_i [Cl^-]_{out}}$$

Legend to equation 2: $[K^+]_{out}$ = Extracellular concentration of K^+ and similar for Na^+ and Cl^- and $[K^+]_{in}$ = Intracellular concentration of K^+ and similar for Na^+ and Cl^-. The intracellular concentrations of ions (40 mM Cl^-, 10 mM Na^+, 110 mM K^+) were taken from a study of Costa et al. (1989).

Experimental determination of ion permeability is based on ion substitution experiments in which the concentration of ion under study is decreased or replaced by another ion of compound assumed to be impermeant (Costa et al., 1989). By varying the ionic composition of external solutions the Nernst potential for each ion type varies and can be used to determine the permeability of that ion type. If one pathway of a single type of ions is favored over another, the ratio would indicate an n-fold higher permeability of that type of ions over another. Permselectivity (P) for Cl^- *vs.* Na^+ and Cl^- *vs.* K^+ can be estimated using **equation 3**, which is derived from the Goldman-Hodgkin-Katz equation.

Equation 3: The permeability ratio.

$$\frac{P(\mathbf{A})}{P(\mathbf{B})} = \frac{[\mathbf{A}]_2 - [\mathbf{A}]_1 \times e^{F/RT\,(\Delta V_{rev})}}{[\mathbf{B}]_2 \times e^{F/RT\,(\Delta V_{rev})} - [\mathbf{B}]_1}$$

Legend to equation 3: A, **B** = K^+, Na^+ or Cl^-; subscript 1 indicates the ion activity in ND96 and subscript 2 indicates its activity in ionic bath solutions. The ΔV_{rev} was determined by comparison of the V_{rev} measured for each external solution in the absence and presence of the peptide. Considering the composition of each ionic solution, calculations also presume that

concentrations of those given ions in ionic solutions which were reduced to 1mM were small enough to contribute minimally to the overall permeation and changes in V_{rev}. *F*, *e*, *R*, and *T* have their conventional definitions. The intracellular concentrations of ions (40 mM Cl^-, 10 mM Na^+, 110 mM K^+) used to estimate the ratios were taken from a study of Costa et al. (1989).

Synthetic ion channels

Ions interact with water molecules that polarize their electron clouds in the intense local field around each ion. The energy required to stabilize water around ions is called the hydration energy. Ions permeate based on their attraction to pore residues relative to their attraction to water; therefore the hydration energy of the ion governs its permeation. Ions with smaller radii attract higher number of water molecules and have higher hydration energies (Hille, 2001). The part of the ion channel actively involved in ion permeation and selectivity is known as selectivity filter. The selectivity filter discriminates ions based on size, and also sets constraints on how well the efficiency of its charged residues will compensate for the hydration energy of the ions (Futaki, 1998; Stoikov et al., 2003; Fyles, 2007). Mutations altering the structural properties of the selectivity filter provide evidence of the great importance of its diameter as well as its electrostatic properties for ion selectivity. Substitutions of charged amino acids with similarly charged amino acids but shorter side chains yields larger pore diameter and modify the electrostatic interactions between the permeating ions and side chains of the new pore-lining residues (Keramidas et al., 2000, Keramidas et al., 2002). Evidence exists that some mutations in the selectivity filer can also convert the ion channel from being anion to cation selective (Keramidas et al., 2000). A general rule is that any carbonyl oxygens (usually amide bond

carbonyls) in the selectivity filter act as donors to cations and hydroxyl groups act as hydrogen bond donors in interaction with ions (Fyles, 2007).

To study the importance of selectivity filters, the central water-filled and ion-selective pores of many native channels, including transmembrane segments of Glycine receptor and nicotine acetylcholine receptor, have been synthesized and reconstituted to form functional synthetic channels in a variety of natural and artificial membrane systems (Montal et al., 1990; Montal et al., 1993a, 1993b, 1994; Reddy et al., 1993; Iwamoto et al., 1994). In native proteins, the structural basis for selectivity relies upon the concerted activity of several domains of a protein bundle (Adcock et al., 1998), therefore native channels exhibit relatively high ion conductance and anion/cation selectivity simultaneously. Synthetic ion channels lack the structural and functional complexity of their native parent proteins. Evidence exist showing that synthetic peptides both assemble into pores with ion conductive or ion selective properties, but in most cases the resultant pores lack the combination of conductance and selectivity (Tosteson et al., 1989; Montal et al., 1990; Oiki et al., 1988).

Previous studies focusing on the design of the anion selective synthetic channels for application in replacement therapies in treatments of CF yielded the peptide NK_4-M2GlyR p22-T19R, S22W (p22-T19R, S22W). The p22-T19R, S22W has high water solubility as a monomer, no detectable antigenicity at clinically relevant dosages, binds and partitions into the epithelial apical membranes, and forms ion-conductive pores. However, this peptide does not show the desired physiologically relevant anion selectivity. In the present study, p22-T19R, S22W served as the scaffold for structural modifications to address this limitation.

Based on previous findings, threonine residues at positions T13, T17 and T20 line the pore of assembled p22-T19R, S22W (Cook et al., 2004; Bukovnik et al., 2011). Recently,

numerous single substitutions of T13 or T17 were tested. T13 was chosen because it resides at the widest part of the pore whereas T17 is located at the narrowest. A substitute for T13 and T17 with the highest potential for increasing the ion conductance of assembled pores was sought. Substitutes of various coding and non-encoding amino acids were selected based on their hydrogen bonding potential with permeating ions and/or potential for modifications of pore electrostatics. Ussing chambers mounted with MDCK epithelial cell monolayers were used and the ability of a given peptide to induce the transepithelial ion transport across these cells was assessed. Relative to other substituted sequences and non-substituted control sequence, Dap substitutions of either T13 or T17 yielded the highest increase in net transepithelial transport across polarized MDCK cells (Frazier, 2006). Dap (shown in **Figure 2-1**) is a non-natural non-genetically encoded amino acid. Dap possesses a positively charged methyl amino side-chain that retains the free primary amine similar to that found in lysine but without the C_4 hydrophobic alkyl linker. In the pentameric assembly, five Dap residues would form a ring of positive charge predicted to provide a strongly electro-positive environment that would favor the passage of negatively charged ions. However, one possible undesirable consequence is the proximity of the five lysines within the assembly, which could lead to a widening of the pore due to electrostatic repulsion between the charged resides. Such increases in pore diameter have been previously observed with charged residues carrying shortened side chains (Keramidas et al., 2000, Keramidas et al., 2002).

Figure 2-1

Molecular structure of Dap.

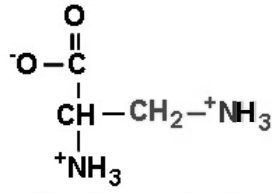

Preliminary molecular dynamics modeling tested this hypothesis and showed that the Dap side chains retain the orientation of the threonines they replaced (*i.e.* facing the interior of assembled pore). Interestingly, introduction of Dap was predicted to widen the pore radius by

several angstroms and increase the selectivity of chloride over sodium. These computational predictions and previous experimentally acquired data sets of transepithelial transport rates in MDCK cells induced by individually replaced T13Dap and T17Dap p22-T19R, S22W peptides provided the impetus for our present and more detailed investigation of the role of Dap in anion selectivity in channel-forming peptides.

Single, double and triple p22-T19R, S22W Dap-substituted p22-T19R, S22W sequences were synthesized and tested ion permeating and ion selective properties by two electrophysiological methods using MDCK cells and *Xenopus* oocytes, respectively. MDCK cells were chosen as representative of the type of epithelial cells that can be affected in CF patients. While the *Xenopus* oocytes were used because of their large cell size, 0.5 to 1.0 mm in diameter, easy manipulation and direct measurements of ion currents through their membrane using whole-cell two-electrode voltage clamp (TEVC) technique (Zűhlke et al., 1995, Cens and Charnet, 2007).

Materials and methods

Peptide synthesis

Peptides were synthesized using solid-phase peptide synthesis by an Applied Biosystems model 431A peptide synthesizer (Foster City, CA) with 9-fluorenylmethoxycarbonyl (F-moc) chemistry (Carpino and Han, 1972; Fields and Noble, 1990; Tomich et al., 1998). CLEAR amide resin, (0.3 mmol/g) (Peptides International, Louisville, KY) and N^{α}-F-moc amino acids (Anaspec Inc., San Jose, CA) were used. The amino acid sequences are shown in **Table 2-1**. Purity of 85 to 90% was obtained by employing an optimized peptide synthesis protocol. Amino acids were recoupled one or two additional times depending on the position in peptide sequence, at 0.5 mmol scale. Residues coupled three times were: Dap, L16, V15, T14, I12, G11, L10, G9, V8, K4, K3, K2 and K1. The following protected amino acids were used: Arg (Pbf), Lys (*t*-Boc), Trp (*t*-Boc), Dap (*t*-Boc), Gln (Trt), Thr (tBu). Fmoc deprotection was carried out with piperidine (99%) and the coupling reagent was a mixture of 0.225 M O-Benzotriazole-N, N, N', N' -tetramethyl-uronium-hexafluoro-phosphate (HBTU) and 0.225 M Hydroxybenzo-triazole (HOBt) in dimethylformamide (DMF). Capping reagent was prepared by mixing 19 mL acetic anhydride, 9 mL N, N-Diisopropylethylamine (DIEA) and 6 mL of a 1 molar solution of HOBt in N-Methyl-2-pyrrolidone (NMP). NMP was added to a final volume of 400 mL. Piperidine, DMF, NMP and DIEA were from American Bioanalytical, Inc. (Natick, MA) and HBTU and HOBt from Anaspec Inc. (San Jose, CA).

Cleavage/deprotection and determination of purity and molecular masses

After the synthesis, the resin was rinsed with few mL of 100% dichloromethane (DCM), dried with vacuum, then suspended in 10 mL of 95% trifluoroacetic acid (TFA) in water solution and allowed to react for 90 minutes. After the cleavage reaction, the peptide was precipitated with 30 mL diethyl ether and washed 5 times with the ether. The peptide was re-dissolved in water containing 15% acetonitrile and then extracted with the ether, 5 additional times. A sample of 10 μL of extracted solution was taken for chemical analysis. The final solution was flash frozen and then dried under vacuum.

The molecular masses, shown in **Table 2-1** and purity of dried peptides were characterized using mass spectroscopy and HPLC respectively. For HLPC analyses, peptide was dissolved in water containing 5% acetonitrile at 5 mg/mL concentration and analyzed on a System Gold HPLC (Beckman Instruments, Fullerton, CA) with Phenomenex (Torrance, CA) reversed-phase C-18 column. A water/acetonitrile gradient was used with solvent A consisting of water containing 0.1 % TFA and solvent B consisting of 90% acetonitrile and 0.1% TFA. Peptides were eluted from the column by a 20-minute linear gradient from 5% to 95% solvent B at a 1.0 mL/min flow rate. After 20-min, the solvent flow was held at 95% of solvent B for 10 min, followed by a return to 5% solvent B in 5 min and then held at 5% solvent B for 6 min. Crude samples were analyzed using 50 μL injections. Peptide elution from the column was monitored at 265 nm (Ivanov et al., 2007). For determination of molecular masses, matrix-assisted-laser desorption time-of-flight mass spectroscopy (MALDI-TOF/TOF) using a Bruker Ultraflex II mass spectrometer was employed.

Table 2-1: Sequences and molecular masses of NK_4-M2GlyR p22-T19R, S22W (p22-T19R, S22W) and Dap substituted peptides.

	Name	Sequence	Molecular weight (Da)
1	NK_4-M2GlyR p22-T19R, S22W (p22-T19R, S22W)	KKKKPARVGLGITTVLTMRTQW	2512.1185
2	p22-T19R, S22W, **T17Dap**	KKKKPARVGLGITTVL**Dap**MRTQW	2497.1067
3	p22-T19R, S22W, **T13Dap**	KKKKPARVGLGI**Dap**TVLTMRTQW	2497.1067
4	p22-T19R, S22W, **T20Dap**	KKKKPARVGLGITTVLTMR**Dap**QW	2497.1067
5	p22-T19R, S22W, **T13Dap, T17Dap**	KKKKPARVGLGI**Dap**TVL**Dap**MRTQW	2482.0949
6	p22-T19R, S22W, **T17 Dap, T20Dap**	KKKKPARVGLGITTVL**Dap**MR**Dap**QW	2482.0949
7	p22-T19R, S22W, **T13Dap, T20Dap**	KKKKPARVGLGI**Dap**TVLTMR**Dap**QW	2482.0949
8	p22-T19R, S22W, **T13Dap, T17Dap, T20Dap**	KKKKPARVGLGI**Dap**TVL**Dap**MR**Dap**QW	2467.0831

Circular dichroism (CD)

Circular dichroism was used to examine the secondary structure of peptides in 40% TFE in water. Spectra were recorded on Jasco J-815 spectropolarimeter (Jasco, Tokyo, Japan) with a Neslab RTE-IIIM circulator set at 25°C using a 1.0 mm path length quartz cuvette. The spectra are an average of five scans and were recorded from 260 to 190 nm using a 1.0 nm spectral bandwidth, 0.2 nm step resolution, 20 nm/min scan speed, and 2 second response time. The data were analyzed with software provided by the manufacturer. Fresh peptide stock solutions were prepared at a concentration of 1 mM in water. In order to calculate the molar ellipticities, peptide concentrations calculated using Beer's Law, $A = \varepsilon bc$, where **A** is the absorbance, **ε** is the molar absorptivity constant in L mol^{-1} cm^{-1}, **b** is the path length in cm, and **c** is the molar concentration of peptide. Absorbance was measured spectrophotometrically, using a Cary 50 Bio UV/Vis spectrophotometer; Varian, Palo Alto, CA. The concentration of each peptide was calculated based on the presence of Trp using its molar extinction coefficient of 5,500 at 280 nm. The final sample concentrations were 100 μM in 40% TFE. The blank spectrum, consisting of this sample solution minus the peptide, was subtracted from each test sample spectrum. All spectra were

recorded in observed ellipticity (θ) units of mill degrees (mdeg) and converted into mean residue ellipticity ([θ]) units of deg cm^2 $decimole^{-1}$ using the following equation: **[θ] = 100(signal)/Cnl**, where **[θ]** = mean residue ellipticity in deg cm^2 $dmol^{-1}$; **signal** = raw output data in mdeg; **C** = peptide concentration in mM; **n** = number of amino acid residues and **l** = cell path length in cm (Myers et al., 1997).

Measurement of transepithelial electrical properties

Madin-Darby canine kidney (MDCK) epithelial cells mounted into the Ussing chamber system were used for the measurements of peptide-induced transepithelial ion transport across the monolayers. MDCK cells allow for easy manipulation because they are grown on permeable supports (Misfeldt et al., 1976).

Chemicals: 1-EBIO (1-ethyl-2-benzimidazolinone; Acros, Pittsburgh, PA) was prepared as 1 M stock solution in dimethyl sulfoxide. Forskolin (*Coleus forskohlii*; Calbiochem, La Jolla, CA) was prepared as 10 mM stock in ethanol. Peptide stock solutions of 5 mM, calculated based on the theoretical molecular weight of synthetic peptides, were prepared in deionized water just prior to use. Unless otherwise noted, all other reagents were purchased from Sigma Chemical (St. Louis, MO).

Epithelial culture

MDCK epithelial cells were a generous gift of Dr. Lawrence Sullivan (KUMC, Kansas City, KS). Cells were grown in 25 cm^2 culture flasks (Cellstar, Frickenhausen, Germany) under conditions of 5% CO_2 and 37 °C. The culture medium was a 1:1 mixture of Dulbecco's modified Eagles medium and Ham's F-12 nutrient mixture (DMEM/F-12; Invitrogen, Carlsbad, CA) supplemented with 5% heat-inactivated fetal bovine serum (FBS; BioWhittaker, Walkersville, MD). Confluent cultures were split for subculture every 6 to 7 days with PBS containing 2.6 mM

EDTA and 0.25% trypsin. For the Ussing chamber experiments, cells were plated on 1.13 cm^2 permeable supports (Snapwell; Costar, Cambridge, MA) at a density of ~$1x10^6$ cells/well and incubated in a solution of DMEM/F-12 supplemented with FBS and 100 IU/mL penicillin G and 0.1 mg/mL streptomycin (P/S) (Lot# 529891 and 417319; Invitrogen) that was refreshed every alternate day for two weeks before being mounted in Ussing flux chambers.

Electrophysiology

Transepithelial ion transport was measured using Ussing chambers (Model DCV9, Navicyte, San Diego, CA) as described previously (Broughman et al., 2004; Broughman et al., 2001). The 14-day post seeding MDCK cell monolayers were mounted in chambers. Apical and basolateral sides of the monolayer were bathed symmetrically in Ringer's solution (120 mM NaCl, 25 mM $NaHCO_3$, 3.3 mM KH_2PO_4, 0.8 mM K_2HPO_4, 1.2 mM $MgCl_2$, and 1.2 mM $CaCl_2$; $\sim$ 290 mOsmol/kg H_2O). The Ringer's solution was prepared fresh daily and all components purchased from Sigma-Aldrich (St. Louis, MO). Temperature of the bathing solution was kept at 37 $^{\circ}C$ and continuously bubbled with 5% CO_2/ 95% O_2 to provide mixing and pH stability. Experiments were conducted on monolayers with a resistance of at least 800 Ohms cm^2. The monolayers were clamped to 0 mV and a 5 s, 1 mV bipolar pulse was generated automatically every 100 s using a voltage clamp (model 558C-5, University of Iowa, Dept. of Bioengineering, Iowa City, IA). Continuously measured short-circuit current with a voltage clamp apparatus reflects the amplitude of the net ion movement across the epithelium.

Experimental design

Once mounted into the Ussing chambers, MDCK monolayers were treated with 1-EBIO (1-ethyl-2-benzimidazolinone) about 10 minutes prior to addition of peptide. 1-EBIO activates of Ca^{2+} dependent basolateral K^+ channels, which hyperpolarizes the cell (Devor, 1996) and increases the electrochemical driving force for Cl^- conductance through any open chloride selective channels in the apical membrane (Broughman et al., 2001). The increase in endogenous transepithelial ion current induced by the EBIO was compared to the currents induced by the peptides. The peptides at concentrations: 10, 30, 60, 100 and 300 μM were added to the apical solution bathing monolayers. Data acquisition was performed at 1 Hz with a Macintosh computer (Apple Computer, Cuppertino, CA) using Aqknowledge software (ver. 3.2.6, BIOPAC Systems, Santa Barbara, CA) with an MP100A-CE interface. The experimental outline is presented in **Figure 2-2.** The raw I_{SC} data correspond to steady-state flux levels. The addition of 1 μM forskolin from 10 mM stock solution to apical and basolateral side of MDCK monolayer, served as an indicator that cells were intact and responsive. Forskolin is an adenylyl cyclase activator that catalyzes the conversion of ATP to cAMP, thereby activating protein kinase A. This in turn activates components of active ion transport pathways, such as CFTR, and results in increased anion secretion (Carlin et al., 2006; Hedin & Rosberg, 1983).It is also known that forskolin drives the uptake of chloride via $Na^+/K^+/Cl^-$-cotransporter (NKCC) (Crook and Polansky, 1994; Andrea-Winslow et al., 2001).

Figure 2-2 Ussing chamber experiment.

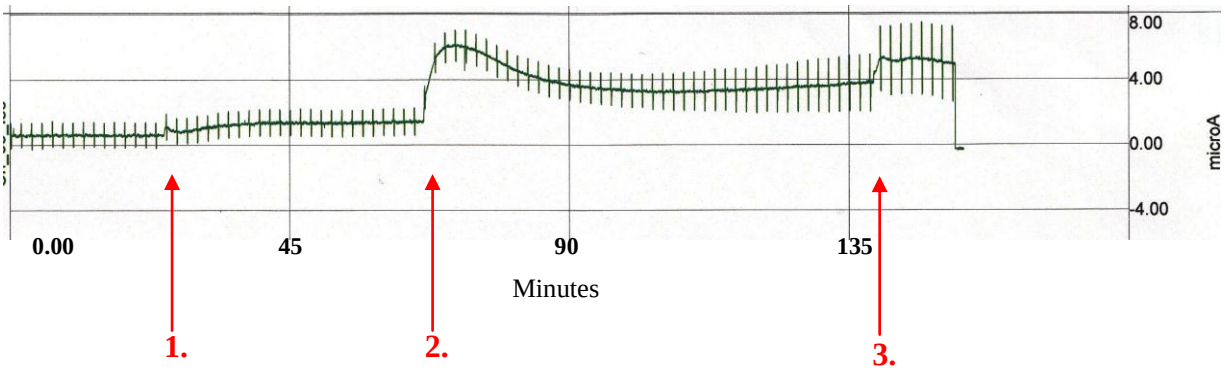

Figure 2-2 shows a typical experimental trace of an Ussing chamber experiment with NK_4-M2GlyR p22-T19R, S22W (10µM). At (1.) 1-EBIO was added to the MDCK cells. (2.) shows addition of peptide to the monolayer. Various concentrations were tested: 10, 30, 60, 100 and 300 µM. At the end of the experiment (3.) 1 µM of forskolin was added to the apical and basolateral side of cells.

Determination of permselectivity

TEVC was used to measure changes in ionic current resulting from peptide function. **Figure 2-3** illustrates the recording configuration used in this study. The membrane of the oocyte is penetrated by two electrodes; a voltage-sensing electrode (#1) and a current injecting electrode (#2). The membrane potential is measured by the voltage sensing electrode (1) connected to an impedance amplifier (left side blue triangle) and compared to a command voltage, sent from the computer (b), while (a) represents the membrane voltage. The difference drives current through electrode 2 from the second amplifier (right side blue triangle). The TEVC system uses the experimentally applied electrical driving force to induce voltage-dependent ion current across the oocyte's

Figure 2-3 A simplistic model of TEVC system.

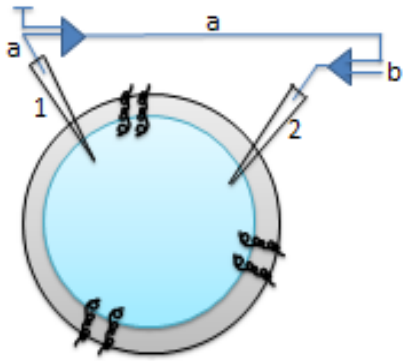

membrane. Ions move down their electrochemical gradient and sign of the electrical driving force is used to predict the induced direction of ion flow across the plasma membrane. When the voltage is negative to the equilibrium potential for the particular ion type, as determined by the Nernst equation, ions move in a direction defined as 'inward'. This indicates the movement of cations into the cell (influx) and anion movement out of the cell (efflux). At positive command voltage pulses, current is defined as outward: cations move out of the cell, whereas anions move into the cell. Measured ionic current (I) is plotted as a function of the corresponding voltage (V), which is referred to as a current-voltage (I-V) plot.

Protocol for TEVC experiments

Isolation of Xenopus oocytes

Mature female *Xenopus laevis* were purchased from Nasco (Fort Atkinson, WI, USA). All animal protocols followed guidelines approved by Washington University, St. Louis, Kansas State University and the National Institutes of Health. Frogs were anaesthetized with 0.1% ethyl-3-amino benzoate methanesulfonate (Tricaine; Sigma-Aldrich) in a solution with 0.1% $NaHCO_3$. A portion of the ovary was surgically removed. Frogs were humanely sacrificed after the final collection. Oocytes were defolliculated by treatment with 1 mg/ml collagenase (Type 1A) in a Ca^{2+}-free solution containing (mM) 82.5 NaCl, 2 KCl, 1 $MgCl_2$, 5 Hepes/Tris (pH 7.5). Stage V-VI oocytes were selected and maintained at 18 °C in a modified Barth's solution Barth's solution (in mM: 88 NaCl, 1 KCl, 2.4, $NaHCO_3$, 0.82 $MgSO_4$, 0.33 $Ca(NO_3)_2$, 0.41 $CaCl_2$, 10 HEPES, pH of 7.4) supplemented with 50 mg/L gentamycin (Sigma), 5.75 mg/L ciprofloxacin (Bayer, West Haven, CT, USA) and 100 mg/L streptomycin sulphate/100 000 units L^{-1} penicillin G

sodium (Gibco, Invitrogen, Carlsbad, CA, USA) (Sala-Rabanal et al., 2006). Oocytes were used up to three days after preparation. All experiments were performed at room temperature.

Electrophysiology: Two-microelectrode-voltage clamp system (TEVC)

A two-microelectrode voltage-clamp system was used to measure the response of oocytes to exposure to the peptides in different ionic environments. The compositions of bath solutions used are presented in a **Table 2-2**.

Table 2-2: Composition of external solutions (in mM).

ND96	**10% Cl^-**	**10% Na^+**	**KD96**	**K-gluconate**
96 NaCl	92.3 Na-gluconate	86.4 choline chloride	96 KCl	96 K-gluconate
1 KCl	9.6 NaCl	9.6 NaCl	1 NaCl	1 Na-gluconate
1 $MgCl_2$	1 KCl	1 KCl	1 $MgCl_2$	1 $MgCl_2$
1.8 $CaCl_2$	1.8 $CaCl_2$	1.8 $CaCl_2$	1.8 $CaCl_2$	1.8 $CaCl_2$
5 Hepes	1 $MgCl_2$	1 $MgCl_2$	5 Hepes	5 Hepes
	5 Hepes	5 Hepes		

The pH was adjusted to 7.5 with Tris for all solutions and osmolality of solutions was ~ 200 mOsm/kg. Typically, an oocyte was mounted in a TEVC setup, superfused in ND96 and held at –30 mV (V_h). The rationale for the use of –30 mV as a holding potential was based on the measured potential when oocyte was impaled and not yet clamped. In basic experiments, the oocyte was exposed to ND96, first in the absence, then in presence of synthetic peptide (50 μM), and then washed with peptide-free ND96 until the initial conditions were completely restored. In experiments with alternate ionic compositions, the oocyte was first stabilized in ND96, subsequently superfused with the appropriate ion-substituted buffer, first in the absence then in presence of the peptide. After peptide exposure, the oocyte was washed first with the alternate

ionic bath solution and then with ND96, to verify reversibility of bath composition-induced changes and to allow comparisons to temporally close controls. Oocytes were exposed to each buffer for a minimum of 10 min, and until stable conditions were reached. At this time, either step or ramp changes in voltage were used to determine reversal potentials and membrane conductance. In the step protocol (**Figure 2-4**) the membrane potential (V_m) was stepped from V_h to a test value for 1000 ms before returning to the holding potential. The test potential varied from +60 to –140 mV in 20 mV increments. Steady-state or pseudosteady-state current-voltage (*I-V*) relationships were measured at the end of 1000 ms.

Figure 2-4: Scheme of step protocol.

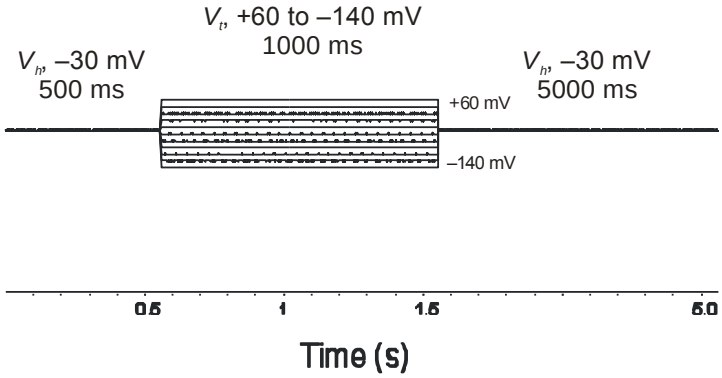

In the linear voltage ramp protocol (**Figure 2-5**), oocytes were held at –30mV, stepped to –140 mV for 1000 ms, ramped from –140 mV to +60 for 2000 ms and back to –140 mV for 50 ms before returning to the holding potential. The ramp protocol was used to determine the V_{rev}. pClamp and Axoscope software (Axon Instruments, Union City, CA, USA)

Figure 2-5: Scheme of ramp protocol.

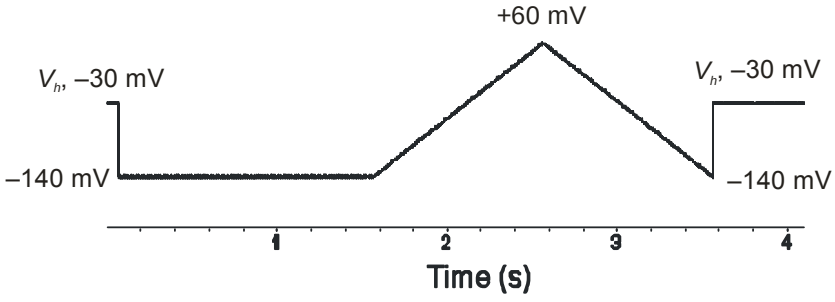

were used for pulse protocols application and data acquisition. The difference in the protocols is that in a ramp protocol the voltage varied progressively, while in a step protocol, the voltage is held at a given voltage for a period of time, then returned to the holding potential before stepping to the next voltage. The oocyte clamp/amplifier does the controlling, according to our specifications.

The voltage drop across the bath grounding electrode (Rb), is indistinguishable from the membrane potential. Therefore the potential recorded by the voltage-recording micropipette is the sum of the transmembrane potential (Vm) and the bath potential (Vb). Problems arise if the product of the clamp current and Rb is significant, meaning the error voltage is more than 10 mV. To record the membrane potential correctly, either bath potential must be made equal to or nearly equal to zero. Usually the grounding and thus minimization of this effect is successfully accomplished through the use of Ag/AgCl pellets. But the direct current (DC) offset of the Ag/AgCl pellets changes with chloride activity. In our experiments, this effect could occur with the change of ND96 for bath solutions with reduced chloride. To avoid this, agar bridges (3M KCl in 3% agar) were used.

Data analyses

For the data analysis, the differences were analyzed using analysis of variance (ANOVA) and unpaired Student's t-test (Excel; Microsoft, Redman, WA). The probability of making a type I error less than 0.05 was considered statistically significant.

$^{86}Rb^{+}$ flux assay

A flux assay using $^{86}Rb^{+}$ was used to assess whether Dap-substituted variants assemble into pores and possess the ion channel properties same as their non-substituted parent, p22 T19R, S22W. The single channel activity of p22 T19R, S22W-assembly, here used as a control, was previously shown in measurements of peptide incorporated into synthetic planar lipid bilayers composed of POPC/POPG (70:30) (Shank et al., 2006).

Liposomes composed of POPE: POPG (3:1) of 70.9 nm in diameter were prepared following the protocol of Heginbotham et al. (1998). As presented in the simplified flux assay scheme (**Figure 2-6)**, the addition of peptide to the solution containing liposomes was tested to determine whether peptides can insert into the membranes, self-assemble into pores and facilitate the permeation of radioactive $^{86}Rb^{+}$ ions.

Figure 2-6 A simplistic scheme of flux assay.

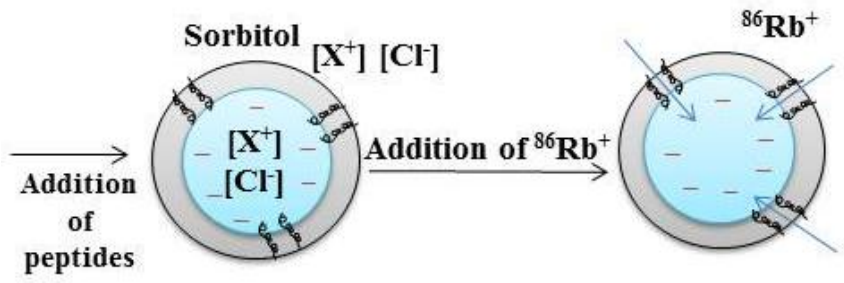

There was no voltage applied and the influx of $^{86}Rb^{+}$ was generated by the concentration gradient. In a control reaction the $^{86}Rb^{+}$ influx into peptide-free liposomes was monitored over the same time course to provide a baseline for the degree of lipid leakiness to $^{86}Rb^{+}$. Valinomycin was used to measure maximal $^{86}Rb^{+}$ uptake. Data were subtracted from uptake counts measured at each time point from protein-free liposomes, and plotted relative to valinomycin-induced uptake counts.

One peptide from each Dap substitute group was chosen, p22 T19R, S22W T20Dap representing single Dap substituted peptides and p22 T19R, S22W T13Dap T17Dap representing double-Dap substituted peptides. The peptide with three Dap substitutes was not used in the assay due to its non-significant induction of ion current compared to doubly substituted peptides, as assessed in Ussing chamber and voltage-clamp experiments.

Flux assay protocol and materials

The protocol for liposomal $^{86}Rb^{+}$ uptake assay was modified from Heginbotham et al. (1998). Experiments were conducted using the following materials: lipids - POPE (1-palmitoyl-2-oleoyl-3-phosphatidylethanolamine) and POPG (1-palmitoyl-2-oleoyl-3-phosphatidylglycerol; Avanti Polar Lipids, Inc.), CHAPS, N-methyl-D-glucamine (NMDG) (Sigma), Dowex 50 X-4-100 (H^{+} form) cation exchange matrix (Sigma), Dowex 50 X-4-100 (H^{+} form) cation exchange matrix (Sigma) (Dowex 50-X8 by Perozo), Polystyrene column bodies (No. 29920, Pierce Chemical Co.), sorbitol, HCl, bovine serum albumin (BSA) and valinomycin.

For preparation of lipids, 4 mg of lipids in chloroform were placed in glass culture tube and dried under a stream of nitrogen gas. For further drying, lipids were put in Speedvac but carefully so that there was no heating at this point of preparation. Then glass tubes were filled with lipids and sealed with parafilm. Tubes were stored in a container filled with nitrogen at -20° C. Lipids were next solubilized in buffer A (450 mM KCl (16.776 g), 10 mM HEPES (1.1915 g), 4 mM NMG (0.3904 g), and pH adjusted to 7.5 with HEPES or NMDG) with 35 mM CHAPS at 10 mg/mL, mixed at a 3:1 mass ratio, and incubated at room temperature for 2 h.

Polystyrene columns (Pierce Chemical Co.) were packed with Sephadex G-50 beads, presoaked overnight in buffer A, and spun on a Beckman TJ6 centrifuge at 3000 rpm. Columns

were always prepared fresh and used on the day of the experiment. 4.0 mL of Buffer A was added to each glass tube containing lipids and sonicated until the lipids were dissolved. Before the final 2 h incubation at room temperature, CHAPS of 37 mM was added to solubilize the lipids. Further, protein (2.5 μg) was added to the lipid (1 mg) (100 μL) for each sample and incubated for 20 min. Liposomes were formed by adding the protein/lipid sample to the partially dehydrated Sephadex G-50 columns and spinning at 2500 rpm. The extraliposomal solution was exchanged by spinning the sample at the same speed in partially-dehydrated columns now containing beads soaked in buffer B (400 mM sorbitol (36.44 g); 10 mM HEPES (1.1915 g); 4 mM NMG (0.3904 g). The pH of Buffer B was adjusted to 7.5 same as for Buffer A. Experiments were conducted using $^{86}Rb^{+}$ (PerkinElmer Life Sciences). The uptake of $^{86}Rb^{+}$ was initiated by adding 400 μL of buffer B containing $^{86}Rb^{+}$. At various time points, aliquots of the liposome uptake reaction were passed through 0.5 mL Dowex cation exchange columns to remove extraliposomal isotope. Dowex columns were prepared by placing 0.5 to 1 mL of Dowex beads in a serum separator column, prewashed with 1 mL of BSA-Sorbitol solution and rinsed with 1 mL of sorbitol. Sorbitol solution (500 mL) was prepared with 400 mM of sorbitol (36.44 g), and BSA of 5 mg/mL in Sorbitol (final volume of 50 mL), using 50 mL of 400 mM of sorbitol and 250 mg of BSA. Columns were prewashed with 100 μg of lipid solution and rinsed with 1 mL of sorbitol.

The aliquots of the liposome uptake reaction were mixed with scintillation fluid and counted in a liquid scintillation counter (Liquid scintillation analyzer 1600TR Tri-Carb Packard, Canberra, Australia). Each experiment was done in triplicate, testing the time course of $^{86}Rb^{+}$ influx. In a control reaction $^{86}Rb^{+}$ flux through the membranes of peptide-free liposomes was monitored over the same time course to provide a baseline to monitor the degree of lipid

leakiness to $^{86}Rb^{+}$. Valinomycin stock set was prepared with 100 μg/mL of the Valinomycin in ethanol and added to the peptide-free liposomes. Valinomycin made liposomes permeable to $^{86}Rb^{+}$ and allows measurement of its maximal uptake. Data were subtracted from uptake counts measured at each time point from protein-free liposomes, and plotted relative to valinomycin-induced uptake counts.

Flux analyses were conducted in collaboration with Dr. Nazzareno D'Avanzo in the laboratory of Dr. Colin Nichols at Washington University of Medicine at St. Louis, MO.

Results

CD analysis

CD measurements were recorded to verify that the introduction of single or multiple Dap substitutions did not significantly alter the secondary structure of the new test peptides. **Figure 2-7** shows that Dap did not alter the secondary structure of any of the peptides. Compared to the secondary structure of the parent p22-T19R, S22W peptide, Dap-substituted peptides displayed similar helical content compared to the parent sequence NK_4-M2GlyR p22-T19R, S22W (Cook et al., 2004, Herrera et al., 2010; Bukovnik et al., 2011). The parent peptide spectra in Figure 2-7 superimposes with the spectra of T13 Dap-substituted peptide. The observed variations in helical content among the different peptides were consistent with previous variances observed for other modified NK_4-M2GlyR peptides in our laboratory. It should be noted that under the conditions tested all of the peptides exist in solution as monomers. However, based on previous computer modeling studies, helical content rises as the peptides assemble in the membrane through a cooperative process (Herrera et al., 2010).

Figure 2-7: CD spectra of NK_4-M2GlyR p22-T19R, S22W (p22-T19R, S22W) Dap-substituted peptides in 40% TFE.

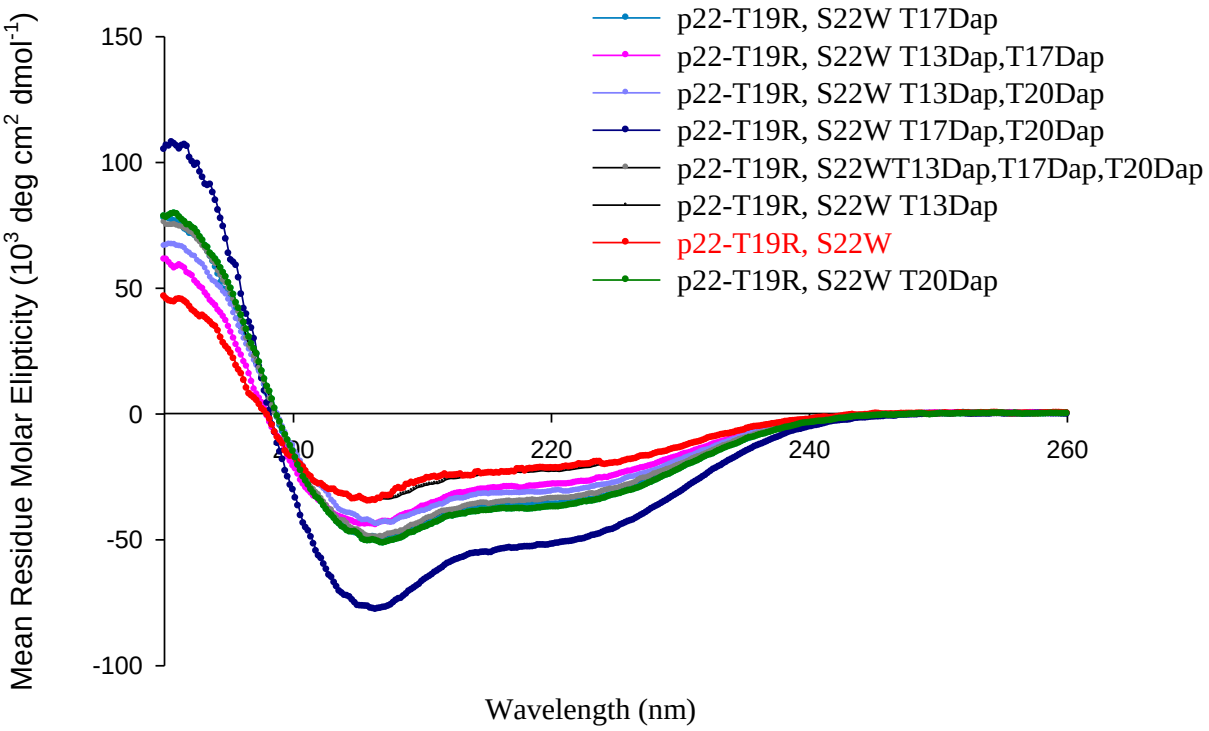

Transepithelial ion transport measurements

Threonine residues at positions 13, 17 and 20 are predicted to line the pore interface of p22-T19R, S22W-assembled channel (Cook et al., 2004; Bukovnik et al., 2011). Threonines 17 and 20 are located at the narrowest part of the pore and threonine 13 at a slightly wider region. Because single substitutions of T13 and T17 with Dap showed increased magnitudes of net ion transport across MDCK cells, a previous reported by Frazier (2006), studies were initiated to assess how Dap affects the biophysical properties of Dap-substituted peptides. All the predicted pore-lining threonines at positions 13, 17 and/or 20 in a sequence were substituted singly, doubly or triply with Dap. Typically, the differences in the measured transepithelial ion transport induced by the peptides were observed within the first 10 minutes after application. I_{SC} was greater with increasing concentration. All the peaks were followed by a gradual response decay

that was greater at higher concentrations, 100 μM and 300 μM. Changes were larger for double or triple Dap-substituted peptides (data not shown). All MDCK epithelial monolayers responded to forskolin at the end of each experiment. Addition of 1 μM forskolin increased *Isc*. The *Isc* peak was followed by a plateau, which indicated an ongoing current (**Figure 2-2**). The *Isc* changes caused by forskolin suggested that MDCK monolayers were still viable and responsive to cAMP-mediated stimulation after the exposure to the peptides.

Results indicate that the sequences tolerated the introduction of Dap. All the Dap-substituted peptides induce transepithelial ion transport across the monolayers of MDCK cells. The I_{SC} increased incrementally with each higher peptide concentration. Experiments were repeated at least six times and the average maximal current (I_{max}) determined for each concentration. The concentration-dependence of I_{SC} for all the peptides is shown in **Figure 2-8**. The solid line represents the best fit of a modified Hill equation to the data set. The Hill equation allowed for the determination of three parameters, the maximal I_{SC} attained by the channel, the concentration of peptide required to reach half maximal short circuit current ($K_{1/2}$), and the degree of cooperativity as quantified by the Hill coefficient. The interpretation of the Hill coefficient is assumed to reflect the cooperativity of peptide monomers in a process of pore assembly. The derived kinetic constants are summarized in **Table 2-3**.

Table 2-3: Kinetic properties of NK_4-M2GlyR T19R, S22W (p22-T19R, S22W) and its Dap-substituted sequences.

Kinetic properties of NK_4-M2GlyR T19R, S22W and its Dap-substituted peptides are shown. I_{max} is maximal I_{SC} and $K_{1/2}$ the concentration required to obtain one-half of I_{max}. Values for I_{max} and $K_{1/2}$ were calculated using the Hill equation with the data presented in **Figure 2-8**.

	Peptide	**Hill Coefficient**	I_{max} **(μA/cm^2)**	$K_{1/2}$ **(μM)**
1	NK_4-M2GlyR T19R, S22W (p22-T19R, S22W)	1.6 ± 0.2	44 ± 5	155 ± 30
2	p22-T19R, S22W **T13Dap**	3.5 ± 0.7	37 ± 1	116 ± 7
3	p22-T19R, S22W **T17Dap**	2.8 ± 0.6	68 ± 14	185 ± 45
4	p22-T19R, S22W **T20Dap**	1.3 ± 0.6	19 ± 0.9	17 ± 0.59
5	p22-T19R, S22W **T13Dap, T17Dap**	2.1 ± 0.2	142 ± 23	218 ± 42
6	p22-T19R, S22W **T17Dap, T20Dap**	3.3 ± 0.4	121 ± 3	114 ± 5
7	p22-T19R, S22W **T13Dap, T20Dap**	3.1 ± 0.8	99 ± 11	150 ± 25
8	p22-T19R, S22W **T13Dap, T17Dap, T20Dap**	2.9 ± 0.2	104 ± 3	139 ± 7

The doubly substituted Dap peptides, T13Dap, T17Dap (142 ± 23 μA cm^{-2}), T13Dap, T20Dap (99 ± 11 μA cm^{-2}), T17Dap, T20Dap (121 ± 3 μA cm^{-2}), and the triply-substituted sequence T13Dap, T17Dap, T20Dap peptide (104 ± 3 μA cm^{-2}), induced higher I_{max} relative to the non-substituted peptide (44 ± 5 μA cm^{-2}) (**Figure 2-8; Table 2-3)**. Among singly substituted peptides, only the 17Dap-substituted peptide showed a greater I_{max} of 68 ± 14 μA cm^{-2} relative to its non-substituted parent (**Figure 2-8, Table 2-3).**

A therapeutic compound ideally functions at low effective concentration. Therefore the concentrations of Dap-substituted peptides required to attain one-half I_{max} values were determined. It is assumed that the amount of water and ion flow induced by such peptide

concentrations would be still adequate to rehydrate the airway and restore mucocilliary clearance in CF patients. Relative to the parent sequence (155 ± 30 μM) the peptides with T13Dap (116 ± 7μM), T20Dap (17 ± 0.59μM) and T17Dap, T20Dap (114 ± 5μM) substitutions possess lower values of $K_{1/2}$ (**Table 2-3**). With the exception of T20Dap-substituted peptide, all the peptides showed greater Hill coefficients than their parent peptide. The T20Dap peptide showed the lowest values of 1.3 ± 0.6 relative to the parent sequence (1.6 ± 0.2). Conversely T17Dap, T20 Dap and T13Dap, T20 Dap sequences showed the highest, with coefficients of 3.3 ± 0.4 and 3.1 ± 0.8, respectively. Hill coefficient might suggest the degree of monomer cooperativity in a multi-step processes of channel assemblies. Whether the cooperative step involves membrane partitioning, assembly of the helical bundles into structures, or a combination of the two is not known. The observed increase in Hill coefficients suggests that membrane association/dissociation mechanisms of assemblies containing Dap-substituted peptides are sensitive to structural changes made by the threonine to Dap substitutions.

Figure 2-8: Concentration dependence of I_{SC} induced NK_4-M2GlyR p22-T19R, S22W (p22-T19R, S22W) and p22-T19R, S22W Dap substituted peptides on MDCK epithelial monolayers.

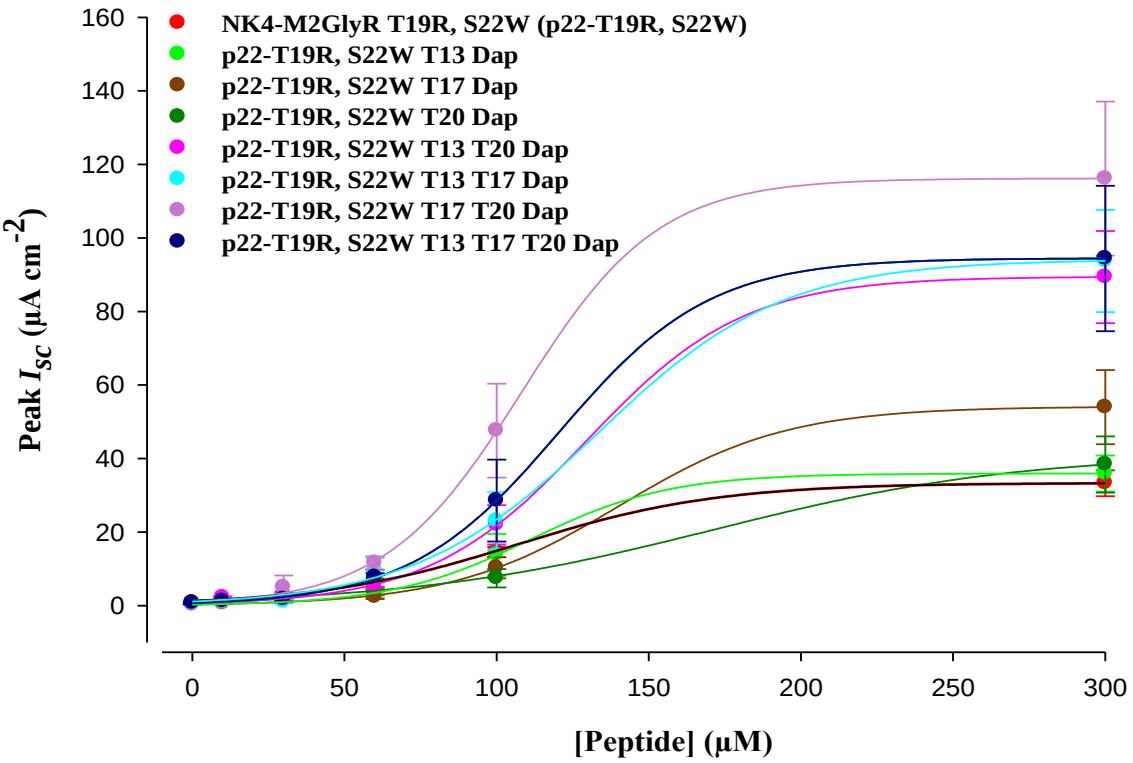

The data points represent the mean peak *Isc* stimulated by the peptides in independent observations at concentrations of 10, 30, 60, 100 and 300 µM. Error bars indicate 6 observations ± S.E.M. The differences between control and treatment data were analyzed using analysis of variance (ANOVA) and unpaired Student's t-test (Excel; Microsoft, Redman, WA). The probability of making a type I error less than 0.05 was considered statistically significant. The lines in **Figure 2-8** are the best fit of a modified Hill equation to the data, $I_{SC} = I_{MAX} * (x^n / (K_{1/2}{}^n + x^n)$; where $K_{1/2}$ is the concentration of peptide that provides a half maximal I_{SC} and n represents the Hill coefficient. Symbols and error bars represent the mean ± S.E.M. of 6 observations for

each concentration tested. Solid lines represent the best fit of a modified Hill equation to each data set. The data points are the mean I_{SC} stimulated by the peptides.

Selective ion permeability

Permselectivity of channels formed by p22-T19R, S22W peptide and its Dap-substituted variants was measured using TEVC of *Xenopus* oocytes. Typically, the results with the non-substituted p22-T19R, S22W peptide show a voltage-dependent increase in the whole-cell oocyte membrane ion conductance. In ND96, this peptide induced voltage dependent, significantly higher inward ion current ($P<0.05$, t-test) (**Figure 2-9**). The increase in whole-cell current was unlikely the result of an increase in ion currents of endogenous channels over time. This was supported by the reversibility of the peptide-induced effect at superfusion of oocyte with ND96; labeled as ND96 final, in **Figures 2-9).**

Figure 2-9: Ion currents induced by exposure of oocyte to p22-T19R, S22W in ND96.

Legend: Raw data represent a superfusion of oocyte with ND96 in absence of the peptide (ND96 initial), presence of p22-T19R, S22W (Peptide) in ND96 solution and again with ND96 in absence of the peptide (ND96 final) (left figure). The right I-V plot summarizes the data corresponding to the raw traces. Symbols represent mean currents induced by exposure of oocyte to either ND96 in the absence of the peptide (ND96 Initial) (circle) (n = 4), ND96 in the presence of peptide (50 μM) (red triangle) (n = 4 from 3 different oocytes) and ND96 in the absence of peptide (ND96 Final) (square) (n = 4). The mean difference currents are plotted at voltages from –140 mV to +60 mV. Error bars indicate the S.E.M. ANOVA was used to calculate significant differences ($P<0.05$, t-test). Significantly higher currents, indicated with the asterisk, were observed at –140 and –120 mV induced by exposure of oocytes to p22-T19R, S22W.

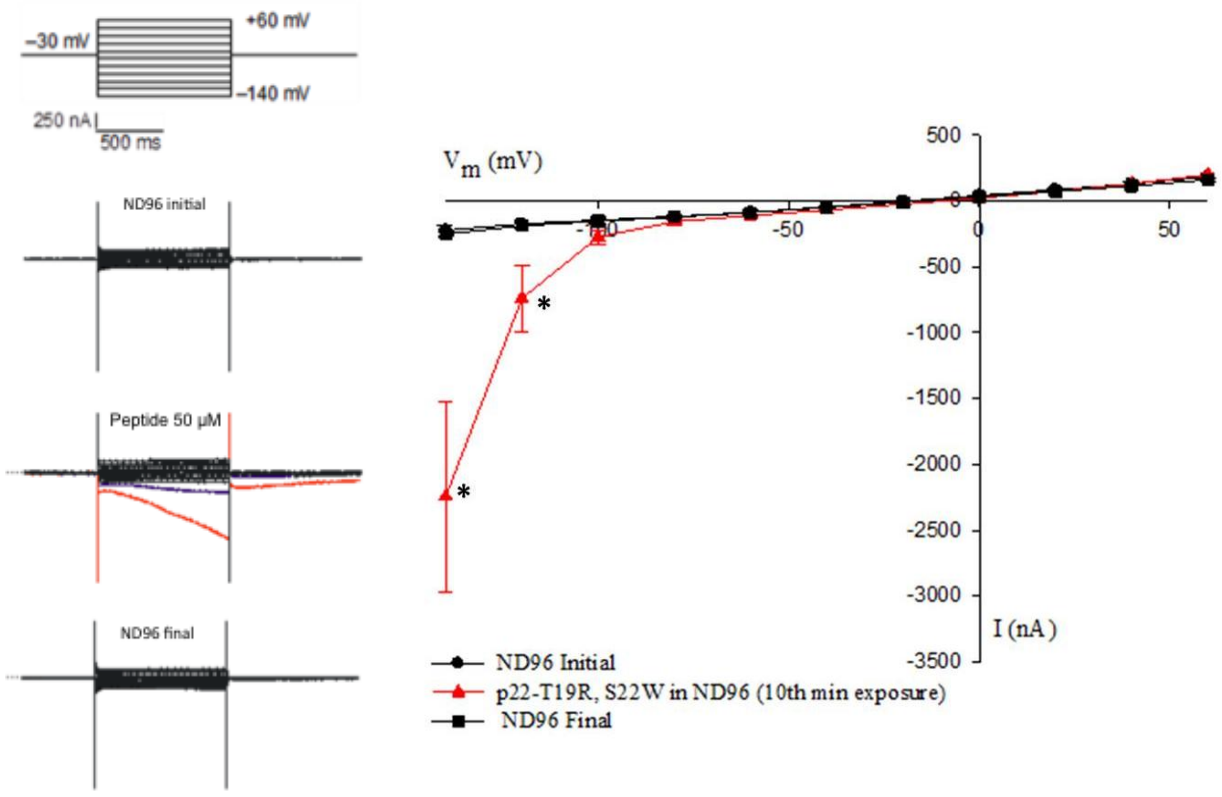

I-V relationships of currents induced by p22-T19R, S22W in response to solutions of varying ionic compositions are summarized in **Figure 2-10**. Altering the concentrations of [Cl^-] (in 10% Cl^- solution), [Na^+] (in 10% Na^+ solution) and [K^+] (in KD96 and K-gluconate solution) in external solutions permits the evaluation of p22-T19R, S22W-assembly permselectivity. Results show larger inward current recorded at very negative pulses (–140 and –120 mV) at 10 mM Na^+ (10% Na^+ bath solution) compared to ND96, with 96 mM Na^+. At positive voltages, the substitution of 96 mM NaCl for 92.3 mM choline chloride in 10% Na^+ bath solution resulted in significantly larger p22-T19R, S22W-induced outward ion flux (**Figure 2-10A**) ($P<0.05$, t-test). The Figures **2-10B** (10% Na^+ solution) and **2-10C** (10% Cl^- solution) were added for illustrative purposes to better explain the specificity of the experimental designs under which results were the most significant.

The increase in whole-cell current was unlikely the result of an increase in ion currents of endogenous channels over time. As for the p22-T19R, S22W-induced currents in ND96 (**Figure 2-9B**), the peptide-induced increase in ion currents was reversed also in experiments using other external solutions.

A change of external solution was associated with a leftward or rightward shift in reversal potential (depending on external solution) lower than 10 mV (**Table 2-5**) and less than the predicted change in reversal potential obtained from Nernst relationship for an ideal chloride selective channel (+46 mV), calculated by Mitchell et al. (2000). The lack of larger peptide-induced shifts in reversal potential also resulted in the permselectivity ratios (**Table 2-6**) ranging from 1.1 ± 0.03 ($n = 4$) for Cl^- over Na^+ and 0.9 ± 0.2 ($n = 4$) for Cl^- over K^+ suggesting that there was no permselectivity between these monovalent ions.

Figure 2-10: (A) I-V relation for currents measured in oocytes exposed to p22-T19R, S22W under different ionic conditions. Schematic presentation of ion flows under conditions of experimentally applied voltage and (B) change of 10%Na^+ and (C) 10% Cl^- external solution.

(A) I-V relation for currents induced in oocytes exposed to p22-T19R, S22W under different ionic conditions. Symbols represent the mean and standard errors of currents induced in oocytes exposed to the peptide p22-T19R, S22W (50 μM) dissolved in ND96, 10% Na^+, 10% Cl^- , KD96 or K-gluconate ionic solution (n = 4 for all). Error bars indicate the standard error of the mean. All data are background subtracted with currents measured in the absence of the peptide in the same oocyte. Statistical analysis was performed using ANOVA to calculate significant differences ($P<0.05$, t-test) between the peptide-induced ion currents under conditions with Na^+, Cl^- or K^+ substituted bath solutions, relative to currents measured in ND96, indicated by (*).

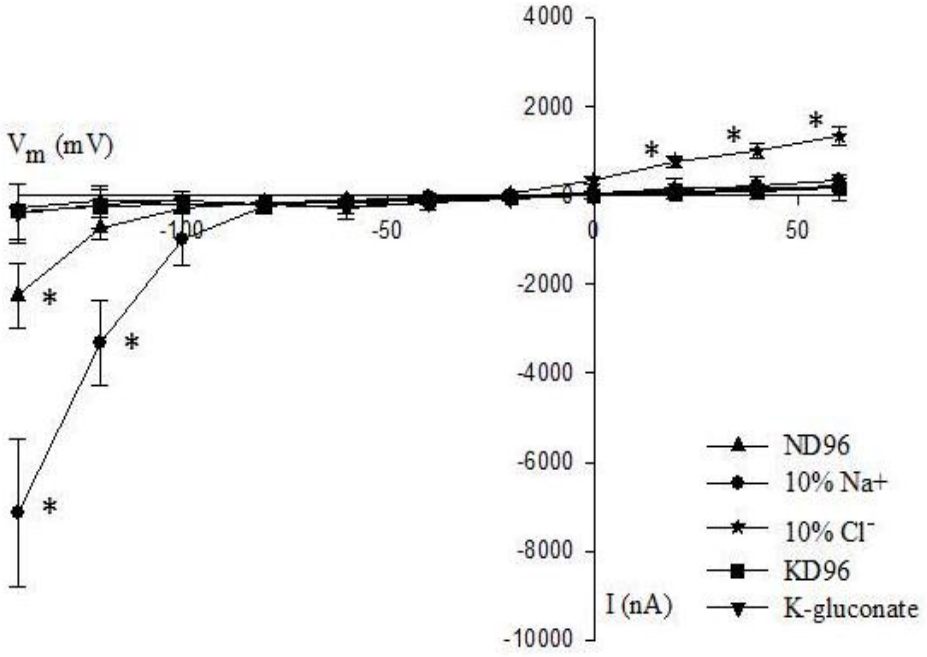

(B) A schematic presentation of ion flows under conditions of 10% Na^+ external solution.

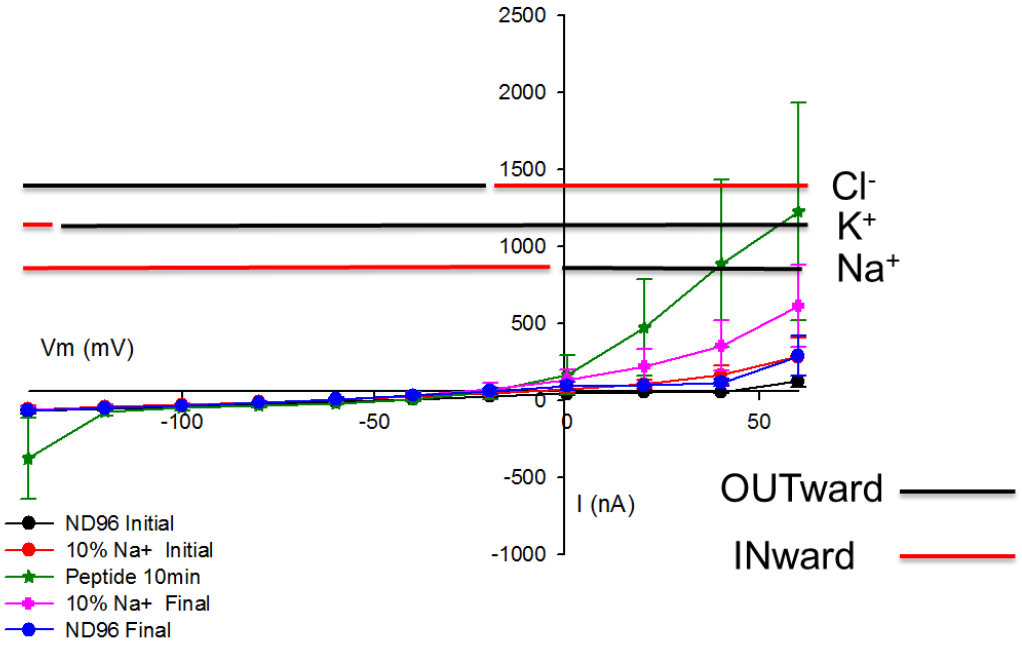

The scheme predicts the flow of Cl^-, K^+ and Na^+ ions based on applied voltages, and concentrations gradients between external bath solution (1 mM K^+, 9.6 mM Na^+, 102.6 mM Cl^-) and oocyte's inter-cellular space (110 mM K^+, 10 mM Na^+, 40 mM Cl^-). The values for ion concentrations in oocytes were obtained from published values (Costa et al., 1989). For the present and all following schemes shown, it was considered that endogenous potassium, chloride and sodium permeable pathways exist in the oocytes. For clarity, only the predicted flows of Cl^-, K^+ and Na^+ ions are illustrated as we were primarily interested in examining the Cl^-/Na^+ and Cl^-/K^+ permselectivity ratios. Needed to be mentioned, are the choline and divalent ions such as Ca^{2+} and Mg^{2+} present, which can permeate the oocyte membrane as well, at the same time as the ions presented in the scheme.

The equilibrium potentials using Nernst equation were calculated for each ion type. When the equilibrium potential for potassium ions (E_{K+} in 10% Na^+ solution = –119 mV) is more negative than the membrane voltage (E_m), the inward movement of K^+ ions is expected at applied pulses of –140 and –120mV. At voltages more positive than –119 mV, K^+ would flow outward. Similar is expected for sodium ions. Na^+ ions move inward as long as E_m is more negative than equilibrium potential for Na^+ (E_{Na+} in 10% Na^+ solution = –1 mV), and outward at voltages more positive than –24 mV. The movement of chloride ions is reverse. The outward movement of chloride ions is induced at voltages more negative than –24 mV (E_{Cl-} in 10% Na^+ solution), and inward movement of ions at voltages more positive than E_{Cl-}.

(C) A schematic presentation of ion flows under conditions of 10% Cl^- external solution.

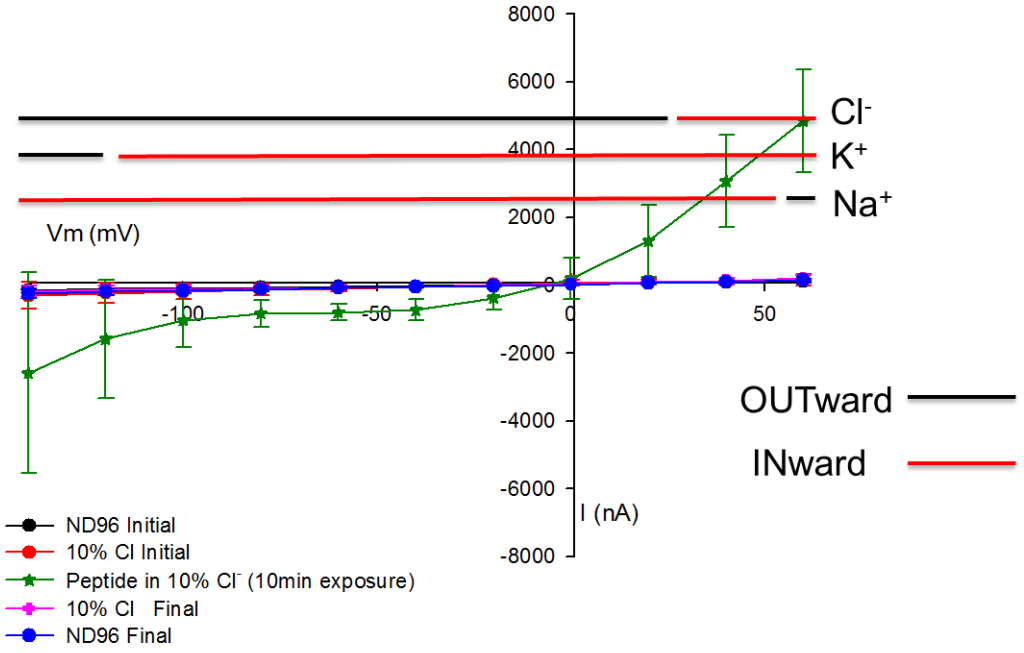

Same as in scheme B, the scheme C predicts the movement of Cl^-, K^+ and Na^+ ions based on applied voltages, and the concentration gradients between the external bath solution (1 mM K^+, 101.9 mM Na^+, 16.2 mM Cl^-) and the inter cellular space using published values (Costa et al.,

1989). For clarity, only predicted movements of Cl^-, K^+ and Na^+ ions are presented. It must be mentioned that gluconate and divalent cations present in 10% Cl^- solution can permeate the oocyte membrane simultaneously as well. The predicted equilibrium potential for K^+ is –119 mV, which means that the inward movement of K^+ ions is expected at applied pulses more negative or equal to 119 mV. At more positive voltages, K^+ ions are expected to move outward. Na^+ ions are expected to move inward as long as E_m is more negative than E_{Na+} (E_{Na+} in 10% Cl^- = +60 mV) which means that we expect the inward movement of sodium ions at all negative and all positive pulses except at +60 mV. The Cl^- ions are predicted to move outward as long as E_m is more negative than E_{Cl-} (E_{Cl-} in 10% Cl^- = +23 mV) and inward at voltages more positive than +23 mV.

In a further set of experiments, Dap-substituted peptides were examined for their ability to increase whole cell ion currents. **Figure 2-11** demonstrates typical peptide-induced voltage-dependent ion currents of a few selected peptides under conditions where 102.6 mM Cl^- (ND96) was changed to 14.2 mM in external bath (10% Cl^- solution), while the Na^+ and K^+ concentrations remained constant. The p22-T19R, S22W was used as a non-substituted, control peptide; its T20Dap-substituted variant was a choice to represent peptide-induced ion currents commonly observed for single Dap-substituted peptides, while the T17Dap, T20Dap-substituted peptide was a chosen to show the responses induced by double Dap-substituted peptides. Additionally, also the triply Dap-substituted peptide was tested.

The doubly substituted peptide, T17Dap, T20Dap, gave higher amplitude currents at voltages lower than –60 mV. Relative to non-substituted peptide, a similar finding was observed for triply Dap-substituted peptide under –120 mV ($P<0.05$, t-test). At +60 mV, all Dap-

substituted peptides induced significantly higher outward current relative to the non-substituted parent peptide ($P<0.05$, t-test) (**Figure 2-11**). Changing the external solution was associated with a total shift in reversal potential, lower than 10 mV (**Table 2-4**). The permselectivity ratios for Cl^-/Na^+ and Cl^-/K^+ ranged slightly above or below unity, which indicates non-selectivity (**Table 2-5**).

Figure 2-11 I-V relation for ion currents measured at exposure of oocytes to selected peptides measured in 10% Cl^- solution.

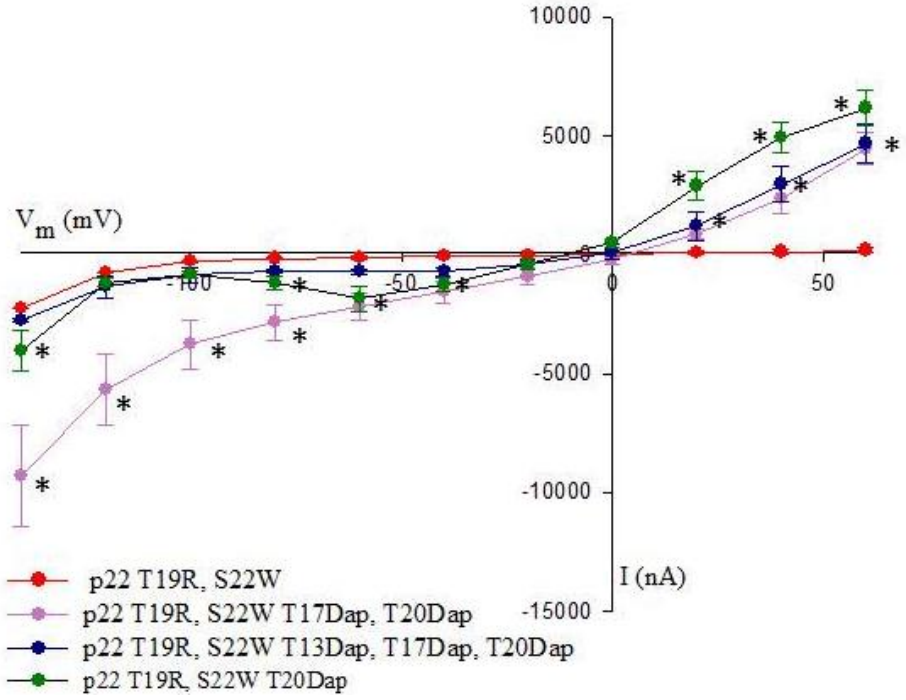

The I-V plot shows differences in ion currents induced by exposure of oocytes to p22-T19R, S22W and T20Dap; T17Dap, T20Dap and T13Dap, T17Dap, T20Dap-substituted peptides (all at 50 μM) dissolved in 10% Cl^- bath solution. The mean ion currents induced by p22-T19R, S22W (n = 4), T20Dap-substituted (n = 3), T17Dap, T20Dap (n = 3) and T13Dap, T17Dap, T20Dap-substituted (n = 3) are shown. Error bars indicate the S.E.M. All data are background subtracted with currents measured in the absence of the peptide in the same oocyte. ANOVA was used to calculate significant differences ($P<0.05$, t-test). Relative to the p22-T19R, S22W -induced ion currents, significantly different currents induced by Dap-substituted peptides are labeled (*).

Table 2-4: Shifts in reversal potentials (V_{rev}).

Differences in reversal potential ΔV_{rev} were calculated using the values of V_{rev} measured in oocytes exposed to ionic solution in the absence or the presence of each peptide. Data are shown as mean (mV) ± S.E.M for n samples.

	ΔV_{rev}				
Peptide	**ND96**	**10% Na^+**	**10% Cl^-**	**KD96**	**K-gluconate**
NK_4-M2GlyR T19R, S22W (p22-T19R, S22W)	4.0 ± 1.7 (n = 4)	3.1 ± 2.0 (n=5)	3.9 ± 1.1 (n = 4)	2.4 ± 1.3 (n=4)	6.0 ± 1.3 (n = 3)
p22-T19R, S22W, T13Dap	1.8 ± 2.7 (n = 3)	5.9 ± 1.1 (n=3)	3.3 ± 1.9 (n = 3)	8.1 ± 2.9 (n=4)	6.3 ± 0.8 (n = 3)
p22-T19R, S22W, T17Dap	4.6 ± 2 (n = 3)	5.0 ± 2.8 (n=4)	6.0 ± 2.7 (n = 4)	1.7 ± 2.1 (n=4)	8.5 ± 3.2 (n = 4)
p22-T19R, S22W, T20Dap	5.0 ± 2.5 (n = 3)	0.70 ± 0.77 (n=4)	0.61 ± 0.5 (n = 3)	6.0 ± 1.3 (n=3)	5.7 ± 2.1 (n = 3)
p22-T19R, S22W, T13Dap, T17Dap	5.3 ± 1.4 (n = 3)	6.6 ± 2.5 (n=3)	5.11 ± 3.8 (n = 3)	4.6 ± 2.9 (n=3)	6.5 ± 2.6 (n = 4)
p22-T19R, S22W, T13Dap, T20Dap	2.8 ± 1.6 (n = 3)	6.7 ± 1.6 (n=3)	5.98 ± 0.93 (n = 3)	6.0 ± 1.3 (n=3)	2.5 ± 1.0 (n = 3)
p22-T19R, S22W, T17Dap, T20Dap	4.7 ± 2.4 (n = 3)	3.4 ± 2.5 (n=3)	7.4 ± 0.8 (n = 3)	4.9 ± 2.8 (n=3)	3.53 ± 0.9 (n = 3)
p22-T19R, S22W, T13Dap, T17Dap,T20Dap	4.6 ± 3.9 (n = 3)	2.5 ± 2.0 (n=3)	3.8 ± 2.4 (n = 3)	3.6 ± 1.2 (n=3)	5.12 ± 1.8 (n = 3)

Table 2-5: Calculated ratios of permeability.

Peptide	**P_{Cl^-}/P_{Na^+}**	**P_{Cl^-}/P_{K^+}**
NK_4-M2GlyR T19R, S22W (p22-T19R, S22W**) (n=4)**	1.1 ± 0.03	0.97 ± 0.01
p22-T19R, S22W, **T13Dap (n=3)**	1.15 ± 0.06	1.03 ± 0.10
p22-T19R, S22W, **T17Dap (n=3)**	1.2 ± 0.08	1.03 ± 0.08
p22-T19R, S22W, **T20Dap (n=4)**	1.04 ± 0.02	0.95 ± 0.04
p22-T19R, S22W, **T13Dap, T17Dap (n=3)**	1.2 ± 0.10	0.99 ± 0.09
p22-T19R, S22W, **T13Dap, T20Dap (n=3)**	1.25 ± 0.01	1.09 ± 0.005
p22-T19R, S22W, **T17Dap, T20Dap (n=3)**	1.25 ± 0.05	1.1 ± 0.008
p22-T19R, S22W, **T13Dap, T17Dap, T20Dap (n=4)**	1.15 ± 0.09	0.99 ± 0.1

The highest Dap-substituted peptide-induced currents relative to the non-substituted peptides were observed at reduction in bath [Cl^-] (10% Cl^- solution) and reduction in bath [Cl^-] and [Na^+], retaining [K^+] high (K-gluconate solution), while in other experiments when only [Na^+] was reduced (KD96 solution), or [Cl^-] and [K^+] were reduced (10% Na^+ solution), the magnitude of Dap-substituted peptide-induced currents was lower. Summarized results of peptide-induced outward or inward currents at +60mV and –100mV, respectively (**Figures 2-12B** and **C)**. Dap-substituted peptides induced the largest currents at –100 mV and +60 mV voltages. Therefore, we chose choice to present results obtained under these voltages.

In Figure **2-12A** (K-gluconate solution) was added for illustrative purposes to better explain the specificity of the experimental designs under which results were the most significant. The experimental design under conditions of 10% Cl^- external solution has been explained before **(Figure 2-10C)**.

Figure 2-12 (A) A schematic presentation of ion flows in the presence of K-gluconate-substituted external solution and ion currents (nA) produced by peptide-exposed conditions of applied voltage of +60 mV (B) and (C) –100 mV, under different ionic conditions.

(A) A schematic presentation of experiments under conditions of K-gluconate external solution.

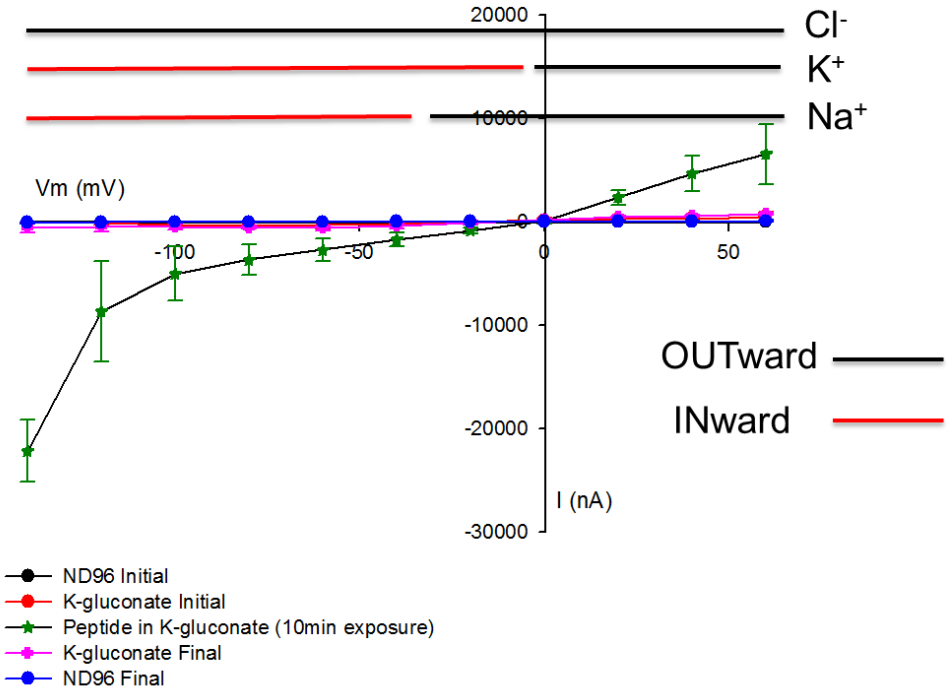

The scheme predicts the flow of Cl^-, K^+ and Na^+ ions based on applied voltages, and concentrations gradients between external bath solution (96 mM K^+, 2 mM Na^+, 2 mM Cl^-) and oocyte's inter-cellular space using published values (Costa et al., 1989). For clarity only the

flows of Cl^-, K^+ and Na^+ ions are presented whereas gluconate and divalent cations can permeate the oocyte membrane at the same time as well. The main property of the K-gluconate bath solution is the replacement of NaCl for K-gluconate and Na-gluconate retaining the concentration of K^+ and lowering concentration of Na^+ and Cl^- ions. The predicted equilibrium potential for K^+ ions is –3 mV. At voltages more negative than –3 mV the inward movement of K^+ ions is expected and the outward movement at all pulses more positive than EK^+. Na^+ ions, are predicted to flow inward as long as E_m is more negative than E_{Na+} (E_{Na+} in K-gluconate solution = –41 mV) and outward at voltages more positive than E_{Na+}. For chloride ions the outward flow is expected as long as E_m is more negative than E_{Cl-}

(E_{Cl-} in K-gluconate = + 76 mV). **(B)** Mean currents and standard errors of 3 or more experiments per peptide under each ionic condition are shown. ANOVA was used to calculate significant differences (P<0.05, t-test). Statistically significant differences (*) between the currents induced by a non-modified peptide p22-T19R, S22W (red colored bars) and its Dap-substituted peptides inside each treatment are labeled.

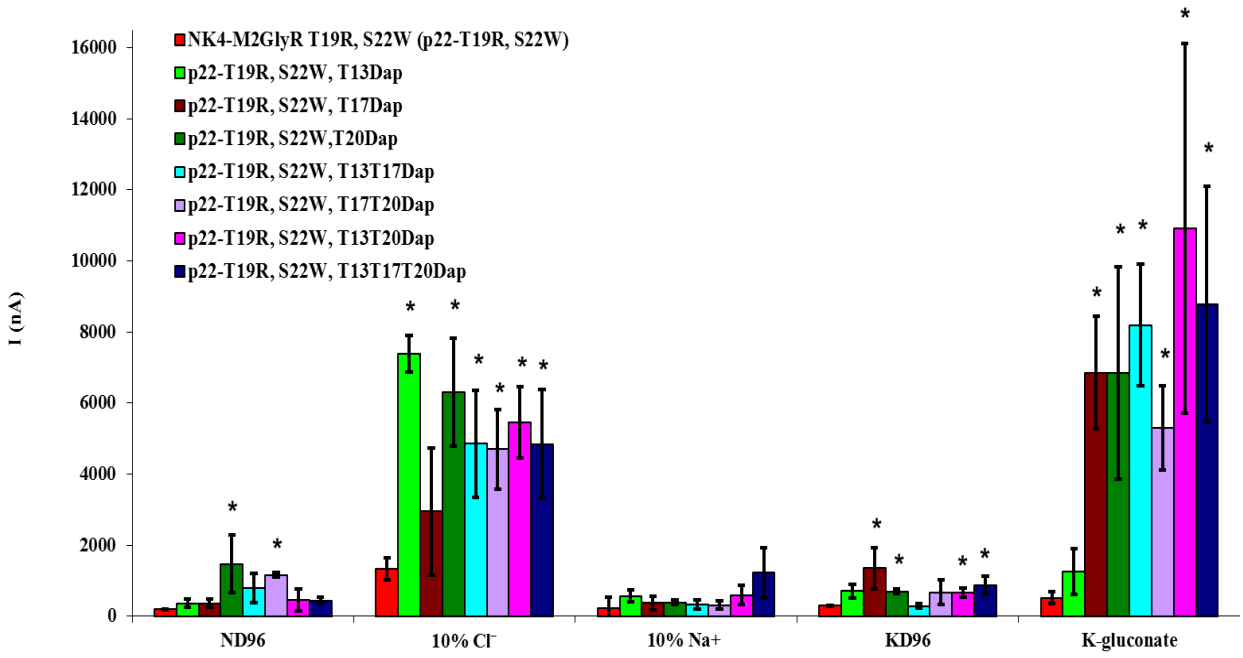

(C) Mean currents and standard errors of 3 or more experiments per peptide under each ionic condition are shown. ANOVA was used to calculate significant differences ($P<0.05$, t-test). Statistically significant differences (*) between the currents induced by a non-modified peptide p22-T19R, S22W (red colored bars) and its Dap substituted peptides inside each treatment are labeled.

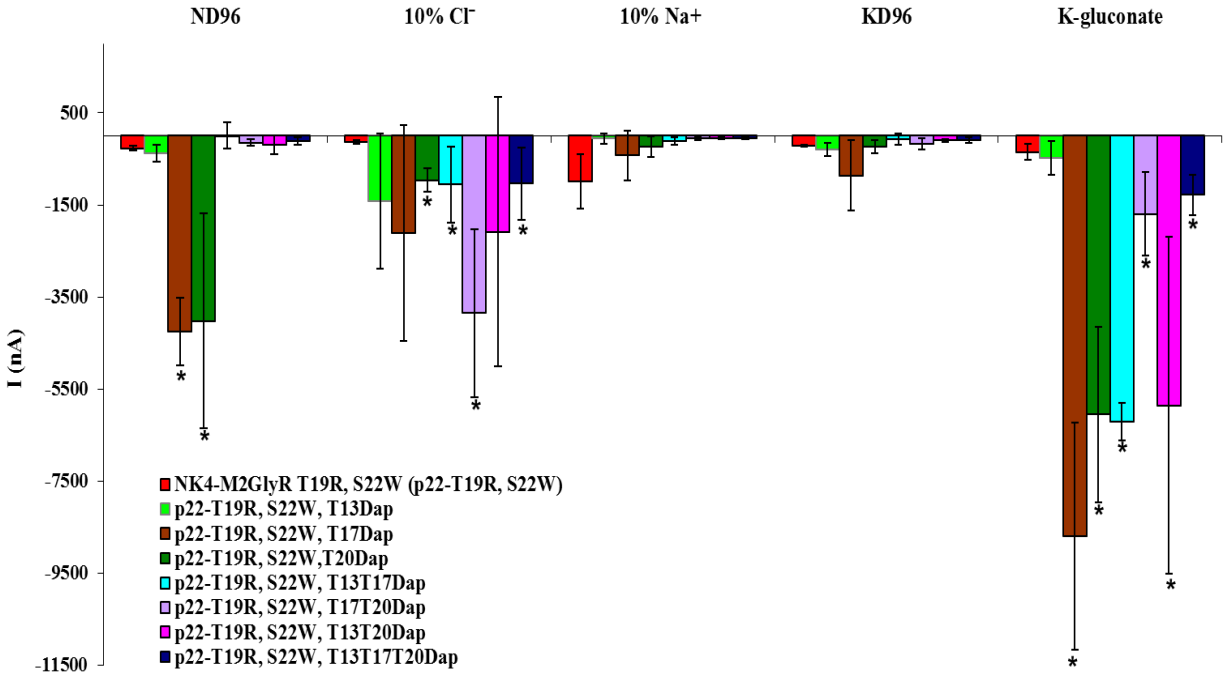

Additionally, the fold increases in peptide-induced ion currents were calculated. The data for peptide-induced currents were normalized to the background ion currents measured in the absence of peptides. The increase in peptide-induced currents depended on applied voltage and ionic conditions, therefore only the most significant fold-increase in ion currents are mentioned here, measured at -100mV and lowered [Cl^-] in external solution (10% Cl^- solution). The tri- and di- substituted peptides, T13Dap, 17Dap, T20Dap and T17Dap,T20 Dap, induced 10.47 ± 1.4 and 11.47 ± 1.2 fold increase in ion current, respectively, compared to the 2.6 ± 1.4 fold increase observed for the non-substituted peptide. However, the increases were even greater for T13Dap, T17Dap and T17Dap-substituted peptides, 68 ± 9 and 88.23 ± 33.9, respectively.

Similar results were observed for peptide-induced ion current at +60 mV, for the same peptides and under same experimental conditions.

Despite the differences in the peptide-induced ion currents under different ionic conditions, results of calculated permselectivity ratios for Cl^-/Na^+ and Cl^-/K^+ indicate lack of selectivity (**Table 2-5**).

However, the results of the analyses presented here do not address the possibility that the endogenous pathways in *Xenopus* oocyte membrane might be directly or indirectly affected by these peptides. Analyses presented in Chapter 3 address this possibility.

$^{86}Rb^+$ flux assay

The influxes of $^{86}Rb^+$ induced by all the peptides were significantly larger relative to the control sample containing peptide-free liposomes. Thus, all peptides were apparently able to insert into the liposomes membrane and form ion conductive pores (**Figure 2-13**). However, only one of three independent experiments yielded measurable fluxes leaving the experiments for the most part unsuccessful. Testing different lipid compositions and their ratios in liposome preparations await further studies. Nevertheless, our results agree with observations encountered by previous studies examining the channel-forming properties of p22 T19R, S22W peptide and its cysteine-substituted variants using lipid bilayers and liposomes. The large number of unsuccessful experiments with no channel activities detected for p22 T19R, S22W-assemblies in lipid bilayers has been attributed to the higher level of specificity of these peptides for the composition of synthetic membranes (Bukovnik et al., 2011).

Figure 2-13 $^{86}Rb^{+}$ flux assay.

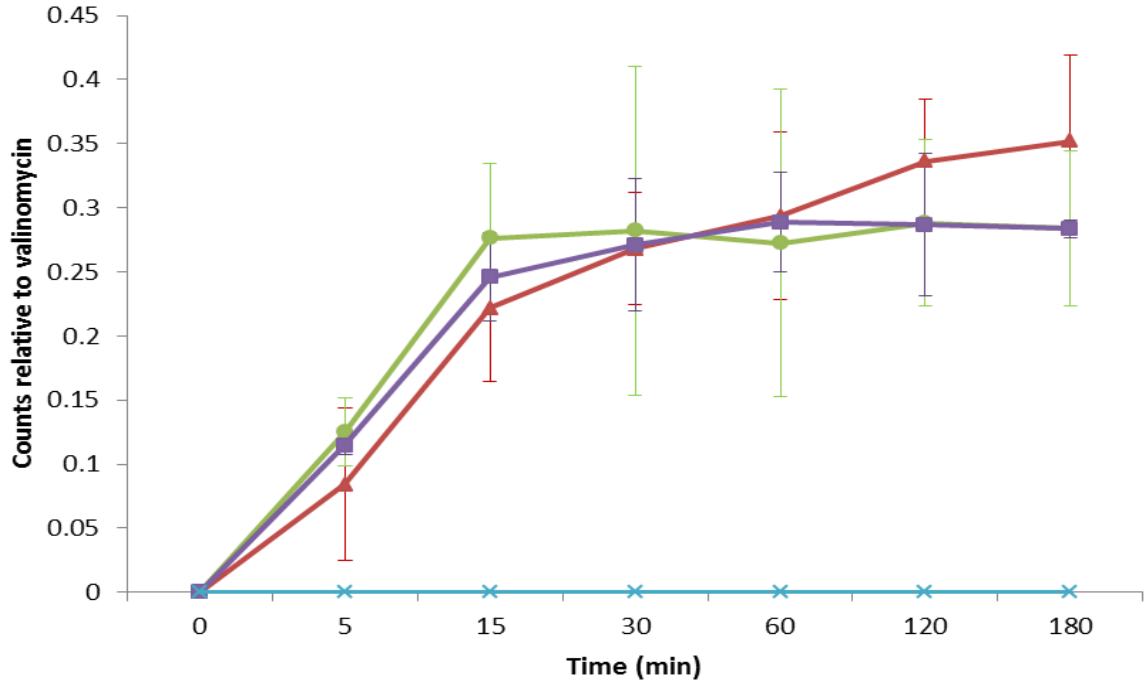

NK_4-M2GlyR p22-T19R, S22W (p22-T19R, S22W) (▲), p22-T19R, S22W, T20Dap (●) and p22-T19R, S22W, T13Dap, T17Dap (■) peptide (n=3 replicates for all peptides tested). Control (×): a sample of peptide-free liposomes.

Discussion

Properties of synthetic channel-forming peptides (CFPs) can be altered, studied systematically, characterized and redesigned to probe specific aspects of channel structure and function. The mechanisms of ion permeation and ion selectivity of CFTR remain incompletely defined and thus present a limiting factor in designs of synthetic CFPs for therapies. The p22-T19R, S22W and its Dap-substituted variants were synthesized as a part of an ongoing project aimed to design anion-selective CFPs as potential therapeutics for CF. The introduction of the cationic amino acid, Dap, into the CFP-pore lining interface was expected to modify the electrostatics of the pore, thereby increasing the ion recognition and providing favorable hydrogen bonding potential for incoming chloride ions. Preliminary computer simulations were performed (**Figure 2-14**) to examine the potential effect of Dap on the geometry and selective properties of the assembled pores. Studies were performed on both singly and doubly Dap-substituted sequences, computing the potential of mean force (PMF) profile for ion permeation. To understand better the mechanisms underlying ion conduction and selectivity of Dap-substituted peptide assemblies, the free energy profiles of K^+ and Cl^- permeation were calculated directly from data collected during 20-ns molecular dynamics simulations. The resulting PMFs suggest similar permeabilities through NK_4-M2GlyR-p22 T19R, S22W for both Cl^- and Na^+, while introduction of the cationic Dap residues favored the passage of Cl^-. The double-substituted T13Dap, T20Dap sequence showed the smallest energy wells where Cl^- could become trapped, suggesting it could be a preferred sequence (Tomich et al., 2011).

Figure 2-14 Summary of preliminary molecular modeling simulations of NK_4-M2GlyR-p22 T19R, S22W and few of the singly-and doubly-Dap-substituted NK_4-M2GlyR-p22 T19R, S22W.

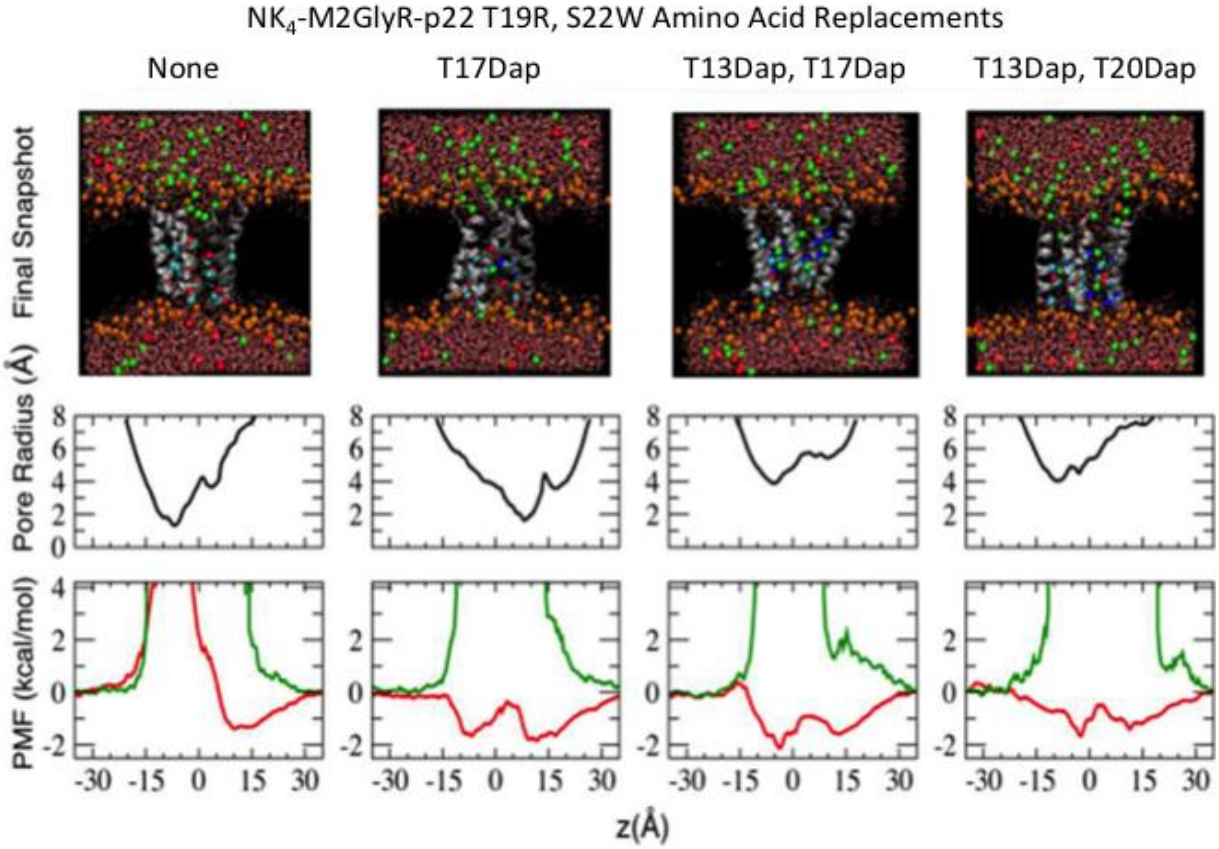

Lane 1: peptide NK_4-M2GlyR-p22 T19R, S22W (p22 T19R, S22W); **lane 2:** p22 T19R, S22W, T17Dap; **lane 3:** p22 T19R, S22W, T13Dap, T17Dap; **lane 4:** p22 T19R, S22W T13Dap, T20Dap. The durations of the simulations in POPC membrane are at least 20 ns. The pore profiles were computed using the HOLE program based on the last snapshots shown. The PMFs were computed from equilibrium ion densities. The red line signifies chloride and the green line sodium (Tomich et al., 2011).

Results for singly- and doubly-Dap-substituted peptide assemblies suggested that Dap residues affected the pore geometry by increasing the pore diameter, shifting the narrowest part of the pore from T17 to L10. Sequences with multiple Dap substitutions are predicted to increase

the diameter of the pore the most, up to 2 Å, compared to the pore diameter observed for the precedent non-substituted peptide-assemblies. This change was suggested to increase the ion conductance and allow the passage of larger anions that were previously impermeable. Experimental results are in agreement with these virtual predictions. The maximal transepithelial ion transport across the MDCK cells was the most significantly increased when cells were exposed to doubly- and triply-substituted peptide(s) (**Figure 2-8**). This suggests that introduced Dap(s) yields fundamental changes in the conductive pathway of Dap-substituted peptide assemblies. The cooperativity of monomers during insertion or assembly, reflected by the Hill coefficients, was increased for the singly substituted T13 and T17 sequences, and was the highest for doubly- and triply-substituted Dap sequences relative to the control (**Table 2-3**). These differences might suggest that at the same density of peptides in the membrane these sequences are more likely to self-associate into channels of higher association numbers. It is however possible that our Dap-substituted peptides, presumed to self-assemble into pentameric pores in MDCK cell membranes and *Xenopus* oocyte membranes, generate species of different oligomeric number accounting for distinct conductances. There is a way to control the pore assembly by the synthesis of template-assembled synthetic proteins (TASP), similarly as described before (Montal et al., 1990, Oblatt-Montal et al., 1994, Iwamoto et al., 1994; Reddy et al., 1994; Futaki et al., 1997). The approach enables the design of defined oligomer numbers with a predetermined parallel arrangement of a synthetic pore. The TASP system involves the covalent attachment of CFPs to template molecules with a set number of attachment sites. Such modules show stabilized peptide-bundle conformation and uniform ion conductances (Grove et al., 1991). Studies using TASPs having controlled channel association numbers provide evidence that the magnitude of ion conductance depends on the increasing association number in peptide

assembly (Matsubara et al., 1996; Futaki et al., 1997). Kersh and colleagues (1989) showed that synthetic peptides which are corresponding to the pore-lining segment of the nicotinic acetylcholine receptor from *Torpedo californica*, a member of the same cys-loop super family of ligand-gated channels as glycine receptor, form assemblies of different association number, predominantly with the number of monomers yielding the most stable pore assembly.

This study led to the assumption that ion-conductive properties of Dap-peptide assembled pores result from a shift from the predominantly pentameric assembly observed for their parent p22-T19R, S22W, hexameric assemblies. Homogeneity of TEVC recordings obtained with five tethered p22-T19R, S22W bundles (schematically presented in **Figure 2-15**) in lipid bilayers or transepithelial measurements using Ussing chambers with MDCK cells would enable a more precise assessment of structure-function relationships specifically pertaining to the predicted pentameric pore structure of a self-assembled p22-T19R, S22W. Although additional examination of the ion conductive properties of six or seven-helix bundle modules made of only p22-T19R, S22W peptides or only

Figure 2-15 Template-assembled synthetic protein comprising 5 helices of NK_4-M2GlyR p22 T19R, S22W.

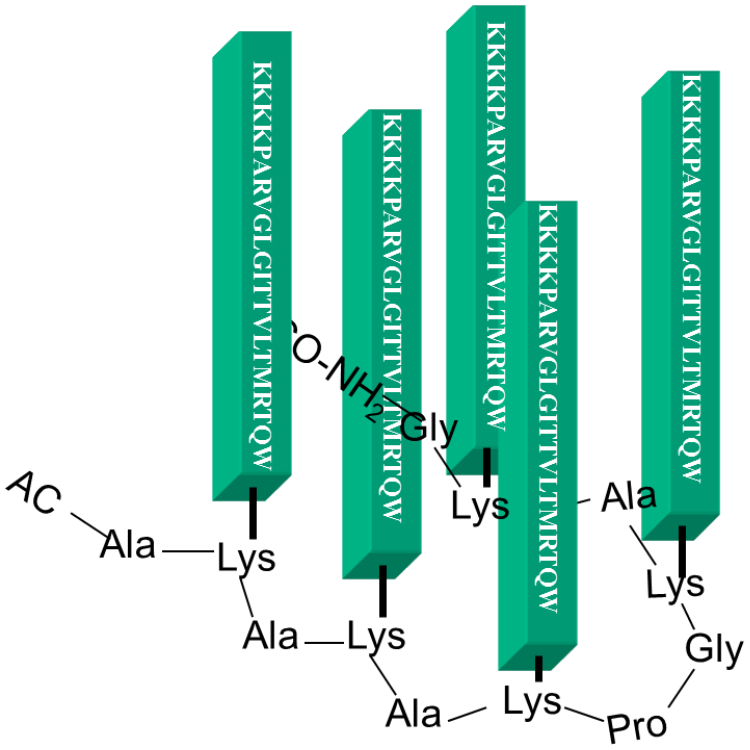

Dap-substituted p22-T19R, S22W peptides would give further insight into the mechanisms of Dap-peptides self-assembly. An attempt has already been made to synthesize the tethered pentameric p22-T19R, S22W peptide model. The synthesis was unsuccessful when performed using F-moc chemistries and high substituted resins. If the substitution number on the resin used for the synthesis is not reduced enough, then inter-assembly aggregation occurs during the peptide-chain synthesis leading to steric hindrances and unsuccessful syntheses. A solution to the problem would be to drop the resin substitution number, enlarge the template spacers between each tethered peptide and also to use the *t*-Boc chemistry throughout template and peptide synthesis.

A decrease in effective peptide concentration is desirable for a CF channel replacement therapy. We identified several Dap-substituted peptides with lower $K_{1/2}$. The non-substituted peptide p22-T19R, S22W has a $K_{1/2}$ of 155 ± 30 μM while T13Dap and T17Dap, T20 Dap-substituted peptides resume the $K_{1/2}$ values, of 116 ± 7 μM and 114 ± 5 μM, respectively, and the T20 Dap-substituted sequence has a $K_{1/2}$ value of 19 ± 0.69 μM (**Table 2-3**). With respect to this characteristic, these peptides can be considered as potential agents for further clinical studies.

Ion selectivity

Previous studies testing anion selectivity of p22 T19R, S22W in artificial bilayers composed of POPC: POPS (70:30) as well as in *Xenopus* oocytes (Shank et al., 2006) showed a slight chloride over sodium selectivity of p22 T19R, S22W-assemblies. Changes made to the sequence to increase the solubility of the monomer and proper peptide insertion into the membranes resulted in reduction of anion selectivity. Knowing the pore-lining residue positions in p22 T19R, S22W-assembled pores (Bukovnik et al., 2011); Dap substitutions in p22 T19R, S22W sequence were strategically positioned. We hypothesized that the introduction of cationic Dap residues to form rings of positive charge at crucial pore-lining positions would change the electrostatic environment of the pore's interior, resulting in enhanced ion charge discrimination. First, preliminary computer modeling studies were employed using the Potential of Mean Force (PMF) function for measuring the energy required to move different ions from one side of the simulated Dap-substituted channel to the other. The resultant models suggested that the introduction of Dap would yield a higher chloride versus sodium permeability ratio. The double substituted T13Dap, T20 Dap sequence shows the smallest energy wells where Cl^- could become trapped, suggesting it as preferred sequence (Tomich et al., 2011).

Selectivity does not necessarily depend on a specific location of charged residue within a pore's cavity, but rather on the orientations of the side chains of pore-lining residues, which must face the channel's central cavity (Bichet et al., 2006). Side chains of the pore-lining threonines in p22 T19R, S22W-assembled pore all face the pore cavity (Cook et al., 2004; Bukovnik et al., 2011), leading to the assumption that the side chains of Dap would orient the same way and interact with permeating ions. Permselectivity of assemblies of Dap-substituted peptides were

tested using whole-cell TEV recordings in *Xenopus* oocytes. Results showed voltage-dependent peptide-induced ion currents, but no selectivity for Cl^-, Na^+ or K^+. In *Xenopus* oocytes, Dap-peptides, compared to the non-substituted peptide, induce the largest ion currents when Cl^- in external solution is replaced by Na- or K-gluconate. Based on our MD simulations, the Dap-peptide-assembled pores have wider pore radii. We therefore speculate that these pores may allow the permeation of larger compounds, such as gluconate. It is possible that (at least in part) gluconate carries this current and permeates. Further experiments are required to confirm the hypothesis that Dap-substituted peptides mediate the passage of molecules as large as gluconate. One suggestion for future testing would be to assess the dose-response relationship of gluconate, using the same experimental setting as in our study, but different concentrations of K- or Na-gluconate in external solution. Measured ion currents would explain possible relationship between the magnitude of the peptide-induced currents and K-gluconate concentration. Furthermore, it is important to examine whether the sizes of Dap-peptide-assembled pores allow gluconate permeation. In this case, radioactively labeled K-gluconate could be injected into the oocytes prior to peptide exposure, using the protocol from the study of Sha and colleagues (2001). The radioactive efflux of K-gluconate measured would address whether Dap-peptide assemblies form *de novo* gluconate pathways.

Gluconate is a well-known Ca^{2+} chelator (Vanoye et al., 1999). It can reduce extracellular Ca^{2+} concentration and whereby extract Ca^{2+} from cells. When replacing monovalent anions with gluconate it is theoretically possible that reduced [Ca^{2+}] causes the increase in ion currents leading to leaky membranes. One of the ways to circumvent this problem is to supplement Ca^{2+} in the solution or to use a large monovalent anion that does not chelate Ca^{2+}, for example isethionate. In our external solutions containing either K- or Na-gluconate, the concentrations of

free Ca^{2+} and free Mg^{2+} were between 600 and 700 μM, as in a similar protocol used by Broughman et al. (2004), an appropriate range to maintain the membrane integrity. Nevertheless, if the observations of the peptide-induced ion currents at the use of K-gluconate external bath result from induced oocyte leakiness, then the currents measured independently of the peptide would also result in continuous and cumulative increase in ion currents. Typically we did not observe big increases in background leak conductance when superfusing oocytes with only buffers containing gluconate and low concentrations of Ca^{2+} and Mg^{2+}. The effects were reversible in all experiments.

The question whether the Dap-peptides are forming *de novo* ion conductive pathways or modulating the ion conductances intrinsic to the oocyte was further addressed. Preliminary studies were initiated to test the functional properties of pores assembled by p22-T19R, S22W Dap-substituted peptides using an $^{86}Rb^{+}$ flux assay. Further studies were done, using shorter peptides corresponding to different sections of a full length p22-T19R, S22W and doubly Dap-substituted peptide and the all-D- p22-T19R, S22W peptide. Findings of latter studies are described in chapter 3.

Chapter 3 - D- NK_4-M2GlyR-p22 T19R, S22W and truncated L-NK_4-M2GlyR-p22 T19R, S22W sequences

Abstract

Two-electrode voltage clamp (TEVC) recordings using *Xenopus* oocytes showed the highest ion current induced by L-NK_4-M2GlyR p22-T19R, S22W and its diaminopropionic acid (Dap) substituted sequences under ionic conditions favoring the activation of either chloride or potassium channels (Chapter 2). Because the ion flow was voltage-dependent and non-selective it was hypothesized that these observations could result from the peptide-induced modulation of ion permeating pathways endogenous to oocyte membranes. First, the studies were conducted using a series of partial segments of the full-length L-NK_4-M2GlyR p22-T19R, S22W and L-NK_4-M2GlyR p22-T19R, S22W T13Dap, T17Dap peptides. The rationale behind this set of experiments was to test whether the observed currents resulted from activation of native channels, then the peptide fragments would induce a similar outcome. Finding an increase in endogenous currents upon the addition of peptide would indicate that the currents observed in the presence of full-length L-NK_4-M2GlyR p22-T19R, S22W are a mixture, with contributions from endogenous oocyte pathways. The central segment of L-NK_4-M2GlyR p22-T19R, S22W sequence did induce significantly higher non-selective inward flow of ions, but under one set of experimental conditions (K-gluconate buffer) and at very negative voltage pulses (bellow –100 mV). Other truncated peptides corresponding to the N-terminal L-NK_4-M2GlyR p22-T19R, S22W, C-terminal L-NK_4-M2GlyR p22-T19R, S22W or di-Dap substituted central part of the L-NK_4-M2GlyR p22-T19R, S22W sequence did not induce ion currents significantly different from the endogenous background currents. The findings suggest that L-NK_4-M2GlyR p22-T19R, S22W monomer does not interact with endogenous channels present in the *Xenopus* oocyte

membrane and that the full length of the L-NK_4-M2GlyR p22-T19R, S22W sequence is required for its observed mode of action. To investigate this assumption that only an assembled L-form might interact with endogenous channels, an all D-amino acid version NK_4-M2GlyR p22-T19R, S22W peptide assembly was prepared and its physiological activity assessed in oocytes. The D-NK_4-M2GlyR p22-T19R, S22W pore is unlikely to have any binding affinity for the endogenous ion channels that might interact with the assembled L-NK_4-M2GlyR p22-T19R, S22W pore. Results from computer modeling demonstrate the different side-chain conformations and handedness of D-NK_4-M2GlyR p22-T19R, S22W. This is in agreement with results obtained with CD measurements showing the secondary structure of D-NK_4-M2GlyR p22-T19R, S22W. D-NK_4-M2GlyR p22-T19R, S22W also shows a distinct physiological profile for D-NK_4-M2GlyR p22-T19R, S22W compared to L-NK_4-M2GlyR p22-T19R, S22W, suggesting that D-NK_4-M2GlyR p22-T19R, S22W either binds and modulates endogenous ion pathways different than L-NK_4-M2GlyR p22-T19R, S22W, or, produces a *de novo* pathway with slightly different properties. The pattern of D-NK_4-M2GlyR p22-T19R, S22W-induced ion currents could be attributed to just a *de novo* pathway while the L-form has a *de novo* plus endogenous activation, or a specific chirality based interaction with different endogenous channels in the oocyte, or the D-NK_4-M2GlyR p22-T19R, S22W channel assembly has a different pore geometry. The amino acids: threonine, valine, isoleucine, tryptophan and proline, present in the sequence of all D-NK_4-M2GlyR p22-T19R, S22W peptides, are known for their strong destabilizing effect on α-helices when present in the D-conformation and could play a role. Based on these initial studies it is not possible to distinguish between these alternatives. Future experiments exploring the pore properties in artificial bilayers could eliminate some of these possibilities.

Introduction

L-NK$_4$-M2GlyR p22-T19R, S22W truncated peptides

Numerous investigations report that natural or synthetic peptide segments of full-length parental peptides or proteins, can display partial to full activity in a variety of artificial bilayer and cell systems including the regulation of ion channels. Examples include the effect of peptide neurotoxins on voltage-gated calcium channels (Pringos et al., 2011), the Arg-Gly-Asp (RGD) sequence in certain synthetic peptides with an indirect impact on potassium channels (Platts et al., 1998), the role of endogenous peptides isolated from rat brains in modulation of Ca^{2+} channels in neuronal and cardiac cells (Callewaert et al., 1989) and the role of peptides from scorpion venoms in regulation of certain chloride ion channels (Thompson et al., 2005; Fuller et al., 2004).

The idea behind our study was to test several truncated portions of L-NK$_4$-M2GlyR p22-T19R, S22W peptides for their ability to induce ion currents across the *Xenopus* oocyte membrane. They were designed to be too short to span the membrane thus preventing their traversing the membrane. Significantly induced ion currents of any of these peptides would be considered an active part of L-NK$_4$-M2GlyR p22-T19R, S22W and provide evidence that the full length L-NK$_4$-M2GlyR p22-T19R, S22W peptide has a direct or indirect effect on the function of channels intrinsic to *Xenopus* oocytes in addition to forming a *de novo* ion conducting pore.

D- NK$_4$-M2GlyR p22-T19R, S22W

Chirality is an important factor influencing functionality of biological molecules in many biological systems (Krause et al., 2000). The L-form of amino acids is by far the predominant

enantiomer in nature but D-forms are also found in certain circumstances. D-amino acids are synthesized in bacteria in response to stress (Lam et al., 2009) or are building blocks of opioid peptides from the skin of amphibians and antibacterial peptides (Kreil, 1994). In human tissues and fluids free D-amino acids are found in cerebrospinal fluid (Fisher et al., 1994), saliva, oral epithelial cells (Nagata et al., 2006) and nails (Min et al., 2010).

D-amino acid containing peptides (D-peptides) have properties that make them very attractive to the pharmaceutical industry. D-peptides are less susceptible to proteolytic degradation (Wade et al., 1990; Haack et al., 1997). Proteases primarily recognize L-configured, naturally predominant amino acids. Further, D-peptides can be taken orally as drugs and are effective for a longer time (Welch et al., 2007). In diastereomeric antimicrobial peptides, D-amino acids help abolish the difficulty of a systemic administration of several antimicrobial peptides against Gram-positive cocci, which if containing only L-amino acids, would be inactivated by components of a human blood (Braunstein et al., 2004; Pag et al., 2004). Another example is the use of D-peptides in a PIE12-trimer. PIE12-trimer is a leading anti-HIV antiviral drug candidate because D-amino acids enable high affinity binding to the region on the HIV virus essential for its successful entry into the human cells (Welch et al., 2007; Welch et al., 2010). A D-enantiomeric peptide of otherwise L-peptide antagonist of the oncoproteins that negatively regulate the activity of tumor suppressor protein p53, binds to the oncoproteins with higher affinity and specificity, and activates p53 (Liu et al., 2010). Apart from the potential for use of D-peptides in various cancer and antiviral therapies, this and many recent studies aimed at assessing the specificity of distinct binding properties of D-peptides to natural L-proteins.

The all-D amino acid NK_4-M2GlyR p22-T19R, S22W peptide with lower susceptibility to proteolytic degradation and longer efficacy should not be considered alternative to the use of

NK_4-M2GlyR p22-T19R, S22W peptides in therapies of CF. Since CF patients would be taking this compound for an extended period, the longer stability and limited proteolytic degradation of D- NK_4-M2GlyR p22-T19R, S22W would result in a systemic accumulation of the compound and have potential toxic side effects. There is little published on the long-term effects of D-peptides therapies used for chronic conditions.

In this group of studies, the D-NK_4-M2GlyR p22-T19R, S22W sequence was used in structure-function experiments. Different chirality of D-peptides (Wade et al., 1990; Krause et al., 2000) makes them suitable for examining potential ligand-receptor relationships of their L-enantiomer parent assembly (Scarborough et al., 1988). Since lipids appear to show no preference for chiral molecules, *de novo* channel-forming peptides have been shown to be active in both the all D– and all L- stereo configurations (Wade et al., 1990). A difference might be expected if in addition to forming a channel, the L-sequence also activated an endogenous channel through some chiral interaction.

Results of TEVC experiments with *Xenopus* oocytes exposed to the different NK_4-M2GlyR p22-T19R, S22W-derived peptides (Chapter 2) did not eliminate the possibility that these assemblies may act as modulators of ion channels intrinsic to *Xenopus* oocytes.

Materials and Methods

Peptide synthesis

All peptides (**Table 3-1**) were synthesized using solid-phase peptide synthesis by an Applied Biosystems model 431A peptide synthesizer (Foster City, CA) with 9-fluorenylmethoxycarbonyl (F-moc) chemistry (Carpino, 1972; Fields, 1990; Tomich et al., 1998). CLEAR amide resin, (0.3 mmol/g) (Peptides International, Louisville, KY) and L- and D-N^{α}-F-moc amino acids (Anaspec Inc., San Jose, CA) were used. The following protected amino acids were used: Arg (Pbf), Lys (*t*-Boc), Trp (*t*-Boc), Dap (*t*-Boc), Gln (Trt), Thr (tBu) for both L- or D-amino acids. F-moc deprotection, the step of cleaving the peptide off the resin and peptide protecting-group deprotection were performed as previously described in Chapter 2, under the section Materials and Methods. Purity values of 85 to 90% for the synthetic peptides were obtained by the optimizing the reaction steps and resin substitution levels during the synthesis. The purity of peptides and molecular masses and were determined using HPLC and mass spectroscopy, respectively. The peptides were lyophilized and stored as dry powders at room temperature. The C-terminal amino acids of NK_4-M2GlyR p22-T19R, S22W central (T20W), NK_4-M2GlyR p22-T19R, S22W central Dap (T20W) and NK_4-M2GlyR p22-T19R, S22W N-terminal (V15W) peptides included tryptophan at the positions indicated. Tryptophan served as a UV absorbing tag for determining accurate peptide concentrations, using UV absorbance spectroscopy.

Table 3-1: Sequences and molecular masses of L-NK_4-M2GlyR T19R, S22W, D-NK_4-M2GlyR T19R, S22W and L-NK_4-M2GlyR T19R, S22W truncated peptides.

	Name	Sequence	Molecular weight (Da)
1	L-NK_4-M2GlyR T19R, S22W	KKKKPARVGLGITTVLTMRTQW	2512.12
2	D-NK_4-M2GlyR T19R, S22W	KKKKPARVGLGITTVLTMRTQW	2512.12
3	C terminal (residues 12 to 22)	GITTVLTMRTQW	1405.68
4	Central (residues 7 to 19)	RVGLGITTVLTMRW	1601.98
5	Central Dap (T13Dap and T17Dap) (residues 7 to 19)	RVGLGIDapTVLDapMRW	1571.96
6	N-terminal (residues 1 to 14)	KKKKPARVGLGITTW	1682.09

CD analysis of D-NK_4-M2GlyR T19R, S22W

Analyses were conducted as described in Chapter 2 (Section Materials and Methods, CD analysis) and the spectra obtained with an average of five scans. The only difference was that D-NK_4-M2GlyR T19R, S22W was dissolved in 50% TFE in water instead of 40% TFE in water, as in experiments with NK_4-M2GlyR T19R, S22W Dap-substituted peptides. There was no significant difference in the D-NK_4-M2GlyR T19R, S22W's secondary structure observed when the peptide was dissolved in 40 (*data not shown*) or 50% TFE solution.

Electrophysiology

Two-microelectrode-voltage clamp (TEVC) measurements

Xenopus oocytes were measured by TEVC methodology to test induced ion current and selectivity for all of the peptides. The protocols used were the same as those described previously in Chapter 2 (Section Materials and Methods). The only modification was the choice of external solutions: only ND96, 10% Cl^- and K-gluconate buffers were used. This choice was made based

on the observation that superfusion with solutions containing high concentration of Na-gluconate or K-gluconate produced greater increase in ion currents associated with most of the NK_4-M2GlyR T19R, S22W-Dap substituted peptides (**Chapter 2, Figures 2-12B and C**).

Results

L-NK_4-M2GlyR T19R, S22W and L-NK_4-M2GlyR T19R, S22W truncated peptides

TEVC recordings using *Xenopus* oocytes were employed to examine the effect of L-NK_4-M2GlyR T19R, S22W and truncated L-NK_4-M2GlyR T19R, S22W peptides on ion current and selectivity. These were assessed from the resultant ion-dependent changes in V_{rev}. Typical results of the peptide-induced ion flow under conditions of ND96 are summarized in **Figure 3-1**. The full-length L-NK_4-M2GlyR T19R, S22W peptides induces significantly higher voltage-dependent ion current compared to L-NK_4-M2GlyR T19R, S22W truncated peptides. None of these peptides induced current equal or higher than the full length peptide. Concomitant reduction in bath [Na^+] and [Cl^-] resulted in significantly higher inward voltage-dependent current induced by the peptide corresponding to the central part of L-NK_4-M2GlyR T19R, S22W but not by either the truncated peptides or the full-length L-NK_4-M2GlyR T19R, S22W (**Figure 3-2**). Other truncated peptides did not induce amplitudes of ion current equal of higher from the background current (data not shown). **Figure 3-3** shows that the observed current amplitudes induced by the Central peptide were not an artifact of the oocytes becoming leaky. The currents measured independently of the peptide did not result in continuous and cumulative increase in ion currents.

Figure 3-1 I-V plot summarizing data on exposure of oocytes to L-NK$_4$-M2GlyR T19R, S22W and L-NK$_4$-M2GlyR T19R, S22W truncated peptides measured in ND96.

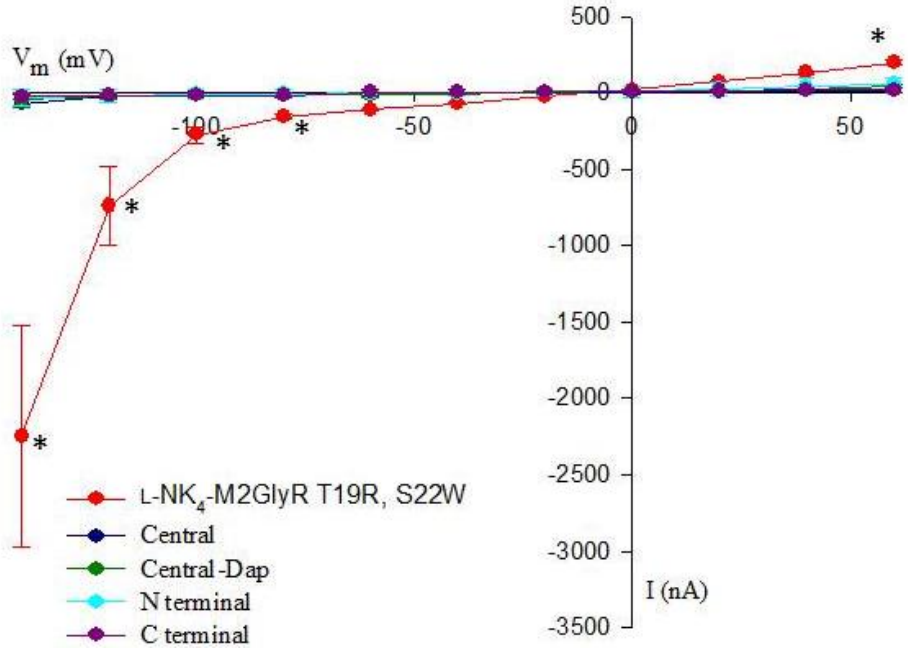

Central = central part of L-NK$_4$-M2GlyR T19R, S22W (7th to 19th amino acid residue); **Central-Dap** = central part of L-NK$_4$-M2GlyR T19R, S22W with T13Dap and T17Dap (7th to 19th amino acid residue), **N terminal** = N-terminal part of L-NK$_4$-M2GlyR T19R, S22W (1st to the 14th amino acid residue), **C terminal** = C-terminal part of L-NK$_4$-M2GlyR T19R, S22W (12th to the 22nd amino acid residue). Summary of $n \geq 4$ experiments per peptide (50 μM) with oocytes from 3 frogs. The background currents measured in the absence of peptide under conditions of ND96 solution have been subtracted to show only the peptide-induced currents. Asterisks indicate significantly different currents induced by L-NK$_4$-M2GlyR T19R, S22W compared to L-NK$_4$-M2GlyR T19R, S22W truncated peptides.

Figure 3-2 I-V plot summarizing data on exposure of oocytes to L-NK$_4$-M2GlyR T19R, S22W and L-NK$_4$-M2GlyR T19R, S22W truncated peptides measured in K-gluconate solution.

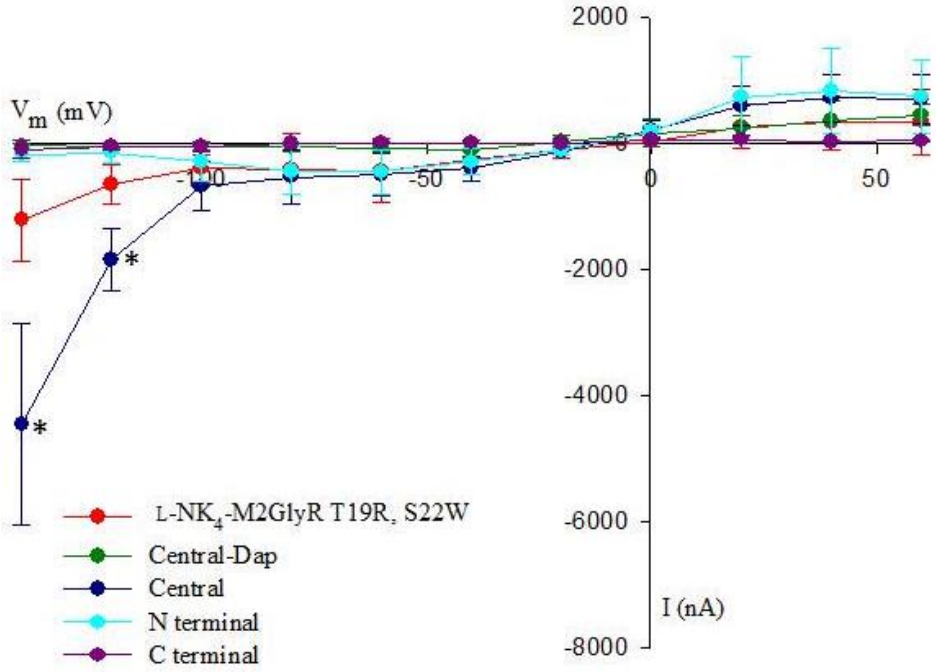

Central = central part of L-NK$_4$-M2GlyR T19R, S22W (7th to 19th amino acid residue); **Central-Dap** = central part of L-NK$_4$-M2GlyR T19R, S22W T13 Dap and T17Dap (7th to 19th amino acid residue), **N terminal** = N-terminal part of L-NK$_4$-M2GlyR T19R, S22W (1st to the 14th amino acid residue), **C terminal** = C-terminal part of L-NK$_4$-M2GlyR T19R, S22W (12th to the 22nd amino acid residue). Summary of $n \geq 4$ experiments per peptide (50 μM) with oocytes from 2 to 3 frogs. The background currents measured in the absence of peptide have been subtracted to show only the peptide-induced currents. Asterisks indicate significantly different currents induced by Central-NK$_4$-M2GlyR T19R, S22W compared to L-NK$_4$-M2GlyR T19R, S22W and other truncated peptides.

Figure 3-3 I-V plot summarizing data on exposure of oocytes to the Central L-NK$_4$-M2GlyR T19R, S22W truncated peptide measured in K-gluconate solution.

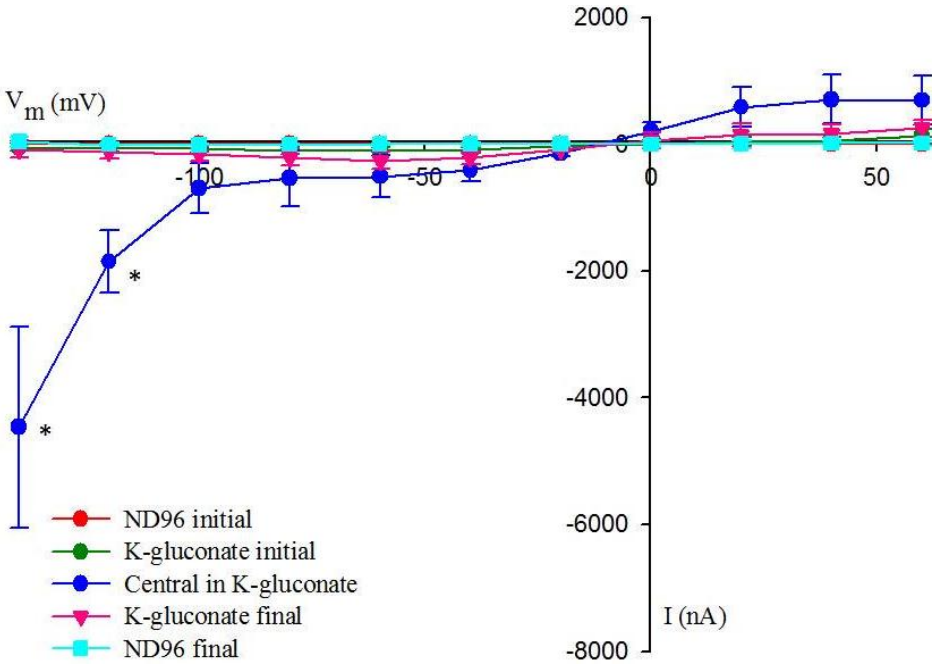

Central = the central part of L-NK$_4$-M2GlyR T19R, S22W peptide (7th to 19th residue); **ND96 initial** = superfusion of oocytes for 10 minutes with ND96 buffer at the beginning of the experiment; **K-gluconate initial** = superfusion of oocyte with K-gluconate solution (10 min); **Central in K-gluconate** = currents induced at the 10th of exposure of oocyte to the truncated peptide with a sequence corresponding to the central part of L-NK$_4$-M2GlyR T19R, S22W, dissolved in K-gluconate buffer; **K-gluconate final** = superfusion of oocyte with K-gluconate solution for 10 minutes, after the exposure to the peptide; **ND96 final** = final superfusion of oocyte with ND96 buffer for 10minutes; Summary of 4 experiments ± S.E.M. per peptide (50 μM) from 2 frogs. Asterisks indicate significant currents induced by Central- L-NK$_4$-M2GlyR T19R, S22W compared to the background currents.

In another set of experiments testing K or Na-gluconate substitutions of [Cl^-], the truncated peptides failed to induce currents different from those of the endogenous currents (*data not shown*). Thus, the inward and outward currents induced by truncated peptides were compared to those induced by the full-length parent peptide. The difference was most pronounced for peptide-induced outward currents ($P<0.05$, t-test; indicated by asterisks) (**Figure 3-4**).

The reversal potentials, V_{rev}, measured in external solution in the absence (control) or the presence of truncated peptides are given in **Table 3-2**. There was no significantly different peptide-induced shift in V_{rev} relative to the background V_{rev} measured in the absence of peptides ($P<0.05$, t-test).

Table 3-2 Reversal potentials measured at exposure of oocytes to L-NK_4-M2GlyR T19R, S22W truncated peptides.

Ionic solution	N-terminal	C-terminal	Central	Central-Dap	Control
ND96	−17 ± 3 (n=3)	−27 ± 9 (n=4)	−27 ± 6 (n=3)	−26 ± 2 (n=3)	−5 ± 8 (n=37)
10% Cl^-	−28 ± 7 (n=3)	−26 ± 3 (n=3)	−30 ± 1 (n=4)	−31 ± 7 (n=4)	−33 ± 5 (n=11)
K-gluconate	−17 ± 3 (n=4)	−17 ± 2 (n=3)	−13 ± 2 (n=4)	−16 ± 4 (n=3)	−21 ± 6 (n=14)

Central = central segment of L-NK_4-M2GlyR T19R, S22W (7^{th} to 19^{th} amino acid residue); **Central-Dap** = central segment of L-NK_4-M2GlyR T19R, S22W T13Dap and T17Dap (7^{th} to 19^{th} amino acid residue), **N terminal** = N-terminal segment of L-NK_4-M2GlyR T19R, S22W (1^{st} to the 14^{th} amino acid residue), **C terminal** = C-terminal segment of L-NK_4-M2GlyR T19R, S22W (12^{th} to the 22^{nd} amino acid residue). Data are shown as mean (mV) ± S.E.M for n samples. V_{rev} measured at exposure of oocytes to each buffer in absence of peptides are given in a Control column.

Figure 3-4 I-V plot summarizing data in exposure of oocytes to L-NK$_4$-M2GlyR T19R, S22W and L-NK$_4$-M2GlyR T19R, S22W truncated peptides measured in 10% Cl^- solution.

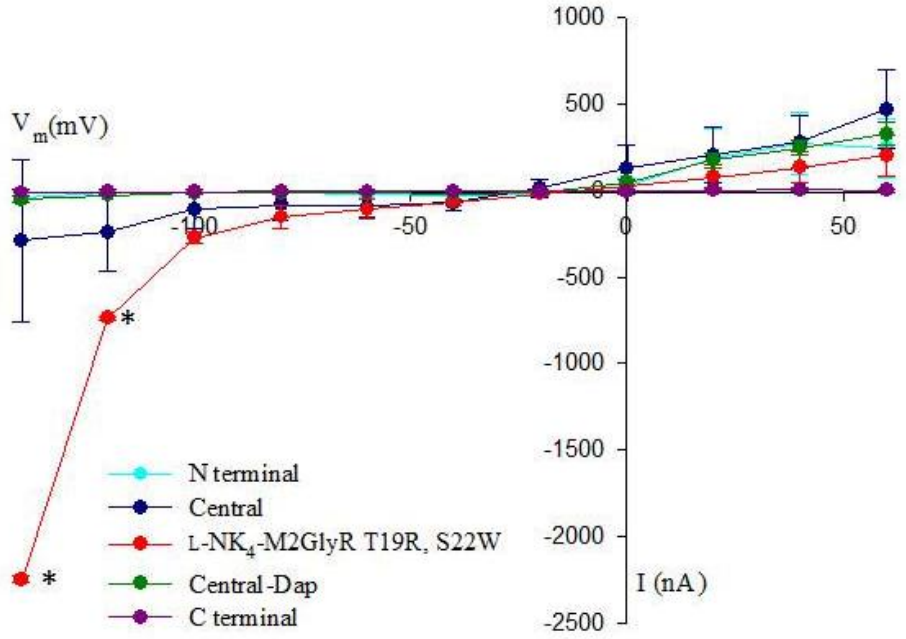

Central = central part of L-NK$_4$-M2GlyR T19R, S22W - (7th to 19th amino acid residue); **Central-Dap** = central part of L-NK$_4$-M2GlyR T19R, S22W with T13Dap and T17Dap (7th to 19th amino acid residue), **N terminal** = N-terminal part of L-NK$_4$-M2GlyR T19R, S22W (1st to the 14th amino acid residue), **C terminal** = C-terminal part of L-NK$_4$-M2GlyR T19R, S22W (12th to the 22nd amino acid residue). Summary of $n \geq 4$ experiments per peptide (50 μM) with oocytes from 2 to 3 frogs. The background currents measured in the absence of peptides have been subtracted to show only the peptide-induced currents. Asterisks indicate significant currents induced by a full length L-NK$_4$-M2GlyR T19R, S22W peptide compared to the currents induced by exposure of oocyte to truncated peptides.

Secondary structure and biophysical properties of D- NK_4-M2GlyR T19R, S22W

Secondary structure of D- NK4-M2GlyR T19R, S22W

D-NK_4-M2GlyR T19R, S22W, at a final concentration of 100 μM, in 50% TFE in water adopted α-helical structure with characteristic minimum near 192 and maxima near 208 and 222 (**Figure 3-5**). Circular dichroism spectroscopy indicated that D-NK_4-M2GlyR T19R, S22W generates a mirror image spectrum compared to the L-NK_4-M2GlyR T19R, S22W peptide (Cook et al., 2004; Shank et al., 2006; Herrera et al., 2010; Bukovnik et al., 2011). The effect is due to contribution from the profoundly different side chain topologies and opposite helical handedness between right handed D- and left handed L-enantiomers of NK_4-M2GlyR T19R, S22W as shown in our preliminary molecular models (**Figure 3-6**).

Figure 3-5 Secondary structure of D-NK_4-M2GlyR T19R, S22W in 50% TFE in water.

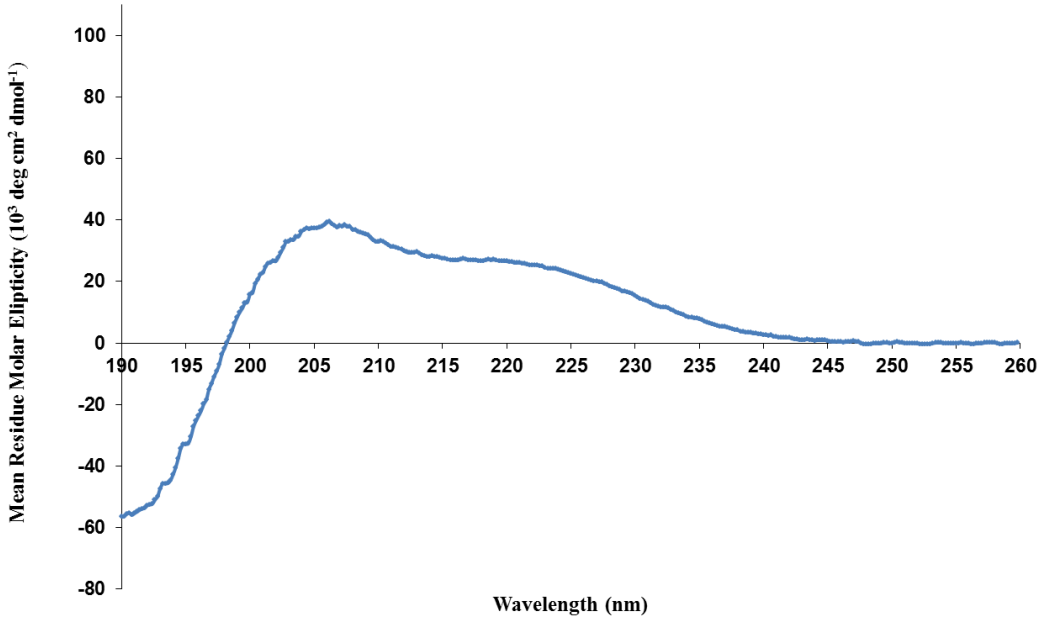

Figure 3-6 Modeled L-NK_4-M2GlyR T19R, S22W overlaid with D-NK_4-M2GlyR T19R, S22W

This model was prepared by Dr. Jianhan Chen. It illustrates the orientations of residue side chains for L-NK_4-M2GlyR T19R, S22W (blue and red) relative to D-NK_4-M2GlyR T19R, S22W (green).

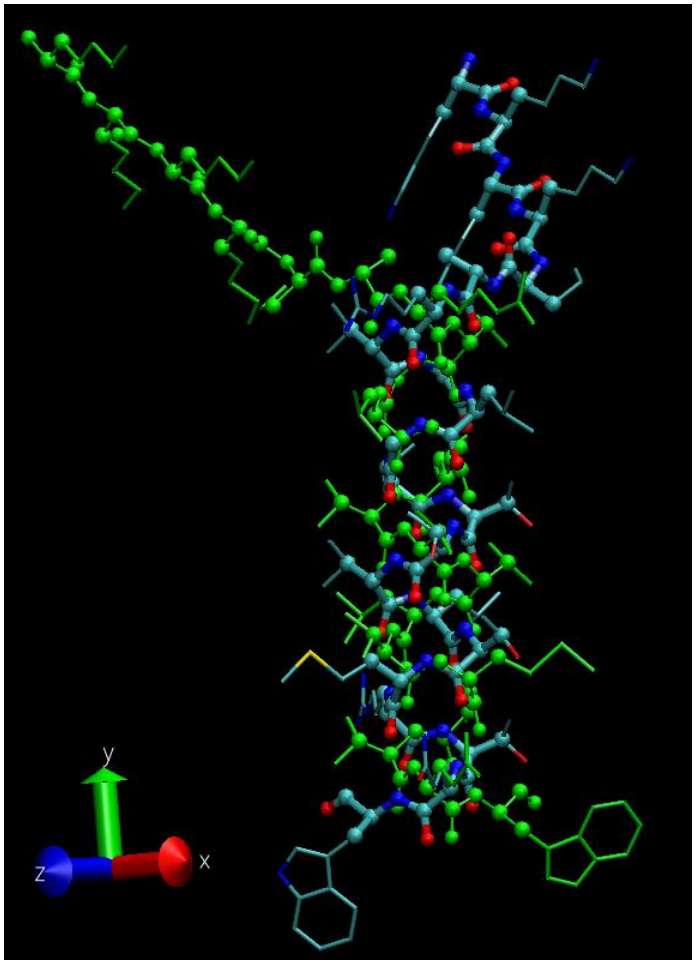

Biophysical properties of D-NK$_4$-M2GlyR T19R, S22W

The ion currents and permselectivity induced by exposure of oocytes to D-NK$_4$-M2GlyR T19R, S22W were examined. The whole-cell D-NK$_4$-M2GlyR T19R, S22W-induced I-V relationship showed a different, voltage-dependent increase in ion current relative to L-NK$_4$-M2GlyR T19R, S22W. In ND96, D-NK$_4$-M2GlyR T19R, S22W-induced smaller inward and outward currents than those measured for L-NK$_4$-M2GlyR T19R, S22W (**Figure 3-7**).

To determine whether D-peptide-induced current was sensitive to changes in external concentration of [K^+] and [Cl^-], currents were measured in the presence of 10% Cl^- and K-gluconate buffer. **Figure 3-8** summarizes the current induced by D-peptide compared to L-peptide. The mean values of peptide-induced currents shown in the figure were obtained by subtracting the background currents measured under the same experimental conditions in the absence of peptide. Relative to the L-NK$_4$-M2GlyR T19R, S22W sequence, D-NK$_4$-M2GlyR T19R, S22W induced an increase of inward current at voltages more negative than –80 mV and an increase of outward current at +60 mV. Little to no change in whole-cell current was seen when oocytes were superfused with K-gluconate buffer only, thus providing evidence that the increase in ion currents observed in cells treated with peptides was unlikely the result of an increase in background leak current. **Figure 3-9** shows a significant increase in peptide-induced currents compared to the background current measured before and after the peptide treatment. The background currents were reversed after the peptide treatment. The same pattern of current reversibility was observed in all our experiments.

Figure 3-7 I-V plot summarizing data on exposure of oocytes to L-NK_4-M2GlyR T19R, S22W and D-NK_4-M2GlyR T19R, S22W measured in ND96 solution.

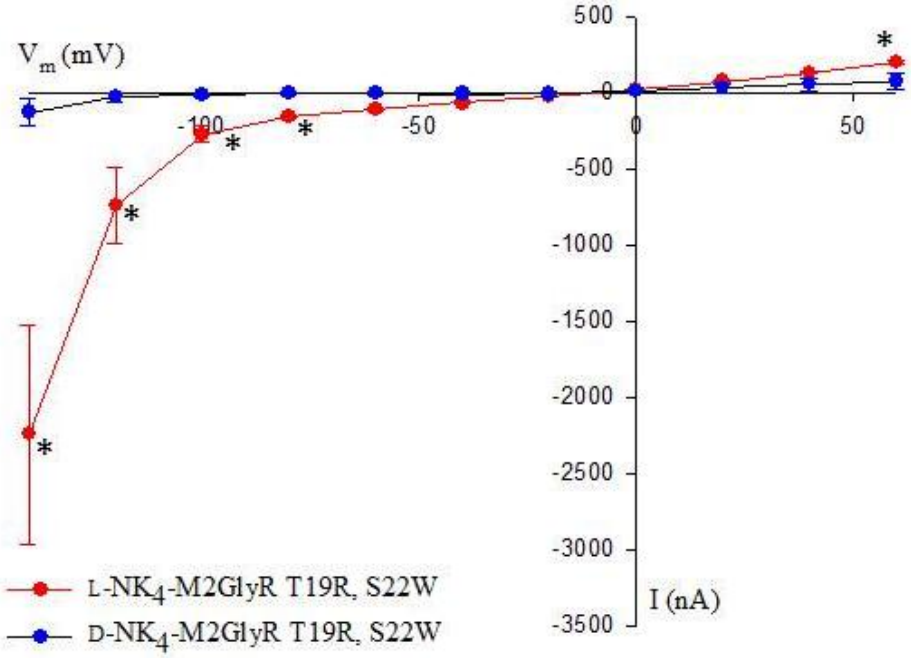

I-V relation shown was obtained by exposure of oocytes to the peptide L-NK_4-M2GlyR T19R, S22W in ND96 or D-NK_4-M2GlyR T19R, S22W in ND96 for 10 minutes. The plots represent the mean with an n > 4 experiments per peptide (50 μM) with oocytes from 3 frogs. The mean background-subtracted currents are plotted at voltages from –140 mV to +60 mV. Error bars indicate the S.E.M. Asterisks indicate significantly different currents induced by exposure of oocytes to D-NK_4-M2GlyR T19R, S22W compared to L-NK_4-M2GlyR T19R, S22W ($P<0.05$; t-test).

Figure 3-8 Effect of external K-gluconate solution on I-V relationship obtained by exposure of oocytes to L-NK$_4$-M2GlyR T19R, S22W and D-NK$_4$-M2GlyR T19R, S22W.

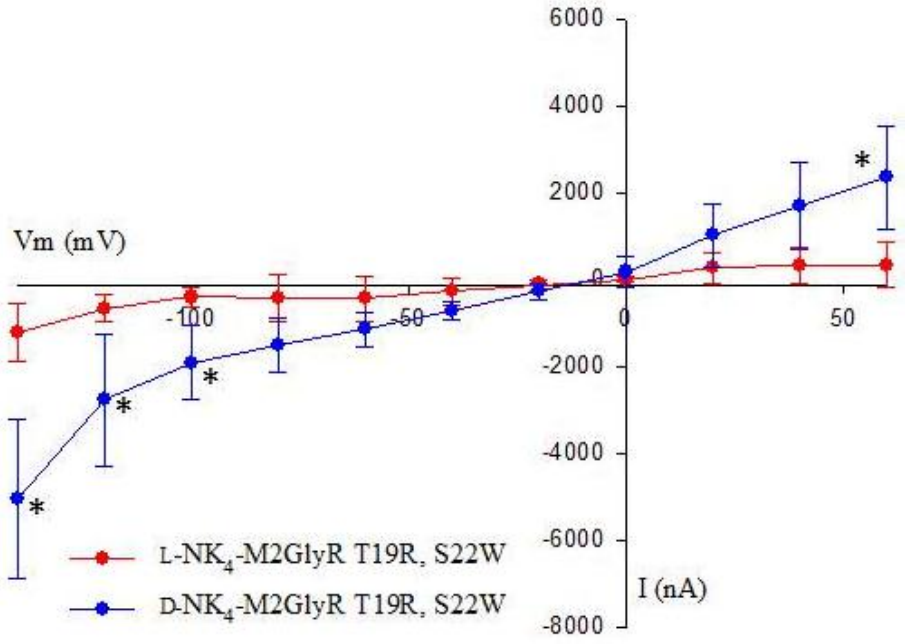

I-V plot summarizes currents induced by exposure of oocytes to the peptide L-NK$_4$-M2GlyR T19R, S22W and D-NK$_4$-M2GlyR T19R, S22W in K-gluconate solution for 10 minutes. Summary of n=4 ± S.E.M. per peptide (50 μM) with oocytes from 3 to 4 frogs. The mean background-subtracted currents are plotted at voltages from –140 mV to +60 mV. Error bars indicate the S.E.M. Asterisks indicate significantly different currents induced by exposure of oocytes to D-NK$_4$-M2GlyR T19R, S22W compared to L-NK$_4$-M2GlyR T19R, S22W ($P<0.05$; t-test).

Figure 3-9 I-V plot summarizing data on exposure of oocytes to D-NK$_4$-M2GlyR T19R, S22W measured in K-gluconate solution.

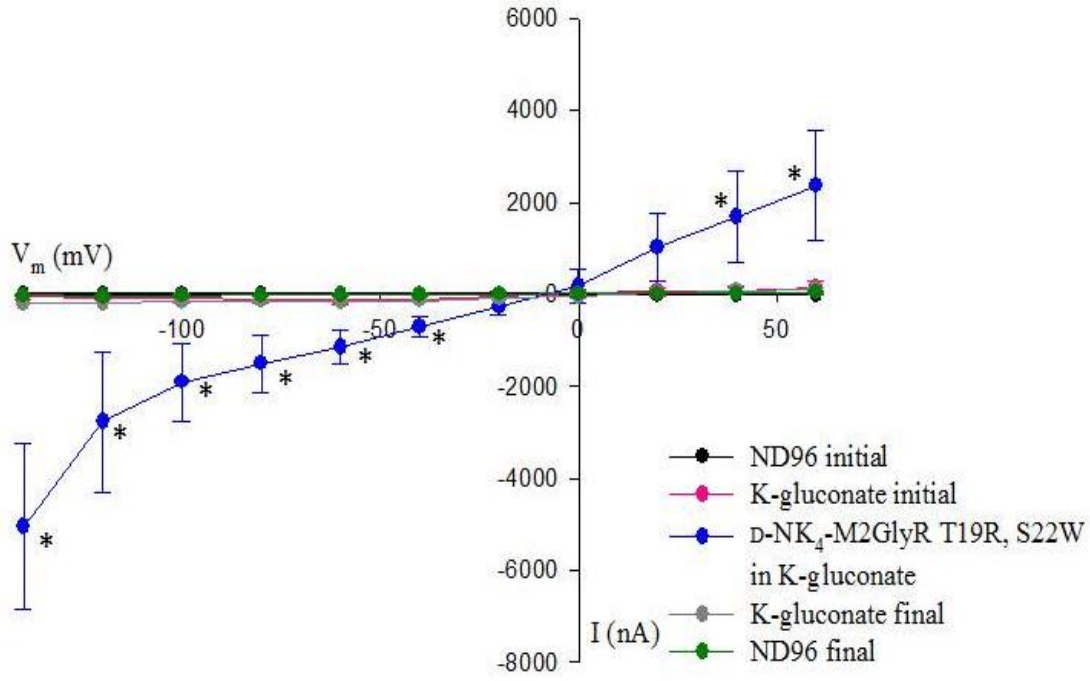

ND96 initial = superfusion of oocytes (10 min) with ND96 solution at the beginning of the experiment; **K-gluconate initial** = superfusion with K-gluconate solution (10 min); **D-NK$_4$-M2GlyR T19R, S22W in K-gluconate** = exposure of oocyte to the peptide in K-gluconate solution (10 min); **K-gluconate final** = superfusion with K-gluconate solution (10 min) after the exposure of oocyte to the peptide; **ND96 final** = final superfusion with ND96 (10 min); Summary of n = 6 experiments ± S.E.M. per peptide (50 µM) with oocytes from 4 frogs. The mean currents are plotted at voltages from –140 mV to +60 mV. Error bars indicate the S.E.M. Asterisks indicate different currents induced by D-NK$_4$-M2GlyR T19R, S22W compared to the background currents ($P<0.05$; t-test).

To determine whether D-peptide-induced current was sensitive to changes in external [Cl^-], chloride was substituted by gluconate while leaving [K^+] and [Na^+] constant. Thus, if D-NK_4-M2GlyR T19R, S22W induces anion selective ion currents, the inward current would be expected to increase. This increases the driving force for chloride efflux by lowering the external chloride concentration. At the same time, a shift in V_{rev} induced by the peptide treatment relative to the V_{rev} induced by the background would indicate anion selective permeability.

Figure 3-10 shows the I-V relations induced by D-NK_4-M2GlyR T19R, S22W and L-NK_4-M2GlyR T19R, S22W peptide. D-NK_4-M2GlyR T19R, S22W induced a significantly higher inward and outward current, as well as small shift in V_{rev}, 2.3 ± 2.0 mV (n=3) in 10% Cl^- solution and a small shift in V_{rev} in K-gluconate solution, 4.5 ± 2.0 mV (n=3) (**Table 3-3**). The permselectivity ratios ranged from 1.06 ± 0.05 (n=3) for Cl^- over Na^+, and 0.99 ± 0.01 (n=3) for Cl^- over K^+, suggest that there was no permselectivity between these monovalent ions.

Figure 3-10 I-V plot summarizing data on exposure of oocytes to L-NK_4-M2GlyR p22-T19R, S22W and D-NK_4-M2GlyR T19R, S22W measured in 10% Cl^- solution.

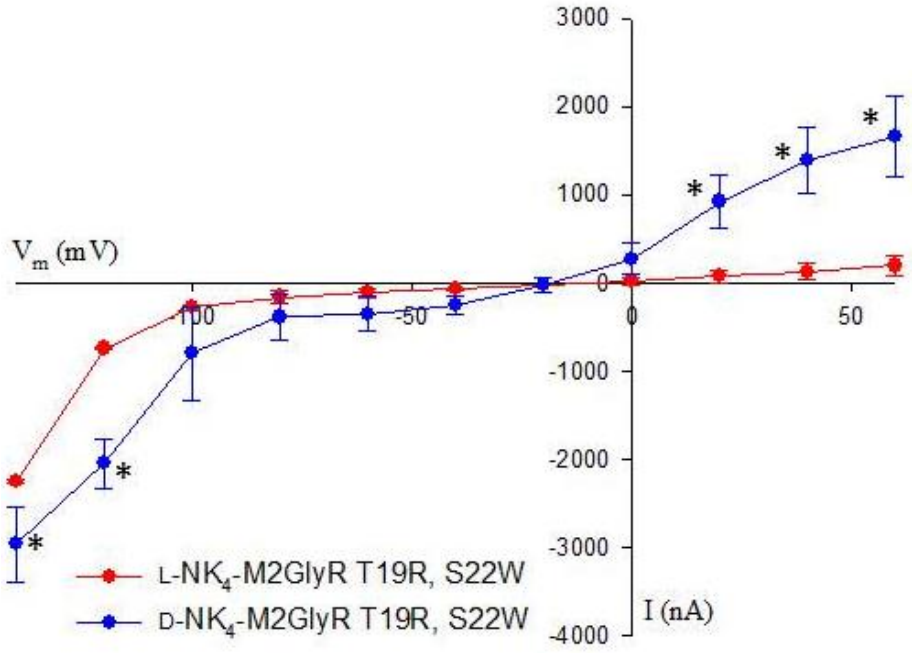

L-NK_4-M2GlyR T19R, S22W = exposure of oocyte to L-NK_4-M2GlyR p22-T19R, S22W in 10% Cl^- buffer for 10 minutes; D-NK_4-M2GlyR T19R, S22W = exposure of oocyte to all-D-NK_4-M2GlyR p22-T19R, S22W in 10% Cl^- for 10 minutes; Summary of n = 4 ± S.E.M. per peptide (50 µM) with oocytes from 3 to 4 frogs. The mean background-subtracted currents are plotted at voltages from –140 mV to +60 mV. Error bars indicate the S.E.M. ANOVA was used to calculate significant differences ($P<0.05$, t-test). Asterisks indicate different currents induced by D-NK_4-M2GlyR T19R, S22W.

Table 3-3 Shifts in reversal potential measured by solution changes performed on oocytes exposed to D-NK_4-M2GlyR T19R, S22W.

A difference in reversal potential ΔV_{rev} was calculated using the values of V_{rev} measured in oocytes exposed to each external solution in the absence or the presence of D-peptide. Data are shown as mean (mV) ± S.E.M for n samples.

External solution	ΔV_{rev} -NK_4-M2GlyR T19R, S22W
ND96	5.0 ± 1.7 (n=3)
10% Cl^-	2.3 ± 2.08 (n=3)
K-gluconate	4.5 ± 2 (n=3)

Discussion

L-NK_4-M2GlyR T19R, S22W truncated peptides and D-NK_4-M2GlyR T19R, S22W

Relative to NK_4-M2GlyR T19R, S22W, the Dap-substituted NK_4-M2GlyR T19R, S22W peptides induce the highest increase in ion currents across the *Xenopus* oocyte membranes when the extracellular solution is switched from high [NaCl] to high [Na-gluconate] or high [K-gluconate]. Here we examine the controversy whether the Dap-substituted peptides and their parent peptide solely forms a *de novo* ion conductance pathway, modulates conductances intrinsic to *Xenopus* oocytes or are a combination of both effects.

The truncated peptides of L-NK_4-M2GlyR T19R, S22W and L-NK_4-M2GlyR T19R, S22W T13Dap, T17Dap were synthesized and tested for their ability to induce ion flow across the *Xenopus* oocyte membrane. Assuming a thickness of the membrane lipid bilayer of about 28.5Å for the hydrophobic acyl core, a 4.5Å pitch of the turn in α-helix and 3.6 amino acid

residues per turn the predicted minimal length of peptide to span the membrane would be 18 amino acid residues. The lengths of our truncated peptides were below 15 amino acid residues.

The sequence (RVGLGITTVLTMRW) corresponding to the central segment of a full length L-NK_4-M2GlyR T19R, S22W (with a descriptive name, Central) induced significantly higher inward flow of ions relative to the background currents of *Xenopus* oocytes. The activity was observed only under very negative voltages (> –100mV) and when extracellular solution was switched from high [NaCl] to high [K-gluconate] (**Figure 3-8**). The sequence of the Central L-NK_4-M2GlyR T19R, S22W corresponds to the most hydrophobic part of the full-length peptide. The peptide does contain residues (R and W) that show preference for interfacial localization. Thus the activity of the Central truncated peptide could be attributed to its hydrophobic nature in combination of the C-terminal tryptophan membrane-seeking anchoring properties as well as the oriented dipole moments of its side chain (Kelkar and Chattopadhyay, 2007). This means the Central truncated peptides could reach the membrane embedded regions of endogenous channels, where it could bind and thus modulate channel activities. It would also adopt an alternate orientation in which the WR and R residues both reside at the water-membrane interface with the hydrophobic region partially inserting in a bowed manner into the hydrophobic core. The peptide-induced ion currents are significantly larger compared to the background currents only in the presence of extracellular K-gluconate buffer (**Figure 3-8**). Under the same experimental conditions, the full length L-NK_4-M2GlyR T19R, S22W peptide induced a different pattern of current amplitudes (**Figures 3-7 to 3-10**). If the Central truncated peptide adopted an orientation similar to the full-length peptide in the bilayer thereby recapitulating the activating portion of the full-length parent peptide, then we would expect to see a similar pattern of current amplitudes induced by this peptide. This was not observed.

The sequences of other truncated peptides corresponding to the N-terminal and C-terminal parts of NK_4-M2GlyR T19R, S22W or the middle part of di-Dap substituted L-NK_4-M2GlyR T19R, S22W also possessed the C-terminal tryptophan, but were less hydrophobic compared to the central NK_4-M2GlyR T19R, S22W segment. With such properties, these peptides were more likely to bind to the solvent-exposed parts of endogenous channels of *Xenopus* oocyte membrane. None of these truncated peptides showed the ability to induce significantly higher ion current compared to background currents, suggesting that these peptides do not and likewise the full-length peptide do not have extracellular or interfacial activating domains that alter the activities of channels intrinsic to *Xenopus* oocytes. To further clarifying the membrane binding properties of the truncated peptides used in this study, binding studies using lipid vesicles and measurements of blue shift of the Trp could more directly assess the position of these peptide fragments relative to the parent sequence.

Nevertheless, the present results suggest that the full length L-NK_4-M2GlyR T19R, S22W is required for inducing detected in our studies (Chapter 2 and 3) and that ion currents induced by this peptide most likely do not result from modulation of intrinsic conductances. It is possible that only the assembled sequences having more fixed geometries activate intrinsic oocyte conductances. To further test this possibility, the activity of all-D-amino acid D-NK_4-M2GlyR T19R, S22W peptide was tested and found to assemble and produce *de novo* conductances. If the L-NK_4-M2GlyR T19R, S22W acts as a modulator of certain endogenous channels, then a D-configuration of this peptide, having a significantly different orientation of side chains, would prevent and/or eliminate the binding of D-peptide to the same endogenous channels and provide further evidence of the activity of its L-peptide (**Figure 3-2**). This hypothesis does not preclude the binding of the D- assembly with different ion-conducting molecules in the oocyte.

The D-NK_4-M2GlyR T19R, S22W peptide induced a voltage-dependent and non-selective ion current across the *Xenopus* oocyte membrane. A change in bath solution from ND96 to K-gluconate buffer resulted in D-NK_4-M2GlyR T19R, S22W-induced, voltage-dependent increase of inward and/or outward ion flows relative to the L-sequence (**Figure 3-8**). Substitution of ND96 with external solution with lowered [Cl^-] and physiological levels of [K^+] and [Na^+] (10% Cl^- buffer), resulted in a significantly higher increase in inward ion flow induced by exposure of oocytes to the D-peptide (**Figure 3-10)**. There was a small shift in V_{rev} induced by D-NK_4-M2GlyR T19R, S22W, 2.3 ± 2.0 mV (n=3) (10%Cl^- solution) and a small shift in V_{rev} induced by D-NK_4-M2GlyR T19R, S22W (K-gluconate solution) 4.5 ± 2.0 mV (n=3), relative to V_{rev} induced by endogenous oocyte channels under same conditions (**Table 3-3**). The Cl^- -to-Na^+ permselectivity of 1.06 ± 0.05 (n=3), and Cl^- -to- K^+ permselectivity of 0.99 ± 0.01 (n=3) for Cl^- over K^+, suggested no selectivity between these monovalent ions.

It has been previously shown that D-enantiomers of naturally occurring L-antibiotics possess the same mode of action in artificial bilayers and form ion channels similar but not identical to the corresponding L-enantiomer parent peptides (Wade et al., 1990). A distinct D- versus L-NK_4-M2GlyR T19R, S22W peptide-induced ion current could be attributed to a different geometry of the D-NK_4-M2GlyR T19R, S22W-assembled pore. In amphiphilic peptides, D-amino acids can act as α-helix destabilizers. Based on the strength of destabilization, they are divided into a group of strong or weak helix destabilizers. Leucine, arginine, methionine, lysine, tryptophan and alanine belong to a group of weak helix destabilizers, and threonine, phenylalanine, valine, isoleucine, tryptophan and proline to a group of strong destabilizers. The effect depends on the amino acid side chains. Bulky and β branched side chains are strong destabilizers because of a steric clash of their side chains with a preceding turn of the helix

(Krause et al., 2000). The D-NK_4-M2GlyR T19R, S22W sequence contains: D-threonine, D-valine, D-isoleucine and D-proline. Thus, the strong helix-destabilizers which could affect the stability of the pore and hence confer different biophysical properties to the D-NK_4-M2GlyR T19R, S22W -assembled pore. The computer molecular modeling simulations of the pentameric D-NK_4-M2GlyR T19R, S22W-assembled pore can directly address this possibility.

Altogether, the results of our studies using D-NK_4-M2GlyR T19R, S22W peptide did not provide a complete answer to the question on the role of L-NK_4-M2GlyR T19R, S22W as a modulator. However, the experiments with a diastereomeric NK_4-M2GlyR T19R, S22W peptide could further address this question. Kovacs and colleagues (2006) report, that peptides substituted with L- or D-amino acids retain the hydrophobicity/hydrophilicity between different amino acids in L- and D-series of substitutions. But the nearest-neighbor effects of L- and D-amino acids restrict the conformational space of their side chains. The alternating L- and D-amino acid side chain positions may lead to an inability of diastereomeric NK_4-M2GlyR T19R, S22W peptides to assemble into functional *de novo* pores and provide further insight into the role of L-NK_4-M2GlyR T19R, S22W as a modulator.

Chapter 4 - Summary and Future Studies

The search for therapies for CF has led to an array of strategies and their combinations, targeted at ameliorating disease progression and thereby enhancing the quality of life for CF patients. Since none of the approaches is fully successful at treating all forms of the disease, novel therapeutic options are needed. Our research represents an approach that addresses the underlying cause of the disease at the cellular or tissue level, namely reduced anion conductance that sets the chemi-osmotic driving force for both paracellular and transcellular fluid movement. The novelty of our design arises from its simplicity and ease of delivery to affected airway cells. We produced a channel-forming peptide (CFP) with an ability to deliver itself to the epithelial cell membranes without the use of any special delivery system, insert into targeted membranes and self-assemble into ion conducting *de novo* pores. Since the therapy would require a repeated administration, the candidate CFP needs to be effective at low concentrations, non-antigenic and not persistent in the membrane for longer than a few hours. Synthetic anion selective channels constitute a therapeutic modality also because they are independent of genetic mutations, meaning that as a drug, a CFP would be equally efficient if administered to patients expressing different CF gene mutations.

The synthetic channel-forming peptides derived from the second transmembrane segment (M2), of the spinal cord Glycine receptor. When assembled in a pentameric array, this transmembrane sequence defines the anion selective pore of this ligand-gated channel. From the initial demonstration that such exogenously applied sequences support anion movement similar to their parent protein (Reddy et al., 1993; Wallace et al., 1997), the peptide has gone through numerous modifications to increase aqueous solubility (Tomich et al., 1998; Broughman et al.,

2001, Broughman et al., 2002) and efficiency of targeted insertion into epithelial membranes (Cook et al., 2004; Shank et al., 2006). The resulting synthetic channel-forming candidate NK_4-M2GlyR p22-T19R, S22W, now represents our best candidate, possessing all the above mentioned favorable properties but no anion selectivity (Tomich et al., 2011). The present investigations focused on addressing this issue by modifying the electrostatic properties of the channel. For this purpose, the non-encoding amino acid, 2, 3-Diaminopropionic acid (Dap) was used to replace pore-lining residues in the assembled NK_4-M2GlyR p22-T19R, S22W channel. The rationale behind using Dap was based on its hydrophilicity and ability to extend into the water-filled pore and its single positive charge at neutral pH. Therefore, we hypothesized that Dap fundamentally changes the electrostatic environment of peptide-assembled pore, favoring selectivity for chloride ions.

One of the important aspects of our studies was to address the question whether the Dap-peptides are forming *de novo* ion conductive pathways or modulating the ion conductances intrinsic to *Xenopus* oocytes. We tested shorter peptides corresponding to different sections of a full length p22-T19R, S22W and doubly Dap-substituted peptide and the all-D- p22-T19R, S22W peptide for their role in modulating ion conductances intrinsic to *Xenopus* oocytes (Chapter 3). The sequence (RVGLGITTVLTMRW) corresponding to the central segment of a full length NK_4-M2GlyR T19R, S22W induced significantly higher inward flow of ions relative to the background currents of *Xenopus* oocytes. The activity depended on voltage and ionic conditions. The Central NK_4-M2GlyR T19R, S22W corresponds to the most hydrophobic part of the full-length peptide, and contains residues (R and W) that show preference for interfacial localization. Thus the activity of the Central truncated peptide could be attributed to its hydrophobic nature and ability to reach the membrane embedded regions of endogenous

channels, where it could bind and modulate channel activities. Nevertheless, the pattern of currents induced by the Central truncated peptide was not similar to those induced by the full-length peptide. The sequences of other truncated peptides corresponding to the N-terminal and C-terminal parts of L-NK_4-M2GlyR T19R, S22W or the central part of di-Dap substituted L-NK_4-M2GlyR T19R, S22W were less hydrophobic compared to the central L-NK_4-M2GlyR T19R, S22W segment, and did not induce ion current significantly higher than background currents in *Xenopus* oocytes. Results suggest that these peptides, as well as the full-length peptide, do not have extracellular or interfacial activating domains that alter the activities of endogenous channels in *Xenopus* oocytes. It is possible that the Central truncated peptide adopts an alternate orientation in which the WR and R residues both reside at the water-membrane interface with the hydrophobic region inserting in a bowed manner part way into the hydrophobic core. Future studies should focus on studying the membrane binding properties of this peptide without the N-terminal arginine, using lipid vesicles to better assess the position of this peptide relative to the parent sequence.

It is possible that only the assembled full-length sequences, which have more fixed geometries, activate channels endogenous to *Xenopus* oocytes. We tested this assumption by synthesizing the all-D-amino acid D-NK_4-M2GlyR T19R, S22W peptide which is presumed to assemble into *de novo* pores. If the L-NK_4-M2GlyR T19R, S22W acts as a modulator of certain endogenous channels, then a D-configuration of this peptide would prevent and/or eliminate the binding of D-peptide to the same endogenous channels and provide evidence of L-NK_4-M2GlyR T19R, S22W activity. However, the hypothesis did not preclude the binding of the D- assembly with different ion-conducting channels in the oocyte. D-NK_4-M2GlyR T19R, S22W induced a voltage-dependent, non-selective ion current across the *Xenopus* oocyte membrane. A distinct D-

versus L- NK_4-M2GlyR T19R, S22W peptide-induced ion current was attributed to the different geometry of D-NK_4-M2GlyR T19R, S22W-assembled pore.

Alternating L- and D-amino acid side chain positions may lead to inability of diastereomeric NK_4-M2GlyR T19R, S22W peptides to assemble into functional *de novo* pores. Therefore, future experiments with a diastereomeric NK_4-M2GlyR T19R, S22W peptide may provide a more complete answer the question on the role of L-NK_4-M2GlyR T19R, S22W as a modulator.

Our results suggest that the full length L-NK_4-M2GlyR T19R, S22W is required for the current amplitudes detected in our studies (Chapter 2 and 3) and that ion currents induced by this peptide most likely do not result from monomeric L-NK_4-M2GlyR T19R, S22W-induced modulation of channel activities intrinsic to the oocyte. The flux assays showed that the full-length Dap-substituted peptides form *de novo* pathways. However, the results were inconsistent and further studies using different types and ratios of lipids for preparation of artificial membranes will be required.

We further focused on more detailed studies of biophysical properties of a full-length L-NK_4-M2GlyR T19R, S22W and its Dap-substituted variants. The preliminary computer simulations (Chapter 2) of pores formed by singly or doubly Dap-substituted peptides indicated that placing Dap at positions T17, T20 or T13, T20 widens the pore, especially at its middle and bottom portions, by about 2Å. This is in agreement with other studies showing that the substitution of charged amino acids with similarly charged amino acids with shorter side chains yields larger pore diameter (Keramidas et al., 2000, Keramidas et al., 2002). The changes in pore diameter were presumed to manifest in increased ion conductance. Experimental results supported by predictions of the simulations. All double- and a triple-Dap-substituted peptide(s) showed increases in maximal I_{SC} in MDCK monolayers, compared to singly Dap-substituted

peptides or their non-substituted parent peptide. This first suggests that the introduced Dap residues yield fundamental changes to pore geometry. Not examined, but clearly possible, is the possibility that the conductances also differ depending upon the sequence. This can be tested by altering the number of monomers involved in the self-assembly of the pore (i.e. increasing from five to six helices per pore-forming bundle). Relative to the non-substituted peptide, the cooperativity of monomers at pore assembly, reflected by the Hill coefficients, was higher for singly Dap-substituted peptides and the highest with multiple Dap-substituted sequences. The differences in Hill coefficients that suggest that, given the same density of peptides in the membrane, these sequences are more likely to self-associate into pores or that the predominant assembly with the most stability has been switched from 5 α-helices (as observed for the non-substituted peptides), to assemblies of 6 or more helical bundles. This assumption is supported by the observation of assembly of higher magnitudes of ion conductances observed for the double and triple Dap-substituted peptide-assemblies. Assembly of synthetic pores is uncontrolled and thought to produce a distribution of assemblies centered about the most stable form. The functionality of undesirable assemblies could be circumvented by employing tethered bundles with a prescribed number of helices thus yielding uniform ion conductances. However, these syntheses would be too costly to produce and purify to homogeneity for use in the clinic.

TEVC studies on the permselectivity of Dap-peptide assemblies provide convincing evidence that introduction of Dap in either multiple positions or number does not result in pores with increased anion selectivity. The charged side chains of Dap modify the electrostatic environment of the pore, but not in the intended manner. The large increases in conductance and possible permeability to gluconate suggest that a much larger pore diameter is generated by the ring(s) of repelling, like charge. A large water-filled pore, most likely decreases the interactions

of permeating ions with the Dap side chains, thus obviating any electrostatic exclusion of cationic ions. Future studies should therefore focus on narrowing the pore diameter. One approach is to mix single, double and triple Dap-substituted peptides in various ratios. The idea behind this approach is to find the best possible combination of staggered charge in the pore. Preliminary computer simulations have already been conducted by Dr. Jian Gao from Dr. Chen's laboratory. The pentameric channels were simulated and individual peptides used, labeled as A, B, C, D and E (**Table 4.1**).

Table 4-1 Combinations of Dap-substituted and non-substituted peptides used in computer simulations of pentameric channels.

	Dap-substituted individual peptides				
Pentamer	**A**	**B**	**C**	**D**	**E**
T13AC Dap	T13Dap	no Dap	T13Dap	no Dap	no Dap
T17AC Dap	T17Dap	no Dap	T17Dap	no Dap	no Dap
T13AC-T20BD Dap	T13Dap	T20Dap	T13Dap	T20Dap	no Dap
T17AC-T20BD Dap	T17Dap	T20Dap	T17Dap	T20Dap	no Dap
T13AC-T17BD T20CE Dap	T13Dap	T17Dap	T20Dap	T17Dap	T20Dap

Results suggest that the pores with only two introduced Dap residues either at position T13 (T13AC Dap) or T17 (T17AC Dap) give unstable pentameric channel formations after 10 ns simulations. Other simulated pores with at least four Dap substitutes are stable (**Figure 4-1**). Previous computer simulations (**Figure 2-14**) (Tomich et al., 2011) suggested that Dap substitution of threonine at position 20 in T13Dap, T20Dap-assembled pores narrows the pore diameter compared to pores composed of T13Dap, T17Dap peptides. In contrast, Dap substitution at position T17 opens the pore the most. This suggests that single T20Dap-substituted peptides should be tested first in various mixes and ratios with single T13Dap-substituted peptides, double substituted T20Dap, T13Dap peptide or even non-substituted parent peptide. Ussing chamber experiments using MDCK cells can be the first experimental system,

followed and/or accompanied by lipid bilayer studies and TEVC recordings using *Xenopus* oocytes.

Figure 4-1 Snapshots of computer simulations of five Dap-substituted peptide-assembled channels at 0 and 10 ns.

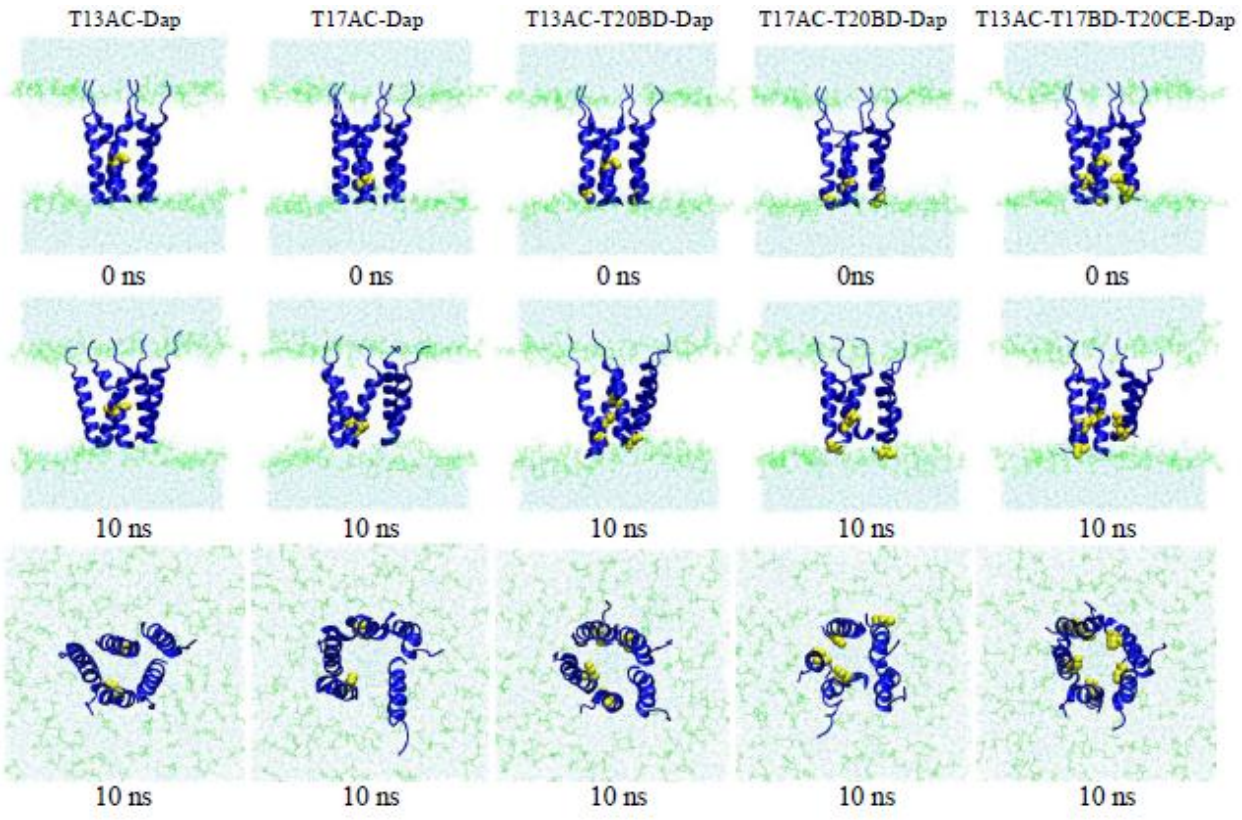

The yellow beads represent Dap residues; cyan lines are head of lipids; the tails are not shown. The top snapshots are the structures at the beginning of production simulations in POPC membranes; the middle are simulations at 10 ns and the bottom are the top views at 10 ns simulations.

Overall, the study yielded new knowledge regarding the design and construction of ion channels. Dap-substitutions show potential for pore geometry modifications but not anion selectivity. Therefore, the ongoing computer modeling studies are aimed at predicting the effect of combinations and ratios of Dap-substitutes on narrowing the pore width. These results will open a new horizon for designs of narrower pores with more tunable anion selectivity.

Clearly, there continues to be a need for new and novel therapeutic agents to treat CF. In this regard, future synthetic Dap-substituted CFPs designed in our laboratory can constitute a therapeutic modality with ample potential.

References

Abel, E., Maguire, G. E. M., Meadows, E. S., Murillo, O., Jin, T., Gokel, G. W. (1997). Planar bilayer conductance and fluorescence studies confirm the function and location of a synthetic, sodium-ion-conducting channel in a phospholipid bilayer membrane. *Journal of American Chemical Society*, 119, 9061-9062.

Adcock, C., Smith, G. R., Sansom, M. S. P. (1998). Electrostatics and the ion selectivity of ligand-gated channels. *Biophysical Journal*, 75(3), 1211-1222.

Anderson, M. P., Sheppard, D. N., Berger, H. A., Welsh, M. J. (1992). Chloride channels in the apical membrane of normal and cystic fibrosis airway and intestinal epithelia. *American Journal of Physiology*. 263(1 Pt 1), L1-L14.

Andrea-Winslow, L. D., Strohmeier, G. R., Rossi, B., Hofman, P. (2001). Identification of a sea urchin $Na^+/K^+/2Cl^-$ cotransporter (NKCC): microfilament-dependent surface expression is mediated by hypotonic shock and cyclic AMP. *The Journal of Experimental Biology*, 204, 147-156.

Arikace™ - Clinical trials (n.d.). Retrieved from http://www.insmed.com/arikace.php.

Atkuri, K. R., Mantovani, J. J., Herzenberg, L. A., Herzenberg, L. A. (2007). N-Acetylcysteine-a safe antidote for cysteine/glutathione deficiency. *Current Opinion in Pharmacology*, 7(4), 355-359.

Barra, E., Socha, J., Teisseyre, M., Celińska-Cedro, D., Stolarczyk, A., Pertkiewics, J., …M., Wawer, Z. (1999). Lipids digestion disturbance in children with cystic fibrosis and chronic pancreatitis. Pediatrica Wspólczesna. *Gastroenterologia, Hepatologia i Żywienie Dzicka*, 1(2/3), 165-167.

Braunstein, A., Papo, N., Shain, Y. (2004). In vitro activity and potency of an intravenously injected antimicrobial peptide and its DL amino acid analog in mice infected with bacteria. *Antimicrobial Agents and Chemotherapy*, 48(8), 3127-3129.

Becq, F. (2010). Cystic fibrosis transmembrane conductance regulator modulators for personalized drug treatment of cystic fibrosis. *Drugs*, 70(3), 241-259.

Bichet, D., Grabe, M., Jan, Y. N., Jan, J. Y. (2006). Electrostatic interactions in the channel cavity as an important determinant of potassium channel selectivity. *Proceedings of the National Academy of Science*, 103(39), 14355-14360.

Bilton, D., Robinson, P., Cooper, P., Gallagher, C., Kolbe, J., Fox, H., Jaques, A., Charlton, B. (2011). Inhaled dry powder mannitol in cystic fibrosis: An efficacy and safety study. *European Respiratory Journal*. Advance online publication.
Doi: 10.1183/09031936.00187510.

Bompadre, S. G., Sohna, Y., Li, M. Hwang, T. C. (2007). G551D and G1349D, two CF-associated mutations in the signature sequences of CFTR, exhibit distinct gating defects. *Journal of General Physiology*, 129(4), 285-298.

Boucher, R. C. (2007). Cystic fibrosis: a disease of vulnerability to airway surface dehydration. *Trends in Molecular Medicine*, 13(6), 231-240.

Braunstein, A., Papo, N., Shai, Y. (2004). *In Vitro* activity and potency of an intravenously injected antimicrobial peptide and its D-amino acid analog in mice infected with bacteria. *Antimicrobial Agents and Chemotherapy*, 48(8), 3127-3129.

Broughman, J. R., Shank, L. P., Takeguchi, W., Schultz, B. D., Iwamoto, T., Mitchell, K. E., Tomich, J. M. (2002). Distinct structural elements that direct solution aggregation and membrane assembly in the channel-forming peptide M2GlyR. *Biochemistry*, 41(23), 7350-7358.

Broughman, J. R., Mitchell, K, Iwamoto, T., Schultz, B. D., Tomich, J. M. (2001). Amino-terminal modification of a channel forming peptide increases capacity for epithelial anion secretion. *American Journal of Physiology - Cell Physiology*, 280(3), C451-C458.

Bukovnik, U., Gao, J., Cook, G. A., Shank, L. P., Seabra, M. B., Schultz, B. D., Iwamoto, T., Chen, J., Tomich, J. M. (2011). Structural and biophysical properties of a synthetic channel-forming peptide: Designing a clinically relevant anion-selective pore. *Biochimica Biophyica. Acta*. Advance online publication. Doi:10.1016/j.bbamem.2011.07.037.

Callewaert, G., Hanbauer, I., Morad, M. (1989). Modulation of calcium channels in cardiac and neuronal cells by an endogenous peptide. *Science*, 243(4891), 663-666.

Carlin, R. W., Sedlacek, R. L., Quesnell, R. R., Pierucci-Alves, F., Grieger, D. M., Schultz, B. D. (2006). PVD9902, a porcine vas deferens epithelial cell line that exhibits neurotransmitter-stimulated anion secretion and expresses numerous HCO_3^- transporters. *American Journal of Physiology - Cell Physiology*, 290(6), C1560-C1571.

Carpino, L. A. & Han, G. Y. (1972). The 9-fluorenylmethoxycarbonyl amino-protecting group. *Journal of Organic Chemistry*, 37, 3404-3409.

Cascio, M. (2004). Structure and function of the Glycine receptor and related nicotinicoid receptors. *Journal of Biological Chemistry*, 279(19), 19383-19386.

Cheng, S. H., Fang, S. L., Zabner, J., Marshall, J., Piraino, S., Schiavi, S. C., …Smith, A. E. (1995). Functional activation of the cystic fibrosis trafficking mutant ΔF508-CFTR by overexpression. *Lung Physiology*, 268(4 Pt 1), L615-L624.

Cheer, S. M., Waugh, J., Noble, S. (2003). Inhaled tobramycin (TOBI): a review of its use in the management of *Pseudomonas aeruginosa* infections in patients with cystic fibrosis. *Drugs*, 63(22), 2501-2520.

Choi, J. Y., Muallem, D., Kiselyov, K., Lee, M. G., Thomas, P. J., Muallem, S. (2001). Abberant CFTR-dependent HCO_3^- transport in mutations associated with cystic fibrosis. *Nature*, 410(6824), 94-97.

Cens, T., Charnet, P. (2007). Use of *Xenopus* oocytes to measure ionic selectivity of pore-forming peptides and ion channels. *Methods in Molecular Biology*, 403, 287-302.

Clarke, L. L., Harline, M. C., Gawennis, L. R., Walker, N. M., Turner, J. T., Weisman, G. A. (2000) Extracellular UTP stimulates electrogenic bicarbonate secretion across CFTR knockout gallbladder epithelium. *American Journal of Physiology*, 279, G132–G138.

Clinical trials – GS-9411. (2010). A randomized, double-blind, placebo-controlled multiple dose trial of GS-9411 in healthy volunteers. Retrieved from http://clinicaltrials.gov/ct2/show/NCT00999531.

Cook, G. A., Prakash, O., Zhang, K., Shank, L. P., Takeguchi, W. A., Robbins, A., …Tomich, J. M. (2004). Activity and structural comparisons of solution associating and monomeric channel-forming peptides derived from the glycine receptor M2 segment. *Biophysical Journal*, 86(3), 1424-1435.

Costa, P. F., Emilio, M. G., Fernandes, P. L., Ferreira, H. G., Ferreira, K. G. (1989). Determination of ionic permeability coefficients of the plasma membrane of *Xenopus* oocytes under voltage clamp. *Journal of Physiology*, 413, 199-211.

Crook, R. B., & Polansky, J. R. (1994). Stimulation of Na^+, K^+, Cl^--contransport by forskolin-activated adenyl cyclase in fetal human non pigmented epithelial cells. *Investigative Ophthalmology and Visual Science*, 35(9), 3374-3383.

Davis, P.B. (2006). Cystic fibrosis since 1938. *American Journal of Respiratory and Critical Care Medicine*, 173(5), 475-482.

De Boeck, K., Weren, M., Proesmans, M., Kerem, E. (2005). Pancreatitis among patients with cystic fibrosis: correlation with pancreatic status and genotype. *Pediatrics*, 115(4), e463-e469.

Devidas, S. & Guggino, W. B. (1997). CFTR: domains, structure and function. *Journal of Bioenergetics and Biomembranes*, 29(5), 443-451.

Devor, D. C., Singh, A. K., Frizzell, R. A., Bridges, R. J. (1996). Modulation of Cl^- secretion by benzimidazolones. I. Direct activation of a $Ca(^{2+})$-dependent K^+ channel. *American Journal of Physiology*, 271(5 Pt 1), L775-L784

Dodge, J. A. (1986). Gastrointestinal tract and nutrition in cystic fibrosis: pathophysiology. *Journal of the Royal Society of Medicine*, 79(Suppl.12), 27-31.

Dutzler, R., Campbell, E. B., MacKinnon, R. (2003). Gating the selectivity filter in ClC chloride channels. *Science,* 300(5616), 108-112.

Fahy, J. V. & Dickey, B. F. (2010). Airway mucus function and dysfunction. *New England Journal of Medicine*, 363(23), 2233-2247.

Faraldo-Gómez, J. D. & Roux, B. (2004). Electrostatics of ion stabilization in a ClC chloride channel homologue from *Escherichia coli*. *Journal of Molecular Biology*, 339(4), 981-1000.

Fields, G. B. & Noble, R. L. (1990). Solid phase peptide synthesis utilizing 9-fluorenylmethoxy-carbonyl amino acids. *International Journal of Peptide Protein Research,* 35(3), 161-214.

Frazier, S. J. (2006). Structure-activity study on pore-lining residue replacements of a self-assembling M2GLYR derived channel-forming peptide. (Unpublished master's thesis). Kansas State University, Manhattan, Kansas.

Fuchs, H. J., Borowitz, D. S., Christiansen, D. H., Morris, E. M., Nash, M. L., Ramsey, B. W., …Wohl, M. E. (1994). Effect of aerosolized recombinant human DNase on exacerbations of respiratory symptoms and on pulmonary function in patients with cystic fibrosis. *New England Journal of Medicine*, 331(10), 637-42.

Futaki, S., Aoki, M., Fukuda, M., Kondo, F., Niwa, M., Kitagawa, K., Nakaya, Y. (1997). Assembling of the four individual helices corresponding to the transmembrane segments (S4 in repeat I-IV) of the sodium channel. *Tetrahedron Letters*, 38(40), 7071-7074.

Fuller, M. D., Zhang, Z. R., Cui, G., Kubanek, J., McCarty, N. A. (2004). Inhibition of CFTR channels by a peptide toxin of scorpion venom. *American Journal of Physiology - Cell Physiology*, 287(5), C1328-C1341.

Fyles, T. M. (2006). Synthetic ion channels in bilayer membranes. *Chemical Society Reviews*, 36, 335-347.

Gao, L., Broughman, J. R., Iwamoto, T., Tomich, J. M., Venglarik, C. J., Forman, H. J. (2001). Synthetic chloride channel restores glutathione secretion in cystic fibrosis airway epithelia. *American Journal of Physiology Lung Cellular and Molecular Physiology*, 281(1), L24-L30.

Gadsby, D. C., Vergani, P., Csanády, L. (2006). The ABC protein turned chloride channel whose failure causes cystic fibrosis. *Nature*, 440, 477-483.

Gibson, R. L., Burns, J. L., Ramsey, B W. (2003). Pathophysiology and management of pulmonary infections in cystic fibrosis. *American Journal of Respiratory and Critical Care Medicine*, 168(8), 918 -951.

Van Ginkel, F. W., Iwamoto, T., Schultz, B. D., Tomich, J. M. (2008). Immunity of a self-derived, channel-forming peptide in respiratory tract. *Clinical and Vaccine Immunology*, 15(2), 260-266.

Van Goor, F., Hadida, S., Grootenhuis, P. D. J., Burton, B., Cao, D., Neuberger, T., … Negulescu, P. (2009). Rescue of CF airway epithelial cell function in vitro by a CFTR potentiator, VX-770. *Proceedings of the National Academy of Science*, 106(44), 18825-18830.

Grasemann, H., Stehling, F., Brunar, H., Widmann, R., Laliberte, T. W., Molina, L., Doring, G., Ratjen, F. (2007). Inhalation of Moli1901 in patients with cystic fibrosis. *Chest*, 131(4), 1461-1466.

Grove, A., Tomich, J. M., Montal, M. (1991). A molecular blueprint for the pore-forming structure of voltage-gated calcium channels. *Proceedings of the National Academy of Science*, 88(15), 6418-6422.

Grudzinska, J., Schemm, R., Haeger, S., Nicke, A., Schmalzing, G., Betz, H., Laube B. (2005). The beta subunit determines the ligand binding properties of synaptic glycine receptors. *Neuron*, 45(5), 727-739.

Haack, T., Gonzáles, M. J., Sánches, Y., Giralt, E. (1997). D-amino acids in protein design. II. Protein-diastereomerism versus protein-enantiomerism. *Letters in Peptide Science*, 4(4-6), 377-386.

Hedin, L., Rosberg, S. (1983). Forskolin effects on the cAMP system and steroidogenesis in the immature rat ovary. *Molecular and Cellular Endocrinology*, 33(1), 69-80.

Heginbotham, L., Kolmokova-Partensky, L., Miller, C. (1998). Functional reconstitution of a prokaryotic K^+ channel. *Journal of Cell Biology*, 111(6), 741-749.

Herrera, A. I., Al-Rawi, A., Cook G. A., Prakash, O., Tomich, J. M., Chen, J. (2010). Introduction of a C-Terminal Tryptophan in a Pore-Forming Peptide: A Structure/Activity Study. *Proteins: Structure, Function, and Genetics*, 78(10), 2238-2250.

Higgins, C. F. (1995). The ABC of channel regulation. *Cell*, 82(5), 693-696.

Hilf, R. J. C. & Dutzler, R. (2009). Structure of a potentially open state of a proton-activated pentameric ligand-gated ion channel. *Nature*, 457, 115-118.

Hille, B. (Ed.) (2001). Ion channels of excitable membranes (pp. 7-23, 309-343, 347-369). Suderland, MA: Sinauer Associates, Inc.

Ishiguro, H., Steward, M. C., Naruse, S., Ko, S. B. H., Goto, H., Maynard Case, R., Kondo, T., Yamamoto, A. (2009). CFTR fluids as a bicarbonate channel in pancreatic duct cells. *Journal of General Physiology*, 133(3), 315-326.

Ivanov, I., Cheng, X., Sine, S. M., McCammon, J. A. (2007). Barriers to ion translocation in cationic and anionic receptors from the Cys-loop family. *Journal of American Chemistry Society*, 129(26), 8217-8224.

Iwamoto, T., Grove, A., Oblat Montal, M., Montal, M., Tomich J. M. (1994). Chemical synthesis and characterization of peptides and oligomeric proteins designed to form transmembrane ion channels. *International Journal of Peptide Protein Research*, 43, 597-607.

Jaques, A., Daviskas, E., Turton, J. A., McKay, K., Cooper, P., Stirling, R. G., …Charlton, B. (2008). Inhaled mannitol improves lung function in cystic fibrosis. *Chest*, 133(6), 1388-1396.

Kim, D. & Steward, M. C. (2009). The role of CFTR in bicarbonate secretion by pancreatic duct and airway epithelia. *Journal of Medicinal Investigation*, 56 Suppl., 336-342.

Kelkar, D. A., & Chattopadhyay, A. (2007). The gramicidin ion channel: A model membrane protein. *Biochimica Biophysica Acta*, 1768, 2011-2025.

Keramidas, A., Moorhouse, A. J., Frensh, C. R., Schofield, P. R., Barry, P.R. (2000). M2 pore mutations convert the glycine receptor channel from being anion to cation-selective. *Biophysical Journal*, 78, 247-258.

Keramidas, A., Moorhouse, A. J, Pierce, K. D., Schofield, P. R., Barry, P. H. (2002). Cation-selective mutations in the M2 domain of the inhibitory glycine receptor channel reveal determinants of ion-charge selectivity. *Journal of General Physiology*, 119(5), 393-410.

Kersh, G. J., Tomich, J. M., Montal, M. (1989). The M2δ transmembrane domain of the nicotinic cholinergic receptor forms ion channels in human erythrocyte membranes, *Biochemical and Biophysical Research Communications*, 162(1), 352-356.

Kersting, U., Schwab, A., Hebestreit, A. (1998). Measurement of human nasal potential difference to teach the theory of transepithelial fluid transport. *Advances in Physiology Education*, 275, S72-S77.

Van Klompenburg, W., Nilsson, J., von Heijne, G., de Kruijff, B. (1997). Anionic phospholipids are determinants of membrane protein topology. *EMBO Journal*, 16(14), 4261-4266.

Knowles, M. R., Olivier, K. N., Hohneker, K. W., Robinson, J., Bennett, W. D., Boucher, R. C. (1995). Pharmacologic treatment of abnormal ion transport in the airway epithelium in cystic fibrosis. *Chest*, 107, 71S-76S.

Kopito, R. R. (1999). Biosynthesis and degradation of CFTR. *Physiological Reviews*, 79(1 Suppl), S167-173.

Kovacs J. M., Mant, C. T., Kwok, C. S., Osguthorpe, D. J., Hodges, R. S. (2006). Quantitation of the nearest-neighbor effects of amino acid side-chains that restrict conformational freedom of the polypeptide chain using reversed-phase liquid chromatography of synthetic model peptides with L- and D-amino acid substitutions. *Journal of Chromatography A*., 1123(2), 212-224.

Koynova, R., Tarahovsky, Y. S., Wang, L., MacDonald, R. C. (2007). Lipoplex formulation of superior efficacy exhibits high surface activity and fusogenicity and readily releases DNA. *Biochimica et Biophysica Acta*, 1768(2), 375-386.

Krause, E., Bienert, M., Schmieder, P. (2000). The helix destabilizing propensity scale of D-amino acids: the influence of side chain steric effects. *Journal of American Chemical Society*, 122, 4865-4870.

Kreil, G. (1994). Peptides containing D-amino acid from frogs and molluscs. *Journal of Biological Chemistry*, 269(15), 10967-10970.

Kumar, V. V., Pichon, C., Refreigers, M., Guerin, B., Midoux, P., Chaudhuri, A. (2003). Single histidine residue in head-group region is sufficient to impart remarkable gene transfection properties to cationic lipids: evidence for histidine mediated membrane fusion at acidic pH. *Gene Therapy*, 10(15), 1206-1215.

Lam, H., Oh, D. C., Cava, F., Takacs, C. N., Clardy, J., de Pedro, M. A., Waldor, M. K. (2009). D-amino acids govern stationary phase cell wall remodeling in bacteria. *Science*, 325(5947), 1552-1555.

Le Novère, N. & Changeux, J. P. (2001). LGICdb: the ligand-gated ion channel database. *Nucleic acid research*, 29(1), 294-295.

Liedtke, C. M. (1989). Regulation of chloride transport in epithelia. *Annual Review of Physiology*, 51, 143-160.

Liu, M., Li, C., Pazgier, M., Li, C., Mao, Y., Lu, Y., … Lu, W. (2010). D-peptide inhibitors of the p53-MDM2 interaction for targeted molecular therapy of malignant neoplasms. *Proceedings of the National Academy of Science*, 107(32), 14321-14326.

Lowry, F. (2011). FDA panel sends Liprotamase back to the drawing board. Medscape Medical news. Retrieved from http://www.medscape.com/viewarticle/735722.

Linsdell, P. (2006). Mechanism of chloride permeation in the cystic fibrosis transmembrane conductance regulator chloride channel. *Experimental Physiology*, 91, 123-129.

Mall, M., Kreda, S. M., Mengos, A., Jensen, T. J., Hirtz, S., Seydewitz, H. H., …Boucher, R. C. (2004). The ΔF508 mutation results in loss of CFTR function and mature protein in native human colon. *Gastroenterology*, 126(1), 32-41.

Mannitol - Clinical trials and use (n.d.). Retrieved from http://pharmaxis.com.au.

Matsubara, A., Asani, K., Akagi, A., Nishino, N. (1996). Ion-channels of cyclic template-assembled alamethicins that emulate the pore structure predicted by the barrel-stave model. *Chemical Communications*, 17, 2069-2070.

Matsui, H., Grubb, B. R., Tarran, R., Randell, S. H., Gatzy, J. T., Davis, C. W., Boucher, R. C. (1998). Evidence for periciliar liquid layer depletion, not abnormal ion composition, in the pathogenesis of cystic fibrosis airways disease. *Cell*, 95(7), 1005-1015.

McCarty, N. A. (2000) Permeation through the CFTR chloride channel. *Journal of Experimental Biology*, 203, 1947-1962.

McCarty, N. A. & Zhang, A. R. (2001). Identification of a region of strong discrimination in the pore of CFTR. *American Journal of Physiology - Lung Cellular and Molecular Physiology*, 281(1), L852-L867.

Miller, C. (1984). Ion channels in liposomes. *Annual Review in Physiology*, 46, 549-558.

Misfeldt, D. S., Hamamoto, S. T., Pitelka, D. R. (1976). Transepithelial transport in cell culture. *Proceedings of the National Academy of Science*, 73(4), 1212-1216.

Mitchell, K. E., Iwamoto, T., Tomich, J. M., Freeman, L. C. (2000). A synthetic peptide based on a glycine-gated chloride channel induces a novel chloride conductance in isolated epithelial cells. *Biochimica et Biophysica Acta*., 1466(1–2), 47-60.

Moneé, M., Nilsson, J., Johansson, M., Elmhed, N., von Heijne, G. (1998). Positively and negatively charged residues have different effects on the position in the membrane of a model transmembrane helix. *Journal of Molecular Biology*, 284, 1177-1183.

Montal, M. O, Montal, M. S., Tomich, J. M. (1990). Synporins- synthetic proteins that emulate the pore structure of biological ionic channels. *Proceedings of the National Academy of Science*, 87(18), 6929-6933.

Montal, M. O., Buhler, L. K., Iwamoto, T., Tomich, J. M., Montal, M. (1993a). Synthetic peptides and four-helix bundle proteins as model systems for the pore-forming structure of channel proteins. I. Transmembrane segment M2 of the nicotinic cholinergic receptor channel is a key pore-lining structure. *Journal of Biological Chemistry*, 268(20), 14601-14607.

Montal, M. O., Iwamoto, T., Tomich, J. M., Montal, M. (1993b). Design, synthesis and functional characterization of a pentameric channel protein that mimics the presumed pore structure of the nicotinic cholinergic receptor. *FEBS Letters*, 320, 261-266.

Montal, M. O., Reddy, G. L., Iwamoto, T., Tomich, J. M., Montal, M. (1994). Identification of an ion channel-forming motif in the primary structure of CFTR, the Cystic Fibrosis Cl^- channel. *Proceedings of the National Academy of Science*, 91(4), 1495-1499.

Mpex – product development programs (n.d.). Aeroquin (MP-376-Levofloxacin solution for inhalation) clinical program for Cystic fibrosis (CF)). Retrieved from http://www.mpexpharma.com/mp-376.html.

Myers, J. K., Pace C. N., Scholtz, J. M. (1997). Helix propensities are identical in proteins and peptides. *Biochemistry*, 36(36), 10923-10929.

Nimigean, C. M. (2006). A radioactive uptake assay to measure transport across ion channel-containing liposomes. *Nature protocols*, 1, 1207-1212.

Oblatt-Montal, M., Reddy, G. L., Iwamoto, T., Tomich, J. M., Montal, M. (1994). Identification of an ion channel-forming motif in the primary structure of CFTR, the cystic fibrosis chloride channel. *Proceedings of the National Academy of Science*, 91(4), 1495-1499.

Oiki, S., Danho, W., Montal, M. (1988). Channel protein engineering: Synthetic 22-mer peptide from the primary structure of the voltage-sensitive sodium channel forms ionic channels in lipid bilayers. *Proceedings of the National Academy of Science*, 85(7), 2393-2397.

Ouali, M., Ruysschaert, J. M., Lonez, C., Vandenbranden, M. (2007). Cationic lipids involved in gene transfer mobilize intracellular calcium. *Molecular Membrane Biology*, 24(3), 225-232.

Pag, U., Oedenkoven, M., Papo, N., Oden, Z., Shai, Y., Sahl, H. G. (2004). In vitro activity and mode of action of diastereomeric antimicrobial peptides against bacterial clinical isolates. *Journal of Antibacterial Chemotherapy*, 53(2), 230-239.

Pajewski, R., Garcia-Medina, R., Brody, S. L., Leevy, W. M., Schlesinger, P. H., Gokel, G. W. (2006). A synthetic, chloride-selective channel that alters chloride transport in epithelial cells. *Chemical Communications (Camb)*, 3, 329-331.

Pettit, R. S. & Johnson, C. E. (2011). Airway-Rehydrating Agents for the Treatment of Cystic Fibrosis: Past, Present, and Future. *The Annals of Pharmacotherapy*, 45(1), 49-59.

Pillewski, J. M. & Frizzell, R. A. (1999). Lung disease is the chief cause of morbidity and mortality in CF patients. *Physiological Reviews*, 79(Suppl. 1), S215-55.

de Planque, M. R., Bonev, B. B., Demmers, J. A., Greathouse, D. V., Koeppe, R. E. 2nd, Separovic, F., Watts, A., Killian, J.A. (2003). Interfacial anchor properties of tryptophan residues in transmembrane peptides can dominate over hydrophobic matching effects in peptide-lipid interactions. *Biochemistry*, 42(18), 5341-5348.

Planells-Cases, R. & Jentsch, T. J. (2009). Chloride channelopathies. *Biochimica et Biophysica Acta*, 1792, 173-189.

Platts, S. H., Mogford, J. E., Davis, M. J., Meininger, G. A. (1998). Role of K^+ channels in arteriolar vasodilation mediated by integrin interaction with RGD-containing peptide. *American Journal of Physiology - Heart and Circulatory Physiology*, 275(4), H1449-H1454.

Pollack, A. (2011). Vertex Says Trial of Vertex's VX-770, a Cystic Fibrosis Drug, Eased Breathing - NYTimes.com. The Business of Health Care - Prescriptions Blog - NYTimes.com. Retrieved from http://prescriptions.blogs.nytimes.com/2011/02/23/vertex-says-cystic-fibrosis-drug-helped-patients-breathe-easier.

Prasad, S. A., Tannenbau, E. L., Mikelsons, C. (2000). Physiotherapy in cystic fibrosis. *Journal of the Royal Society of Medicine*, 93(Suppl. 38), 27-36.

Pringos, E., Vignes, M., Martinez, J., Rolland, V. (2011). Peptide neurotoxins that affect voltage-gated calcium channels: A close-up on ω-Agatoxins. *Toxins*, 3, 17-42.

Proesmans, M., Vermeulen, F., De Boeck K. (2008). What's new in cystic fibrosis? From treating symptoms to correction of the basic defect. *European Journal of Pediatrics* 167(8), 839-849.

Pulmozyme – Full Prescribing Information (n.d.) Retrieved from http://www.pulmozyme.com/hcp/prescribing-info.jsp#table1.

Pusch, M. (2008). Electrophysiological analysis of ion channels. Protein Science Encyclopedia. Doi: 10.1002/9783527610754.

Ramalho, A. S., Beck, S., Meyer, M., Penque, D., Cutting, G. R., Amaral, M. D. (2002). Five percent of normal cystic fibrosis transmembrane conductance regulator mRNA ameliorates the severity of pulmonary disease in cystic fibrosis. *American Journal of Respiratory and Cell and Molecular Biology*, 27(5), 619-627.

Robinson, M., Hemming, A. L., Regnis, J. A., Wong, A. G., Bailey, D. L., Bantovich, G. J., King, M., Bye, P. T. (1997). Effects of increasing doses of hypertonic saline on mucociliary clearance in patients with cystic fibrosis. *Thorax*, 52(10), 900-903.

Ryan, S. G., Buckwalter, M. S., Lynch, J. W., et al. 1994. A missense mutation in the gene encoding the alpha 1 subunit of the inhibitory glycine receptor in the spasmodic mouse. *Nature Genetics*, 7(2), 131-135.

Reddy, L. G., Iwamoto, T., Tomich, J. M., Montal, M. (1994). Synthetic peptides and four-helix bundle proteins as model systems for the pore-forming structure of channel proteins. III. Transmembrane segment M2 of the brain glycine receptor channel is a plausible candidate for the pore-lining structure. *Journal of Biological Chemistry*, 268(20), 14608-14615.

Riordan, J. R., Rommens, J. M., Kerem, B. S., Alon, N., Rozmahel, R., Grzelczak, Z., … Tsui, L. C. (1989). Identification of the cystic fibrosis gene: Cloning and characterization of complementary DNA. *Science*, 245(4922), 1066-1073.

Roux, B. (2005). Ion conductivity and selectivity in K^+ channels. *Annual Review of Biophysics and Biomolecular Structure*, 34, 153-71.

Rowe, S. M., Miller, S., Sorscher, E. J. (2005). Cystic fibrosis. *The New England Journal of Medicine*, 352(9), 1992 – 2001.

Rowntree, R. K. & Harris, A. (2003). The phenotypical consequences of CFTR mutants. *Annals of Human Genetics*, 67, 471-485.

Quinton, P. M. (1999). Physiological basis of cystic fibrosis: A historical perspective. *Physiological Reviews*, 79(1), S3-S22.

Quinton, P. M. (2001). The neglected ion: HCO_3^-. *Nature Medicine*, 7, 292-293.

Sagel, S. D., Sontag, M. K., Anthony, M. M., Emmett, P., Papas, K. A. (2011). Effect of an antioxidant-rich multivitamin supplement in cystic fibrosis. *Journal of Cystic Fibrosis*, 10(1), 31-36.

Sala-Rabanal M, Loo D. D. F, Hirayama B. A., Turk, E., Wright, E. M. (2006). Molecular interactions between dipeptides, drugs and the human intestinal H^+–oligopeptide cotransporter hPEPT1. *Journal of Physiology*, 574(Pt 1), 149-166.

Scarborough, R. M., McEnroe, G. A., Arsten, A., Kang, L. L., Schwartz, K., Lewicki, J. A. (1988). D-amino acid-substituted atrial natriuretic peptide analogs reveal novel receptor recognition requirements. *Journal of Biological Chemistry*, 263(32), 16818-16822.

Schmieden, V.,Grenningloh, G., Schofield, P. R., Betz, H. (1989). Functional expression in *Xenopus* oocytes of the strychnine binding 48 kD subunit of the glycine receptor. *EMBO Journal*, 8(3), 695-700.

Schwiebert, L. M. (2004). Cystic fibrosis, gene therapy, and lung inflammation: for better or worse? *American Journal of Physiology - Lung Cellular and Molecular Physiology*, 286(4), L715-L716.

Sermet-Gaudelus, I., De Boeck, K., Casimir, G. J., Vermeulen, F., Leal, T., Mogenet, A., … Miller, L. L (2010). Ataluren (PTC124) induces CFTR protein expression and activity in children with nonsense mutation cystic fibrosis. *American Journal of Respiratory and Critical Care Medicine*, 182(10), 1262-1272.

Sears, H., Gartman, J., Casserly, P. (2011). Treatment options for cystic fibrosis: State of the art and future perspectives. *Reviews on Recent Clinical Trials*, 6(2), 94-107.

Sha, Q., Lansbery, K. L., Distefano, D., Mercer, R. W., Nichols, C. G. (2001). Heterologous expression of the Na^+, K^+-ATPase γ subunit in *Xenopus* oocytes induces an endogenous, voltage-gated large diameter pore. *Journal of Physiology*, 535(2), 407-417.

Shank, L. P., Broughman, J. R., Brandt R. M., Robbins, A. S., Takeguchi, W., Cook, G. A., … Tomich, J. M. (2006). Redesigning channel-forming peptides: Amino acid substitutions in channel-forming peptides that enhance rates of supramolecular assembly and raise ion transport activity. *Biophysical Journal*, 90(6), 2138-2150.

Sheppard, D. N. & Welsh, M. J. (1999). Structure and function of the CFTR chloride channel. *Physiological Reviews*, 79(Suppl. 1), S23-44.

Sine, S. M. & Engel, A. G. (2006). Recent advances in Cys-loop receptor structure and function. *Nature*, 440(7083), 448-455.

Smart, O. S., Neduvelil, J. G., Wang, X., Wallace, B. A., Sansom, M. S. P. (1996). HOLE: a program for the analysis of the pore dimensions of ion channel structural models. *Journal of Molecular Graphics*, 14(6), 354-360.

Smith, J. J., Karp, P. H., Welsh, M. J., (1994). Defective fluid transport by cystic fibrosis airway epithelia. *Journal of Clinical Investigation*, 93(3), 1307-131.

Smith, J. J., Travis, S. M., Greenberg, E. P., Welsh, M. J. (1996). Cystic fibrosis airway epithelia fail to kill bacteria because of abnormal airway surface fluid. *Cell*, 85(2), 229-236.

Stoichov, I. I., Antipin, I. S., Konovalov, A. I. (2003). Artificial ion channels. *Russian Chemical Reviews*, 72(12), 1055-1077.

Stoltz, D. A., Meyerholz, D. K., Pezzulo, A. A., Ramachandran, S., Rogan, M. P., Davis, G. J., …Welsh, M. J. (2010). Cystic Fibrosis Pigs Develop Lung Disease and Exhibit Defective Bacterial Eradication at Birth. *Science Translational Medicine*, 2(29), 29ra31.

Tanaka, T., Legat, A., Adam, E., Steuve, J., Gatot, J. S., Vandenbranden, M., … Jacquet, A. (2008). DiC14-amide cationic liposomes stimulate myeloid dendritic cells through Toll-like receptor 4. *European Journal of Immunology*, 38(5), 1351-1357.

Tarran, R. (2004). Regulation of airway surface liquid volume and mucus transport by active ion transport. *The Proceedings of the American Thorack Society*, 1, 42-46.

Taylor, C. J. & Aswani, N. (2002). The pancreas in cystic fibrosis. *Pediatric Respiratory Reviews*, 3(1), 77-81.

Tirouvanziam, R., Conrad, C. K., Bottiglieri, T., Herzenberg, L. A., Moss, R. B. (2006). High-dose oral N-acetylcysteine, a glutathione prodrug, modulates inflammation in cystic fibrosis. *Proceedings of the National Academy of Science*, 103(12), 4628-4633.

Thompson, V. F., Lawson, K. R., Barlow, J., Goll, D. E. (2003). Digestion of mu- and m-calpin by trypsin and chymotrypsin. *Biochimica et Biophysica Acta*, 1648(1–2), 140-153.

TOBI® - Description clinical pharmacology (n.d.).
Retrieved from http://www.pharma.us.novartis.com/product/pi/pdf/tobi.pdf.

Tomich, J. M., Wallace, D. P., Henderson, K., Brandt, R., Ambler, C. A., Scott, A. J., …Iwamoto, T. (1998). Aqueous solubilization of transmembrane peptide sequences with retention of membrane insertion and function. *Biophysical Journal*, 74(1), 256-267.

Tomich, J. M., Bukovnik U., Layman, J., Schultz, B. D. (2011) (In press). Channel replacement therapy for cystic fibrosis. In Sriramulu, D. D. (Ed.), Cystic Fibrosis. Rijeka, Croatia: Intech Open Access Publisher.

Torchilin, V. P., Levchenko, T. S., Rammohan, R., Volodina, N., Papahadjopoulos-Sternberg, B., D'Souza, G. M. (2003). Cell transfection in vitro and in vivo with nontoxic TAT peptide-liposome-DNA complex. *Proceedings of the National Academy of Science*, 100(4), 1972-1977.

Tosteson, M. T., Auld, D. S., Tosteson, D. C. (1989). Voltage-gated channels formed in lipid bilayers y a positively charged segment of the Na-channel polypeptide. *Proceedings of the National Academy of Science*, 86(2), 707-710.

Vanoye, C. G., Altenberg, G. A., Rems, L. (1999). Inhibition of P-glycoprotein-mediated transport by a hydrophobic contaminant in commercial gluconate salts. *American Journal of Physiology - Cell Physiology*, 276(6 Pt 1), C1439-C1442.

VX-770 – product description (n.d.). Retrieved from http://www.vrtx.com/current-projects/drug-candidates/vx-770.html.

Wade, D., Boman, A., Wåhlin, B., Drain, C. M., Andreu, D., Boman, H. G., Merrifield, R. B. (1990). All-D amino acid-containing channel-forming antibiotic peptides. *Proceedings of the National Academy of Science*, 87(12), 4761-4765.

Wagner, J. A. & Gardner, P. (1997). Toward cystic fibrosis gene therapy. *Annual Review of Medicine*, 48, 203-216.

Wallace, D. P., Tomich, J. M., Iwamoto, T., Henderson, K., Grantham, J. J., Sullivan, L. P. (1997). A synthetic peptide derived from the glycine-gated Cl^- channel generates Cl^- and fluid secretion by epithelial monolayers. *American Journal of Physiology - Cell Physiology*, 272(5 Pt 1), C1672-C1679.

Welsh, M. J. (1987) Electrolyte transport by airway epithelia. *Physiological Reviews*, 67, 1143-1184.

Welch, B. D., Vandemark, A. P., Hill, C. P., Kay, M. S. (2007). Parent D-peptide inhibitors of HIV-1 entry. *Proceedings of the National Academy of Science*, 104(3), 16828-16833.

Welch, B. D., Francis, N., Redman, J. S., Weinstock, M. T., Reeves, J. D., Lie, Y. S., … Kay, M. S. (2010). Design of a potent D-peptide HIV-1 entry inhibitor with a strong barrier to resistance. *Journal of Virology*, 84(21), 11235-11244.

White, S. H., & von Heijne, G. (2005). Do protein-lipid interactions determine the recognition of transmembrane helices at the ER translocon? *Biochemical Society Transaction*, 33, 1012-1015.

Wilschanski, M., Miller, L., Shoseyov, D., Blau, H., Rivlin, J., Aviram, M., … Kerem, E. (2011). Chronic Ataluren (PTC124) treatment of nonsense mutation cystic fibrosis. *European Respiratory Journal*, 38(1), 59-69.

VX-770 and VX-809 combination drug release (2011). Interim phase 2 data showed a Combination of VX-770 and VX-809 improved function of the defective protein that causes Cystic fibrosis in people with the most common form of the disease. Retrieved from http://investors.vrtx.com/releasedetail.cfm?releaseid=583683.

Zabner, J., Smith, J. J., Karp, P. H., Widdicombe, J. H., Welsh, M. J. (1998). Loss of CFTR chloride channels alters salt absorption by cystic fibrosis airway epithelia *in vitro*. *Molecular Cell*, 2(3), 397-403.

Zeiher, B. G., Eichwald, E., Zabner, J., Smith, J. J., Puga, A. P., McCray, P. B., … Thomas, K. K. (1995). A mouse model for the delta F508 allele of cystic fibrosis. *Journal of Clinical Investigation*, 96(4), 2051-2064.

Zeitlin, P. L., Boyle, M. P., Guggino, W. B., Molina, L (2004). A phase I trial of intranasal Moli1901 for cystic fibrosis. *Chest*, 125(1), 143-149.

Zhou, L., Dey, C. R., Wert, S. E., Duvall, M. D., Frizzell, R. A., Whitsett, J. A. (1994). Correction of lethal intestinal defect in a mouse model of cystic fibrosis by human CFTR. *Science*, 266(5191), 1705-1708.

Zhou, J. J., Li, M. S., Qi, J., Linsdell, P. (2010). Regulation of conductance by the number of fixed positive charges in the intracellular vestibule of the CFTR chloride channel pore. *Journal of General Physiology*, 135(3), 229-245.

Zűhlke, R. D., Zhang, H. J., Joho, R. H. (1995). *Xenopus* oocytes: A system for expression cloning and structure-function studies of ion channels and receptors. *Methods in Neuroscience*, 25, 67-89.

Xu, Y., Clark, J. C., Aronow, B. J., Dey, C. R., Liu, C., Wooldridge, J. L., Whitsett, J. A. (2003). Transcriptional adaptation to cystic fibrosis transmembrane conductance regulator deficiency. *Journal of Biological Chemistry*, 278(9), 7674-7682.